THESIS

SPATIAL PATTERNS AND PARTICLE SIZE DISTRIBUTIONS OF ATMOSPHERIC AMINES IN

NORTHERN COLORADO

Submitted by

Evelyn J. Bangs

Department of Atmospheric Science

In partial fulfillment of the requirements

For the Degree of Master of Science

Colorado State University

Fort Collins, Colorado

Spring 2020

Master's Committee:

    Advisor: Jeffrey L. Collett, Jr

    Sonia Kreidenweis
    Ellison Carter
    Katherine B. Benedict

ABSTRACT

SPATIAL PATTERNS AND PARTICLE SIZE DISTRIBUTIONS OF ATMOSPHERIC AMINES IN

NORTHERN COLORADO

Emissions of reactive nitrogen along the Front Range in Northern Colorado have

implications for sensitive and protected environments such as those in Rocky Mountain

National Park (RMNP). Nitrogen-containing pollutants exert a variety of adverse effects on the

environment, including visibility impairment and excessive nitrogen input to sensitive alpine

ecosystems. Northern Colorado has many urban, agricultural, and oil and natural gas

production activities that emit various forms of reactive nitrogen to the atmosphere. Model

simulations and past measurements demonstrate that these emissions are capable of being

transported long distances in gaseous and particulate forms. RMNP is particularly exposed to

increased concentrations of reactive nitrogen pollutants during periods of easterly, upslope

flow when emissions along the Front Range and sources from even farther away (e.g. the

Western United States coast) are transported into the mountains. A detailed understanding of

the composition of transported reactive nitrogen pollution is needed to predict environmental

impacts within RMNP. While emissions of ammonia and nitrogen oxides have received

significant attention in previous studies, relatively little is known about organic nitrogen

pollution, despite its ability to contribute to excess N deposition and to formation of particulate

matter (PM). Amines are organic analogs of ammonia, where one or more hydrogen atoms are

replaced by organic functional groups. The animal agriculture industry is known to be a major

source of some amines, while the beer and wine industry, sugar beet industry, leather

manufacturing, and chemical manufacturing are also potentially important sources. Many of

these industries are located along Colorado's Front Range, providing a good opportunity to

study amine atmospheric chemistry. While the chemical lifetime of many gas phase amines is

relatively short (hours), they are strong bases that can compete with ammonia to form longer-

lived particles that are transported over substantial distances. The work carried out in this

study focused on assessing a spatial gradient of particulate amines between RMNP, Fort Collins,

and Greeley. Greater concentrations of many amines were typically observed near source

emissions in Greeley and/or Fort Collins, but significant concentrations of amines such as

dimethylamine, were also observed in the more remote environment at RMNP. To better

understand amines, their chemistry and their contribution to PM, size distributions of 16

different amines were analyzed from measurements with a Micro-Orifice Uniform Deposit

Impactor (MOUDI). Of 16 analyzed amines, nine were found above the detection limits in

summertime Fort Collins and five during the winter. Several organic acids and inorganic acid

anions particle size distributions were also assessed to understand contributions from potential

anion species involved in salt formation with amine cations. Organic acid particle size

distributions, particularly oxalate, overlap with fine particle mode size distributions of both

ammonia and amine cations. The size distribution measurements also reveal important

reactions between gaseous nitric acid and coarse soil particles to generate coarse mode nitrate

particles. Continued measurements of amines and other species size distributions and spatial

gradients at more locations would help improve understanding of amine PM chemistry. This

understanding would allow necessary changes to be made to better protect the health of living beings and the sensitive ecosystems like those found in Rocky Mountain National Park.

ACKNOWLEDGMENTS

TABLE OF CONTENTS

LIST OF TABLES

LIST OF FIGURES

1. Introduction:

1.1 Background

Excess nitrogen deposition has been associated with adverse effects to particularly sensitive ecosystems like those observed in Rocky Mountain National Park (RMNP). Negative environmental effects of excess nitrogen deposition include lake eutrophication, increased nitrate concentrations in lakes, soil acidification, decreased biodiversity and changes to diatom flora(Baron et al., 2000; Bobbink et al., 2010; Cisneros et al., 2010). As places like RMNP are treasured and heavily visited, seeing millions of visitors annually, there is a strong motivation for the preservation of these areas. The geography of the region, semi-arid plains to the east with large population centers residing at the base of the Rocky Mountains from Fort Collins in the north to Colorado Springs in the south, and the Rocky Mountains themselves across western Colorado, makes the location of sources and wind patterns important for understanding the impacts of atmospheric nitrogen emitted from across the state and beyond. Northeastern Colorado is dominated by agricultural and feeding operations, as well as, many oil and natural gas wells and housing developments. Back trajectories from the HYSPLIT model have shown the potential for reactive nitrogen emissions to reach Colorado from locations that originated as far out as the United States west coast. Previous work has shown that many reactive nitrogen species are attributed to sources located outside of Colorado with the exception of ammonia being about 50% attributable to sources in Colorado (Gebhart et al., 2011).

Emissions of nitrogen oxides are regulated by national, state, and regional policies (e.g., the Clean Air Act and associated State Implementation Plans (SIPs)); however, emissions of organic nitrogen compounds and reduced nitrogen compounds such as ammonia are largely unregulated. Stakeholder groups and government agencies (EPA, NPS, CDPHE) in the Colorado Front Range have recognized the importance of reducing emissions of ammonia in agricultural and industrial practices, especially on days when southeasterly flow is predicted either from mountain valley diurnal wind circulations or synoptic weather conditions. During these southeasterly flow periods, studies have documented sharp increases in concentrations of gaseous ammonia and fine mode particulate matter (PM) in RMNP, suggesting that pollution from the Front Range urban corridor and agricultural and oil and natural gas development activities in NE Colorado is transported into RMNP (Beem et al., 2010). Inorganic particles (e.g., ammonium nitrate) and gas phase concentrations of ammonia and nitric acid have been linked to these upslope flow events. However, organic nitrogen species have not been well characterized in the gas or aerosol phase in this region due to a complex variety of organic nitrogen compounds and sources making it difficult to characterize them all with current sampling methods. This is an important gap in our understanding as wet deposition of organic nitrogen has been demonstrated to be an important source of reactive nitrogen inputs into RMNP ecosystems (Beem et al., 2010; Benedict et al., 2013). Additional nitrogen has been shown to have an adverse effect on ecosystems in RMNP due to shallow bed-rock and low soil buffering capacities (Baron et al., 2000). By closing the gap in our understanding of organic nitrogen, these negative effects inflicted on an ecosystem can be better regulated and monitored.

1.2 Organic Nitrogen and Amines

Amines are organic analogs to ammonia, with one or more hydrogens in an ammonia molecule replaced by organic functional groups. Oxidation products of gaseous amines can form species that are known to be carcinogenic (Pitts et al., 1978), such as nitrosamines. Amines are known to be emitted strongly from the agriculture industry and animal feeding operations (Zhang et al., 2011) along with ammonia. Amines known to be emitted in significant concentrations in the gas phase include methylamine, dimethylamine, trimethylamine, and triethylamine (Ge et al., 2011; Hutchinson et al., 1982; Rabaud et al., 2003; Schade and Crutzen, 1995). Some studies have attempted to look at specific sources within an animal feeding operation to determine aspects of the operation that contribute most to emissions, finding that waste treatment processes at cattle operations are one of the greater contributors to amine emissions (Dod et al., 1984). In addition to emissions of gas phase amines, field campaigns have shown that organic nitrogen can contribute significantly to overall organic aerosol mass (Mace et al., 2003; Makela et al., 2016; McGregor and Anastasio, 2001; Williams et al., 2001). Several studies have demonstrated an important role for amines in nucleation of new particles (e.g., Jen et al., 2016, 2014), but additional work is needed to quantify contributions of amines to total organic nitrogen mass in the aerosol phase as amines are known to have toxic properties, impacting health.

Because gas-phase amines are strong bases and compete with ammonia to a high degree, acid-base chemistry is one of the major pathways for particle formation from primary and secondary amines (Murphy et al., 2007). Primary and secondary amines can react with nitrate (NO_3^-), sulfate (SO_4^{2-}), and organic acids to form soluble aminium salts. Tertiary amines

have been shown to form non-salt secondary organic aerosol (SOA) via oxidation reactions with the nitrate radical, ozone (O_3), or the hydroxyl radical (OH) (Murphy et al., 2007; Silva et al., 2008). Estimations of amine dissociation constants in previous studies show that even when ammonia is at typical ambient concentrations in urban regions, amines can compete for acid-base chemical reactions (Murphy et al., 2007). Several amines can be oxidized by oxidant species in the atmosphere but tertiary amines are the only amines known to form non-salt organic aerosol in the presence of OH or O_3. In particular, studies have shown that SOA formation is greatest when the oxidative species are a mixture of nitrogen oxides (NO_x) and O_3 (Silva et al., 2008).

Given potential reactions of sulfuric and nitric acids with amines to form PM, the common assumption that available ammonia first neutralizes sulfate and the excess is available to react with nitric acid to form ammonium nitrate, may not be fully accurate. In addition, there is little understanding about the contribution of organic nitrogen (ON) to overall aerosol mass, but, studies carried out in the early 2000s suggest that a significant amount of organic aerosol mass is made up of ON. There is hardly any insight into the contribution of amines to total ON masses (Mace et al., 2003; Makela et al., 2016; McGregor and Anastasio, 2001; Williams et al., 2001). This study focused on particle size-resolved measurements of amine concentrations with the intent to better understand the chemistry of amines in the atmosphere, their role in aerosol formation, and their contributions to aerosol mass and composition.

1.3 Sources of inorganic and organic nitrogen

It is well known that ammonia is emitted in large quantities from animal feeding operations. Previous studies have shown that amines are also emitted from these same operations. Since the 1970s, amines have been identified in atmospheric emissions from cattle and swine operations (Bethea and Narayan, 1972; Miner and Hazen, 1969; Mosier et al., 1973). Later on, amines were observed to be emitted from dairy operations as well as cattle and swine operations (Filipy et al., 2006; Rabaud et al., 2003). Amines are emitted from these animal industries as a result of decarboxylation reactions in the gastrointestinal tracts of animals. They are also emitted from anaerobic processes in waste treatment (Rappert and Müller, 2005).

Other large amine emitters are vegetation and biomass burning (Ge et al., 2011). Wildfires, dead tree removal from forests, and agricultural and waste burning are large biomass burning activities that contribute greatly to amine emissions. The highest emissions of amines from biomass burning have been observed to occur during smoldering burns (Yokelson et al., 1997).

While animal feeding operations and biomass burning are two of the largest sources of amine emissions, there are other important local sources of amines, including industry, composting, and food industries (e.g. grain, sugar beet, and beer operations.) All of these amine sources are present in Northeastern Colorado and along the Front Range. Amine emissions result from grain, sugar beet, and beer production as a result of the drying processes (for grains and sugar beets) and, in the case of beer, the roasting and drying of grains, as well as, fermentation processes (Daniel et al., 2015; Passant et al., 1993). Composting is another important local source of amines as the processes of composting involves anaerobic activity,

which is known for causing amine emissions (Krzymien et al., 1999). Studies have shown the potential for amine formation and emission from manure, yard waste, cardboard, construction waste, recyclate, and particularly, restaurant and food waste composting (Krzymien et al., 1999; Tsai et al., 2008).

There are also more localized sources of amines. Automobiles, sewage waste, meat cooking, pesticides, and tobacco smoke are known sources of amines, and can potentially be large contributors to fine organic aerosol mass (Rogge et al., 1994, 1993, 1991). Interestingly, amines have even been found to be emitted from common household materials such as indoor textiles (Sollinger et al., 1994, 1993). All of these sources have the potential for amine emissions to the atmosphere, driving the possibility for subsequent aerosol formation.

Amines have been recognized as potentially significant contributors to the nitrogen budget in the atmosphere (Fekete et al., 2010). Some early studies looked into the contribution of amines, particularly trimethylamine, in the formation of secondary organic aerosol (SOA) (Murphy et al., 2007; Silva et al., 2008). Murphy et al. (2007) attempted theoretical calculations based on laboratory chamber experiments to assess aerosol thermodynamic parameters for amines. More recent work (Jen et al., 2016, 2014) further confirmed the importance of amines in new particle formation involving sulfuric acid clusters. Because they are associated with particle formation from the gas phase, amines are expected to be primarily associated with fine mode particles, so high-resolution measurements in the submicron size range have the potential to provide useful insight into the types of particles being formed from amine chemistry.

1.4 Size Resolved Aerosol Measurements and Aerosol Formation Mechanisms

Near sources, PM can be emitted directly as primary organic aerosol (POA) or can be formed from emitted gas-phase constituents via various chemical and physical processes. The formation of ammonium nitrate is one such example. Ammonium nitrate is formed by the following reaction:

$$NH_3\,(g) +\ HNO_3\,(g)\ \leftrightarrow\ NH_4NO_3$$
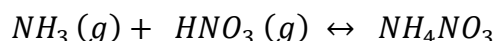
This is a temperature and relative humidity dependent, reversible reaction. This is in contrast to the formation of ammonium sulfate, which is essentially irreversible. Atmospheric sulfuric acid (H_2SO_4) can be formed via reactions of SO_2 in the gas phase and in cloud droplets. When this reaction forms sulfuric acid, a neutralization reaction between H_2SO_4 and NH_3 can form ammonium sulfate.

$$2NH_3 +\ H_2SO_4\ \rightarrow\ (NH_4)_2SO_4$$

A commonly held assumption is that, as the more acidic species, sulfate is likely to react with all available ammonia before ammonia will react with nitric acid. However, some work has shown that in some cases only partial neutralization of SO_4^{2-} was observed in the presence of organic gaseous species due to a competition between ammonia and organic gases for sulfate uptake (Liggio et al., 2011; Silvern et al., 2017). Additionally, there are often ionic imbalances in measurements of PM composition, suggesting incomplete measurement of charged species present in the aerosol and, potentially, a lack of understanding of important aerosol formation

processes and reactions on aerosol already formed. Typically, observed imbalances are anion

deficits and are commonly attributed to unmeasured organic acids (OA). In some cases, studies

have found a cation deficit that has not been well explained (John et al., 1990). By measuring

the traditionally measured inorganic ions (ammonium, sodium, magnesium, calcium, nitrate,

and sulfate) in the same samples as amines, organic acids, and smoke markers, we hope to

improve our understanding of aerosol chemistry sources, contributions to total nitrogen in the

atmosphere, and general aerosol formation mechanisms.

Due to a relatively long atmospheric residence time, PM can be transported from one

location to another with relatively minimal losses due to removal by atmospheric processing;

PM mass often increases as the original aerosol picks up additional, secondary constituents

along the way (Seinfeld and Pandis, 2006). While ambient species like particulate nitrate and

sulfate compounds have been shown to constitute a large amount of aerosol $PM_{2.5}$ mass in the

atmosphere, there remain limited field measurements of the particle size distributions of these

important species as well as the processes that lead to their formation in aerosol. Ammonium

nitrate and ammonium sulfate are typically assumed to be dominant contributors, along with

organic matter, to particles in the submicron size range; however, in some environments these

species are also observed in coarse particles.

Size-resolved measurements of PM composition have shown things like the importance

of fine mode ammonium near animal husbandry, coarse mode nitrate at sites near the ocean

and near heavy agricultural productivity, and oxidation processes of anthropogenic emissions of

sulfate. Lee et al., 2008, for example, demonstrated the common importance of coarse mode

nitrate, especially in acidic aerosol formed in hot, dusty environments, as a result of reactions

of nitric acid with sea salt and/or soil dust. Size resolved data for species such as nitrate, ammonium, and sulfate have been regularly collected and evaluated to understand their role in aerosol chemistry; high resolution size distributions data of organic acids and reduced nitrogen compounds have not typically been included.

1.5 Objectives

In this study, we examined the change in total nitrogen, amine concentrations, and more generally aerosol composition measured at weekly intervals from March 2019 to October 2019 across an east-west transect of the following 3 sites in NE Colorado: (1) from an agricultural source region (Greeley), (2) the Front Range urban corridor (Fort Collins), and (3), a remote site in Rocky Mountain National Park (RMNP). These samples were primarily collected to identify gradients in concentrations of oxidized and reduced nitrogen species, in the gas and particle phases, and to quantify different amines and their relative contributions to PM$_{2.5}$ organic nitrogen.

Additionally, size resolved samples were collected at the Fort Collins sampling site to examine individual inorganic and organic species size distributions. In an attempt to understand ionic species found in PM, this study focused on ten size bins and a variety of ionic species with a special emphasis on quantification of amines, including the more commonly studied ones (trimethylamine, dimethylamine and methylamine.) By analyzing amines, organic acids, and smoke markers together in the same study, in addition to more traditionally measured inorganic ions, this work was designed to inform development of a better understanding of PM composition and formation mechanisms across different size ranges. In the urban region of the

Front Range, it is expected that amines would be found in significant concentrations as there are many known sources of amine emissions in this region. RMNP on the other hand has minimal sources of emissions and therefore, it would be expected that amine concentrations would be in lesser amounts relative to the urban corridor.

2. Methods:

2.1 Sampling Sites

Three aerosol and trace gas monitoring sites were established in Greeley, Fort Collins, and RMNP. Measurements at the three locations were made in tandem with each other for comparison. The spatial measurements reported here across the three sites, using URG denuder/filter-pack samplers, are weekly samples for the month of April 2019. Size-resolved measurements of particle composition, using a cascade impactor, were made only at the Fort Collins site during the months of August 2018 and January 2019 to represent summer and winter seasons, respectively.

2.2 Denuder Filter Pack Sampling

Measurements of PM$_{2.5}$ composition and select trace gases (ammonia, nitric acid, and sulfur dioxide) were taken weekly with sample changes around mid-day, using a nominal flow rate controlled by a mass flow controller of 10 L min^{-1} (CSU and RMNP) and a nominal flow rate of 3 L min^{-1} (Greeley). Previous work has shown high concentrations of gas-phase ammonia at the Greeley site due to proximity of sampling to animal feeding operations prompting a lower flow rate to prevent over-saturation of the gaseous ammonia denuder capacity during a weekly sampling period. RMNP and CSU samples have not been found to have over-loaded ammonia denuders and used a more standard higher flow rate as used in past studies (Beem et al., 2010; Benedict et al., 2018; Lee et al., 2008; Yu et al., 2005).

At each site the ionic composition of particles with an aerodynamic diameter less than

2.5 μm were measured using URG denuder-filter pack sampling. Filters were loaded into the

filter pack at the CSU laboratory and installed in a sampling train along with coated URG

annular denuders. The annular denuders were coated with phosphorous acid for collection of

gas phase ammonia and sodium carbonate for collection of nitric acid and sulfur dioxide (Lee et

al., 2008). The ambient air was drawn up through a Teflon-coated cyclone rated for either a 10

L min^{-1} flow rate or 3 L min^{-1} flow rate for collection of PM$_{2.5}$ (D$_{50}$ = 2.5 μm) depending on the

site. Next in the sample train are the denuders which collect ammonia, nitric acid, and sulfur

dioxide by diffusion onto the appropriately coated surfaces. Next, the air flow was pulled

through a filter pack with a nylon filter (Measurement Technology Laboratories, LLC, 1 μm pore

size and 47 mm diameter). Previous studies have shown high efficiency of nitrate retention on

nylon filters, despite volatilization of ammonium nitrate particulate (NH$_4$NO$_3$), by recapture of

the gas-phase nitric acid (Yu et al., 2005). However, ammonia volatilized from the particulate

has been shown to not be efficiently recaptured by the nylon filters (Yu et al., 2006). Volatilized

ammonia from the NH$_4$NO$_3$ was consequently recaptured by a downstream back-up denuder

coated with the same phosphorous acid solution. The total particulate ammonium was

determined by summing the ammonium found from the filter and the ammonium found in the

back-up denuder.

The flow on the pump was measured using a Mesa BIOS defender dry calibration meter

(Defender 530, Mesa Labs) to ensure the proper flow was being pulled through the pump for

the size cut of the cyclone. The actual sampled air volume was measured separately using a dry

gas meter and was corrected with a measured pressure difference through the sample train at

the start and end of each sampling period. The calculation of total sampled ambient air was

corrected to standard conditions since each site was at a different elevation to allow more direct comparison between site locations. Before deploying the dry gas meters in the field, they were tested in the laboratory with a micro-orifice for a set period of time to check if the proper air volume was recorded. In addition to the sampled filters, a set of blank filters were collected by loading the filters into filter packs and then removing them within one day. This was done as part of a quality assurance check. Blank samples were also generated using coated, but un-sampled denuders.

2.3 Size Resolved Particle (MOUDI) Sampling

2.3.1 Running the MOUDI

In addition to PM$_{2.5}$ measurements at the Fort Collins site, size resolved particle composition measurements were also made. To measure ambient size resolved particulate matter, a Micro Orifice Uniform Deposition Impactor (MOUDI) (Model: 0100-01-1050) was used. Most models of the MOUDI, including the one used for this experiment, allow for rotation to evenly distribute the particulate across the filter. Rotation is most useful when filters are to be analyzed visually with a microscope or x-ray imaging. This type of analysis was not relevant for the experiment carried out here and the MOUDI was operated without rotation. Prior to the initial sampling start, the MOUDI was cleaned by following the cleaning method outlined elsewhere (Lee, 2007). The MOUDI impactor stages collected particles from >0.176 μm at the smallest size (an after-filter collected smaller particles passing this stage) to <18 μm at the largest size across ten stages at a calibrated 30 L min^{-1} flow rate. This flow rate was not corrected to standard conditions. Table 1 shows the relevant size cuts and parameters for the

MOUDI as determined from calibrations in previous studies involving the same instrument and flow rate (Marple et al., 1991).

Table 1. Nominal and calibrated stage cuts are reported below based on the work performed by Marple et al. These stage cuts are calibrated based on a flow rate of 30 L min^{-1} as was used in this experiment.

Stage #	Inlet	1	2	3	4	5	6	7	8	After-filter
Nominal cut-point (μm)	18	10.0	5.6	3.2	1.8	1.0	0.56	0.32	0.18	<0.18
Calibrated cut-point (μm)	18	9.9	6.2	3.1	1.8	1.0	0.56	0.32	0.176	<0.176

Aluminum foil pre-cut round filters (MSP Corp. 47 mm diameter), coated with a silicon spray and baked, were used for the impaction surface of each stage except the after-filter. Each aluminum foil filter was placed on a tray in a glovebox and sprayed with heavy-duty silicon spray from MSP Corporation. Application of silicon spray is used to reduce potential particle bounce. The filters were then transferred into a clean glass dish and placed in an oven pre-heated to 60 °C and allowed to bake for one hour. The baked filters were then transferred to sterile petri dishes (PALL 50x9 mm) and stored in a dry dark place before loading onto the MOUDI stage plates. The largest 9 stages were loaded using the aluminum foil filters but the smallest stage (After-filter) was loaded with a Teflon filter with ring (PALL 2.0 μm pore size, 37 mm diameter, Product ID: R2PL037) to collect remaining smaller particles in the sampled air stream. To obtain the 30 L min^{-1} flow rate, a ¼-hp carbon vane vacuum pump was used (Gast Manufacturing Corp.) along with a flow control valve on the MOUDI. Outside air was pulled through a straight inlet into the MOUDI which was housed in a mobile laboratory parked outside the CSU Atmospheric Science Department. The stream of air cascaded through the top 9 stages and through the first magnehelic. This magnehelic measured the pressure drop across

the top 9 largest stages and was set to 23.5 inches of water by adjusting the flow control valve

as suggested by the MOUDI manufacturer. The second magnehelic measured the pressure drop

between the final stage and the environment. This magnehelic was used as an indicator that

the MOUDI was working properly. Values on the second magnehelic that were too high were an

indication of a clog and values that were too low were an indication of a leak. Neither issue was

found for the samples analyzed in this experiment. The stream of air then left the MOUDI and

was pulled past a third magnehelic and a dry gas meter in tandem. The third magnehelic and

dry gas meter were used along with elapsed time to determine the actual sample volume of air

and to confirm that the MOUDI was accurately operating at a 30 L min^{-1} flow rate.

2.3.2 Inverting size resolved data and corrections

The MOUDI has relatively steep size cuts (Marple et al., 1991). The 50 % cutpoint of a

stage, denoted by d_{50}, is the aerodynamic particle diameter collected with 50% efficiency. The

collection efficiency curve for a stage describes collection efficiency as a function of particle

size. Because even well-designed impaction stages do not exhibit a perfect step-change in

collection efficiency at the stage cutpoint, it is necessary to account for this non-ideality in

reconstructing measured particle size distributions. To account for the slope of the collection

efficiency curve for each stage, an adapted version of the Twomey algorithm was used

(Winklmayr et al., 1990). The original inversion procedure was developed by Twomey and was

successful in smoothing raw size distribution data by applying an iterative nonlinear algorithm

to the size distribution data (Twomey, 1975). The original Twomey algorithm, however,

produces artifacts when applied to cascade impactors with relatively steep size cuts. The

adapted version of the Twomey code accounts for the steepness by applying an additional

calculation for the weighting functions rather than assuming the kernel functions are identical

to the weighting functions (Winklmayr et al., 1990). In this adapted version of the code, a

Fredholm equation is solved in the form below.

$$y_i = \int_{x_{min}}^{X_{max}} k_i(x) f_j(x)\, dx \tag{1}$$

In this function, $k_i(x)$ is the kernel function that depends on the instrument and the

probability of a particle sized x collected on stage i. The integral bounds are the upper and

lower size limits of the instrument stages. In the initial solution of this equation, a guess

function is determined as $f_0(x)$ and then iterations are performed until a stopping criterion is

reached. The initial guess function was determined based on the raw MOUDI data collected for

this study. After successive iterations, the initial guess function becomes modified by

multiplying $f_j(x)$ by the kernel function and a ratio of actual mass to calculated mass.

Fredholm equations of the first order are typically solved by replacing the integration with a

summation. Then equation (1) becomes

$$y_{i\,j} = \sum_d^m k_i(x_d) f_j(x_d) \delta \log[x_d] \tag{2}$$

Where $f_j(x_d)$ is modified in the form

$$f_{j+1}(x_d) = f_j(x_d) * [1 + \left(\frac{y_i}{y_{ij}} - 1\right) a_i(x_d)] \tag{3}$$

and $a_i(x_d)$ is the weighting function that replaces the kernel function such that

$$a_i(x_d) = k_i(x_d) \tag{4}$$

The term $\frac{y_i}{y_{ij}}$ is the ratio of actual mass to the calculated mass, x_d is the particle

diameter, and m is the number of points that the distribution is evaluated at. For this study, m =

100. The weighting function was calculated using the following expressions:

$$k_n(x_d) = E_n(x_d) \tag{5}$$

$$k_i(x_d) = E_i(x_d)[1 - E_{i+1}(x_d)] * \dots [1 - E_n(x_d)] \tag{6}$$

where $i = n - 1, n - 2, \dots, 1$ and n is the number of stages. The term, $E_n(x_d)$, represents the

efficiency function of the largest particle size range and can be determined generally by

$$E(x_d) = \left[1 + \left(\frac{d_{50}}{x_d}\right)^{2s}\right]^{-1} \tag{7}$$

The weighting function is dependent on the particle diameter, x_d; the 50% cutpoint,

d_{50}; and the steepness, s.

The Twomey inversion stops when the improvement in the accuracy parameter, sigma,

is smaller than five percent. Sigma is given by the following formula,

$$SIGMA^2 = \left(\frac{1}{n}\right)\sum_{j=1}^{n}\left[\frac{y_i - y_{ij}}{\delta y_i}\right]^2 \qquad (8)$$

where δy_i is the absolute uncertainty for the mass on the stage, i. The code was only

allowed to run for 100 iterations. When the stopping criteria, sigma, was not attained in 100

iterations, then the code was stopped after the 100th iteration and the final iteration was used

in the output file.

The adaptation used for this study was written in Fortran and can be modified to other

cascade impactors aside from the MOUDI. The adapted Twomey algorithm accounts for non-

ideality in the collection efficiency of the MOUDI and smooths the raw size distribution data

across all measured size bins. The values for d_{50} cutpoints and steepness were adopted from

Marple et al. and integrated into the adapted Twomey algorithm (Marple et al., 1991). The

Fortran code was adjusted to reflect the number of stages and MOUDI size parameters, before

being compiled and run using CodeBlocks software. A note should be made, due to the nature

of the originally written code, a faux size range had to be created to allow for the code to be

run properly. This faux size range was smaller than the after-filter range and represented the

range of 0.05 μm down to 0 μm.

2.4 Sample Analysis

2.4.1 Sample Extraction

URG denuders were immediately extracted upon return to the lab and all sampled filters

were removed promptly from the filter pack or MOUDI housing. All of the collected nylon and

MOUDI filters were placed in 16 mL sterile polystyrene round-bottom tubes with the sampled

side of the filter facing inward from the walls of the tube and then stored in a cold room until

extraction. Extraction for all filters was performed with 7 mL deionized water (DI) purified from

a ThermoScientific Nanopure system. It has been shown that extraction with DI is efficient at

removing the ions from the nylon filters (Yu et al., 2005). After addition of DI water, the sample

tubes were placed in a sonicator (Branson 3510) and allowed to extract for one hour, then

immediately measured on the Dionex IC systems for amines, organic acids, and common

inorganic ions.

2.4.2 Ion Chromatography

Filter and URG extracts were analyzed by several Dionex Ion Chromatograph (DX-500)

systems. Descriptions of the various methods follow:

Amine IC System

The amine Dionex IC system was equipped with an AS50 autosampler, a self-

regenerating cation suppressor, an ED50 electrochemical detector, and a GP50 gradient pump.

In addition to amines, other cationic species were measured using this IC system. The eluent

drawn through the cation IC system was methansulfonic acid (MSA) in a solution with DI water.

Because the amines retention times are so close together, a modified method was developed at

CSU by Amy Sullivan to ensure high resolution of separate amine peaks. The cation separation

occurred on Dionex CS-19 guard (4 x 50 mm) and analytical (4 x 250 mm) columns. Under a 1

mL min^{-1} flow rate, each sample separated over a total of 125 minutes. Initially, the first 68

minutes had an isocratic elution with 0.3 mM MSA in order to detect any +1 charged inorganic

cations. For the next 17.9 minutes, a linear gradient from 0.3 to 6 mM MSA occurred to

separate all the amines. An isocratic elution was performed for 28.7 minutes at 6 mM MSA to

detect +2 charged inorganic cations. For the last 10.4 minutes, a re-equilibration step was used

to return the IC to the starting conditions for the next sample. **Error! Reference source not

found.**Figure 1 shows an example of a chromatogram from the amine IC system.   A total of 16

different amines were analyzed and are listed in order of retention times: ethanolamine,

methylamine, diethanolamine, dimethylamine, allylamine, propylamine, tert-butylamine,

trimethylamine, diethylamine, sec-butylamine, iso-butylamine, butylamine, triethylamine,

dipropylamine, amylamine, and 1,4 diaminobutane.
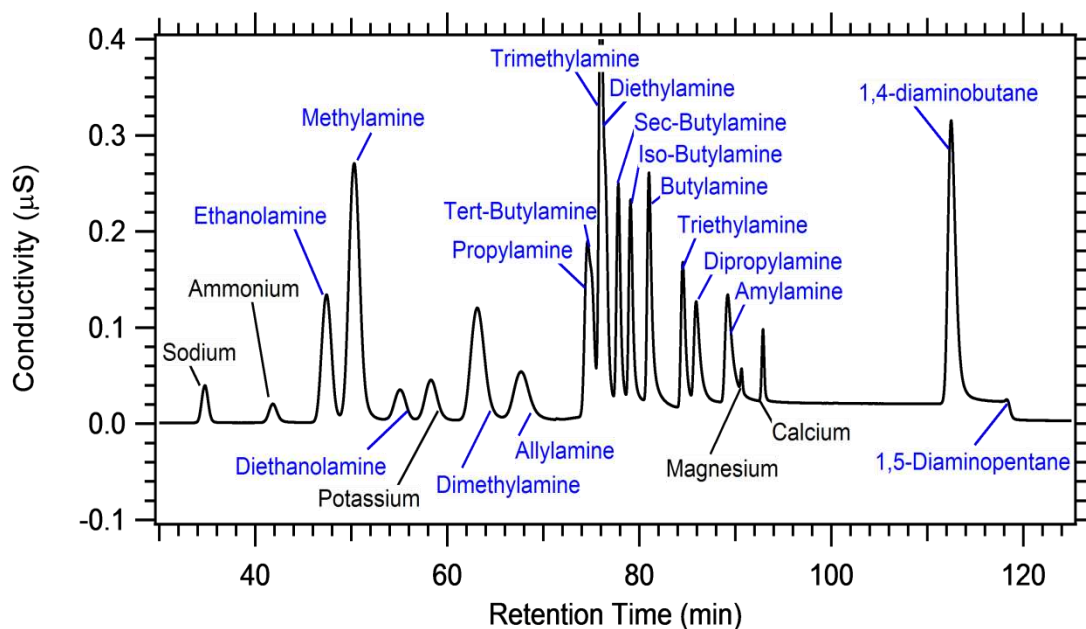
Figure 1. An example of an amine separation chromatogram is presented above. A total of 16 different amines and five inorganic ions were analyzed in this work. Graph courtesy of Amy Sullivan, Colorado State University.

A total of 5 different inorganic cations were measured in the amine separation: sodium,

ammonium, potassium, magnesium, and calcium. Separated amine and inorganic cation peaks

were analyzed using the IC Chromeleon software and concentrations were determined using a

calibration curve developed from standards with known compound concentrations. An

example of a typical calibration plot made from a set of standards is shown in Figure 2.

Ammonium was the only species that exhibited a polynomial signal response. All other species

analyzed for this work were plotted with a linear calibration fit.   The MOUDI substrates and

Teflon and nylon filters were analyzed by this method.
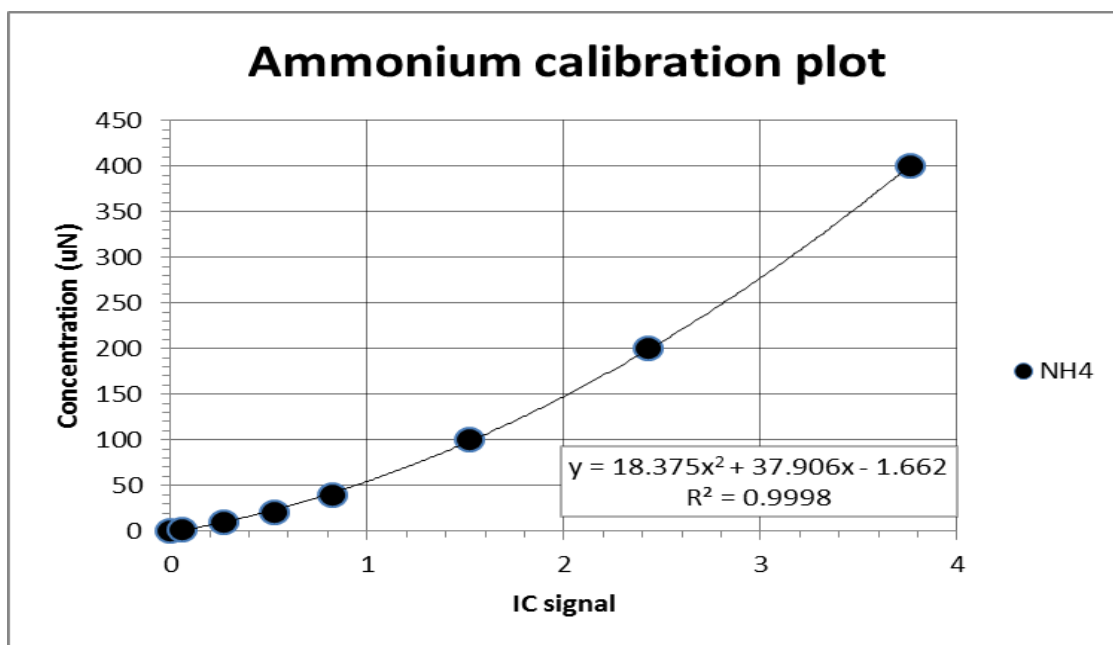
Figure 2. An example of an ammonium calibration plot is shown here. Ammonium is the only analyzed species in this work that has a polynomial signal response; other species have linear responses.

Organic Acid IC System

The organic acid (OA) system consisted of a Dionex ion chromatograph (DX-500) with a

gradient pump, self-regenerating anion suppressor, and a conductivity detector. These species

were separated on a Dionex AS-11HC guard (4 x 50 mm) and analytical (4 x250 mm) columns.

To resolve the peaks of species with similar retention times, a method involving a gradient

change with the eluent was developed at CSU by Amy Sullivan allowing for high resolution

between species peaks. The eluents made for this IC were a 5 mM sodium hydroxide (NaOH)

and 100 mM NaOH solution in DI water along with pure DI water. Each sample was run with a flow rate of 1.5 mL min^{-1} for a total of 65 minutes. The initial 13 minutes had an isocratic elution with 1 mM NaOH before a linear gradient from 1 mM to 15 mM was performed for 20 minutes. Then a linear gradient from 15 mM to 30 mM NaOH was carried out for the next 10 minutes. Next a linear gradient was carried out from 30 mM to 45 mM NaOH for only 5 minutes. Lastly, a re-equilibration step was carried out for 17 minutes to return the IC to the starting conditions for the next sample to be run. A total of 15 OA species were analyzed for this experiment as follows: acetate, propionate, formate, butyrate, methanesulfonate, pyruvate, cis-pinonate, valerate, glyoxylate, glutarate, succinate, malonate, maleate, oxalate and phthalate. In addition to the OA, four inorganic ions were analyzed using this IC method (chloride, nitrite, nitrate, and sulfate).
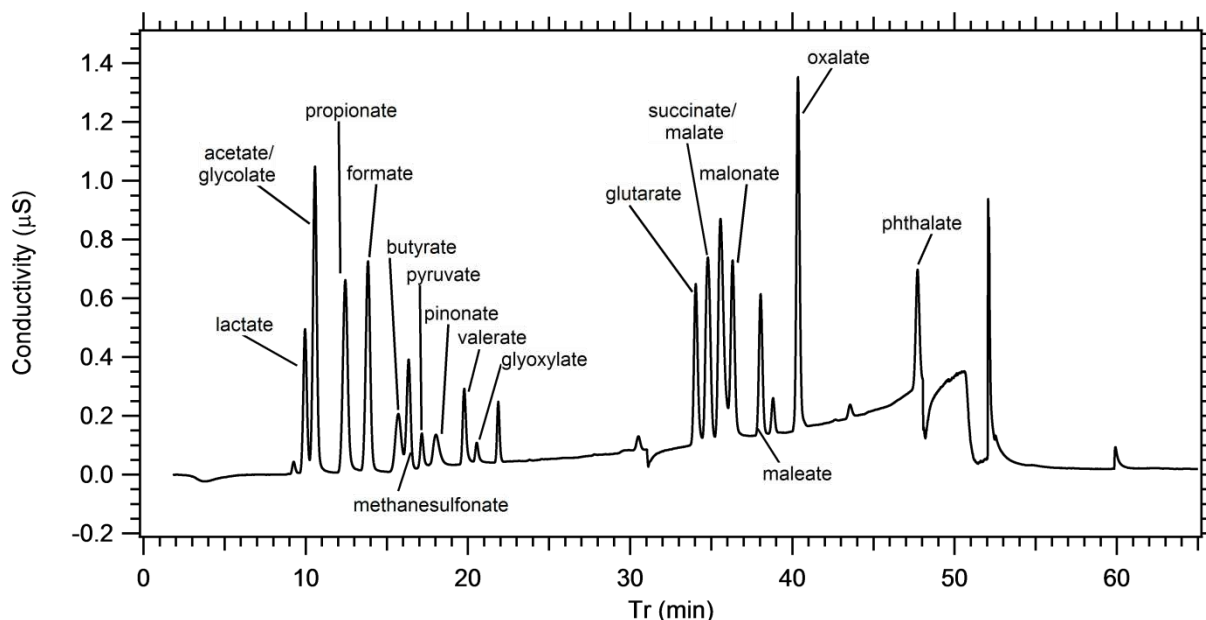
Figure 3. An example chromatogram for OA is shown above. Graph courtesy of Amy Sullivan, Colorado State University.

A set of standards with known concentrations of each of the listed OA above were run and calibration curves were developed. Only the MOUDI substrates were analyzed by this

method due to difficulties in accurately analyzing nylon filters for OA. These difficulties arise in the high background concentration of OA found on the nylon filters, making accurate sample detection unattainable.

Anion IC System

PM$_{2.5}$ nylon filters were analyzed using a Dionex IC equipped with an AS14A IonPac analytical column (4 x 250 mm), a self-regenerating anion suppressor, a CD20 conductivity detector, an IP25 isocratic pump, and a SpectraSYSTEM AS3000 Autosampler. The inorganic anions that were measured are: chloride, nitrite, nitrate, and sulfate. The eluent for this method was an 8 mM sodium carbonate (Na$_2$CO$_3$) and 1 mM sodium bicarbonate (NaHCO$_3$) solution that was operated with a 1 mL min^{-1} flow rate. A series of standards were made to develop a calibration curve for each species measured. The nylon filters were analyzed by this method to obtain inorganic ion data since we were unable to use the organic acid system for this type of filter.

2.4.3 Total Nitrogen Analysis

Total nitrogen (TN) content was measured for the URG nylon filters using a TOC/TN analyzer (Shimadzu TOC-V with TNM-1 attachment). Due to the limited amount of extract volume (2.2 mL total), manual injections were made in the TN analyzer instead of using the attached auto-sampler. Using the TOC-V Sample Table Editor software, the injection volume was adjusted to reflect manual injections but still allowed for three injections of approximately 0.75 mL each. As a consequence of the manual injection method, air bubbles were generally

present in the first injection causing inaccuracies in the signal detection. Therefore, the second

and third injections were averaged and used in the TN determination. A set of standards

consisting of sodium nitrate (NaNO$_3$) was made to create a calibration curve for sample

analysis. The standard concentrations were chosen to reflect the smallest and greatest

concentrated samples. Standard concentrations were 0.2 mg N L^{-1}, 0.5 mg N L^{-1}, 1 mg N L^{-1}, 3

mg N L^{-1}, 5 mg N L^{-1}, and 8 mg N L^{-1}. An example of the TN calibration plot is presented in Figure

4. Samples were analyzed for TN content using the linear fit equation generated by the TN

standards.
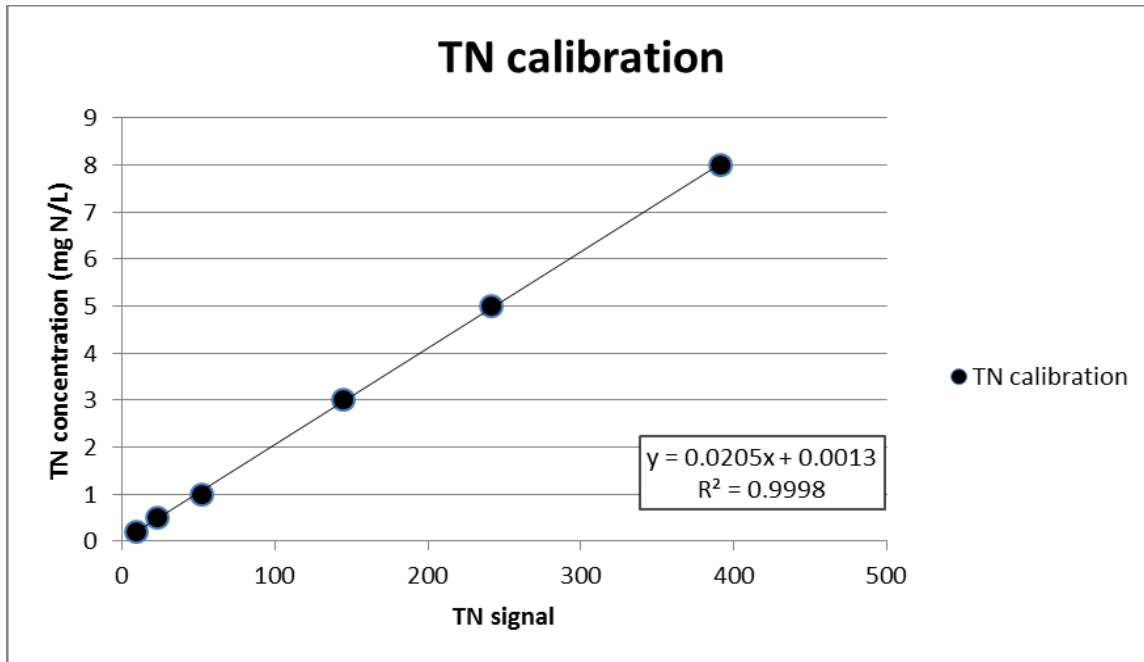
Figure 4. An example of the calibration plot generated for TN analysis of samples is shown above. The standard values were fitted with a linear line and the resulting equation was used in analysis calculations.

2.5 Quality Assurance and Quality Control

Overall measurement precision was calculated using a relative standard deviation (RSD) as outlined in equation (9). Due to limited sample extract volumes, the RSD was calculated using replicate standards that were similar in concentration to the samples.

$$RSD = \frac{S_{pooled}}{\bar{X}} * 100\% \tag{9}$$

where S_{pooled} is the pooled standard deviation and $\bar{X}$ is the average of all replicate samples.

A set of 12 blanks (11 aluminum foil filters, and 1 teflon after-filter) were collected during both the winter and summer seasons for a quality assurance check. The blanks were analyzed and averaged to correct the MOUDI size distribution data and to determine the method detection limit (MDL). The same was done for URG nylon filters. Detection limits were determined using the standard method blank calculation at the 95% confidence limit using the average of three blank samples as shown in the equation below

$$MDL > t * \delta_b * \sqrt{\frac{N_1 + N_2}{N_1 * N_2}} \tag{10}$$

where t is the t value given at the 95% confidence interval for the relevant degree of freedom, δ_b is the blank standard deviation, N_1 is the number of sample measurements, and N_2 is the number of analyzed blanks.

In the cases where species concentrations were found to be below the MDL, the concentrations were replaced with half the MDL value to avoid a bias in calculations of mean concentration values. This issue was only significant for concentration measurements of some trace-level amines. Inorganic ions and most OA species were present at concentrations greater

than the MDL. Table 2 lists MDL values for the different amines analyzed. The final column of

the table indicates which species were found consistently above the detection limit.

Table 2. A table of MDL values for amines is shown below. IC MDL values are in units of μeq/L and MDL values associated with different filter types (MOUDI and URG) and flowrates (3 L/min and 10 L/min)) are in units of neq/m³. The final column has a Y for the species that were consistently above the MDL and a N for species that were not.

Species	MOUDI (μeq/L)	MOUDI (neq/ m³)	URG (μeq/L)	URG (10 L/min) (neq/m³)	URG (3 L/min) (neq/ m³)	Above the MDL in fine mode? (Y or N)
Ammonium	0.001	0.001	0.001	0.001	0.001	Y
Ethanolamine	0.063	0.002	0.063	0.003	0.009	N
Methylamine	0.225	0.009	0.226	0.010	0.034	Y
Diethanolamine	0.018	0.001	0.018	0.001	0.003	N
Dimethylamine	0.180	0.007	0.180	0.008	0.027	Y
Allylamine	0.116	0.005	0.116	0.005	0.017	N
Propylamine	0.033	0.001	0.033	0.002	0.005	N
tert-Butylamine	0.024	0.001	0.024	0.001	0.004	N
Trimethylamine	0.007	0.0003	0.006	0.0003	0.001	Y
Diethylamine	0.038	0.001	0.038	0.002	0.006	N
sec-Butylamine	0.061	0.002	0.061	0.003	0.009	N
iso-Butylamine	0.067	0.003	0.067	0.003	0.010	Y
Butylamine	0.056	0.002	0.056	0.003	0.008	N
Triethylamine	0.048	0.002	0.046	0.002	0.007	N
Dipropylamine	0.070	0.003	0.068	0.003	0.010	N
Amylamine	0.069	0.003	0.073	0.003	0.011	Y
1,4-Diaminobutane	0.177	0.007	0.165	0.008	0.025	N

3. Results:

A total of 5 weekly nylon filter samples for RMNP, Fort Collins, and Greeley were collected in spring 2019 and analyzed for various amines, inorganic ions and total nitrogen content. The figures below show a time series of various species across all three sites. Due to a power outage, the Greeley sample from April 9th was excluded from the data set.

In addition to the nylon filters, MOUDI samples for both winter and summer seasons were analyzed for amines, inorganic ions, and organic acids. A total of 5 samples were collected throughout each season in four day sampling periods and each sampling period yielded 10 samples to be analyzed from fine mode to coarse mode for each collected sample.

3.1 PM$_{2.5}$ TN and inorganic ion spatial distributions

The spatial distribution of PM$_{2.5}$ TN (Figure 5a) showed the greatest nitrogen content in Greeley and smallest in RMNP. The same tendency was observed for PM$_{2.5}$ ammonium (Figure 5b) and nitrate (Figure 5c). The greatest concentrations of TN at Fort Collins and RMNP occurred on April 9th.
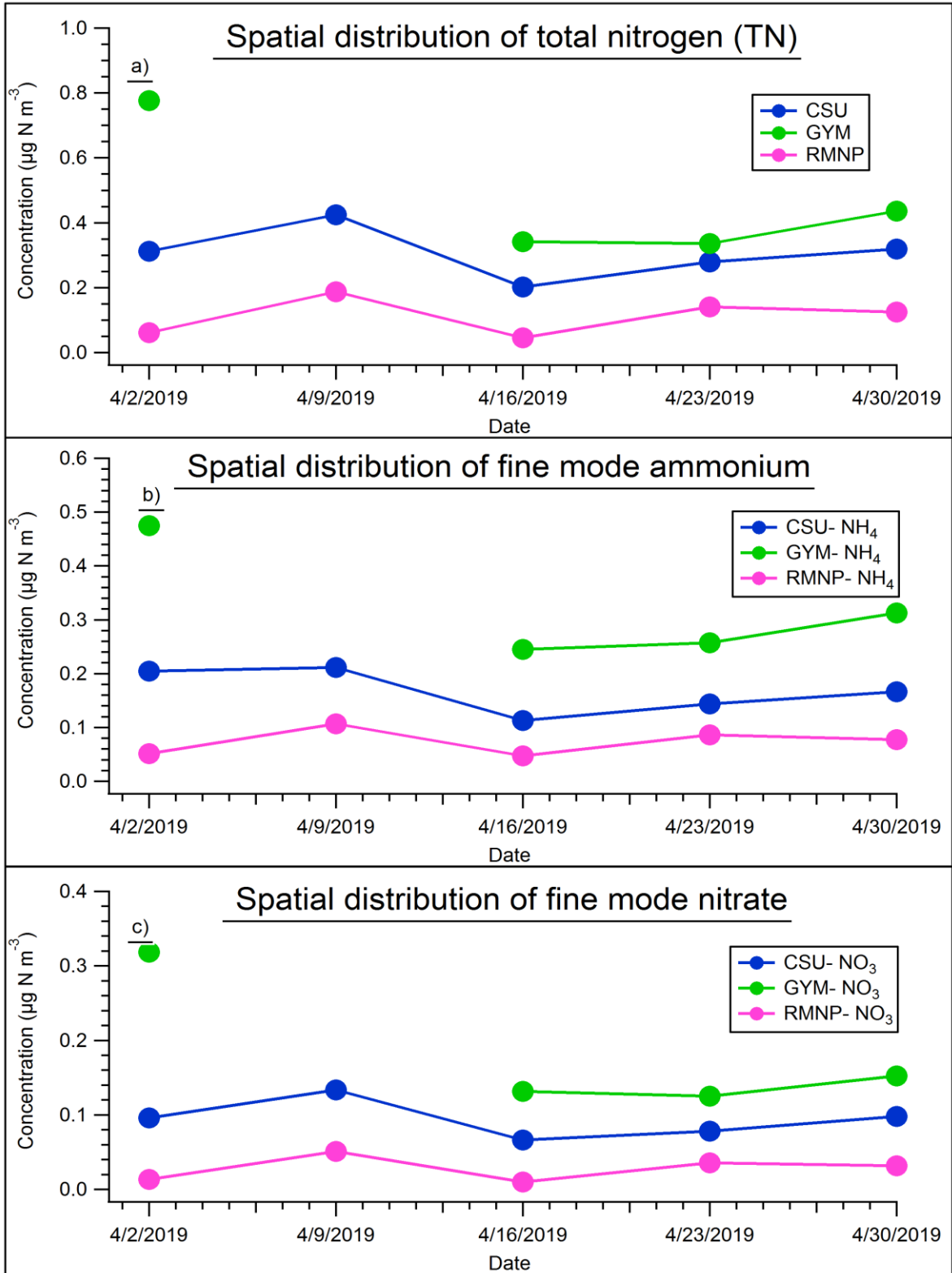
Figure 5. Spatial distributions for TN (a), ammonium (b), and nitrate (c) are shown above for the month of April 2019.

Measurements were made at Greeley (GYM), Fort Collins (CSU) and Rocky Mountain NP (RMNP).

An assessment of inorganic, organic and total nitrogen concentrations showed nearly all of the $PM_{2.5}$ TN is attributed to ammonium plus nitrate for all three sites and across the whole month of April. In other words, inorganic nitrogen (IN) dominated the $PM_{2.5}$ TN observed at the three sites in this study and only small amounts of ON were observed based on TN analysis at Fort Collins and RMNP locations, consistent with results reported in other literature. While Greeley did not exhibit evidence of ON, an assessment of percent error shows that trace amounts of ON are still potentially found in these samples. . Table 3 lists the ammonium to TN and nitrate to TN ratios for the three sites along with the percent errors. Ammonium accounted for approximately half of the TN and nitrate accounted for approximately one-third of the TN consistently during the month of April 2019 at Fort Collins. . Greeley and RMNP generally had higher contributions of ammonium to TN concentrations compared to Fort Collins. Nitrate contributions to TN concentrations were similar at Greeley and Fort Collins and smallest at RMNP.

Ammonium was highest in concentration at Greeley, as can be seen in Figure 5b. The trend remains the same for nitrate with the greatest concentration observed in Greeley and the smallest concentration observed in RMNP. Formation of ammonium nitrate involves the reaction of gas phase ammonia and gas-phase nitric acid. An assessment of gas-phase concentrations of both ammonia and nitric acid is offered further on in this section. Ammonium in $PM_{2.5}$ can also be associated with ammonium salts of sulfate or organic acids.

Table 3. The ratios of ammonium and nitrate to TN along with the associated percent error are shown in the table below for the different sites during the month of April. The RSD for the sum of ammonium and nitrate to TN is calculated from combining the individual errors of ammonium and nitrate.

		4/2/2019	4/9/2019	4/16/2019	4/23/2019	4/30/2019	% Error
$\dfrac{NH_4^+}{TN}$	CSU	0.65	0.50	0.56	0.51	0.52	
	GYM	0.61	n/a	0.71	0.76	0.71	6.8
	RMNP	0.84	0.57	1.03	0.61	0.62	
$\dfrac{NO_3^-}{TN}$	CSU	0.31	0.31	0.33	0.28	0.31	
	GYM	0.41	n/a	0.38	0.37	0.35	8.6
	RMNP	0.22	0.27	0.22	0.25	0.25	
$\dfrac{NH_4^+ + NO_3^-}{TN}$	CSU	0.96	0.81	0.89	0.79	0.83	11.3
	GYM	1.02	n/a	1.10	1.13	1.06	
	RMNP	1.06	0.75	1.25	0.87	0.88	

The spatial distribution of sulfate (Figure 6) follows the same trend as described above for ammonium and nitrate, with the greatest concentration observed in Greeley and smaller, fairly similar concentrations in Fort Collins and RMNP.
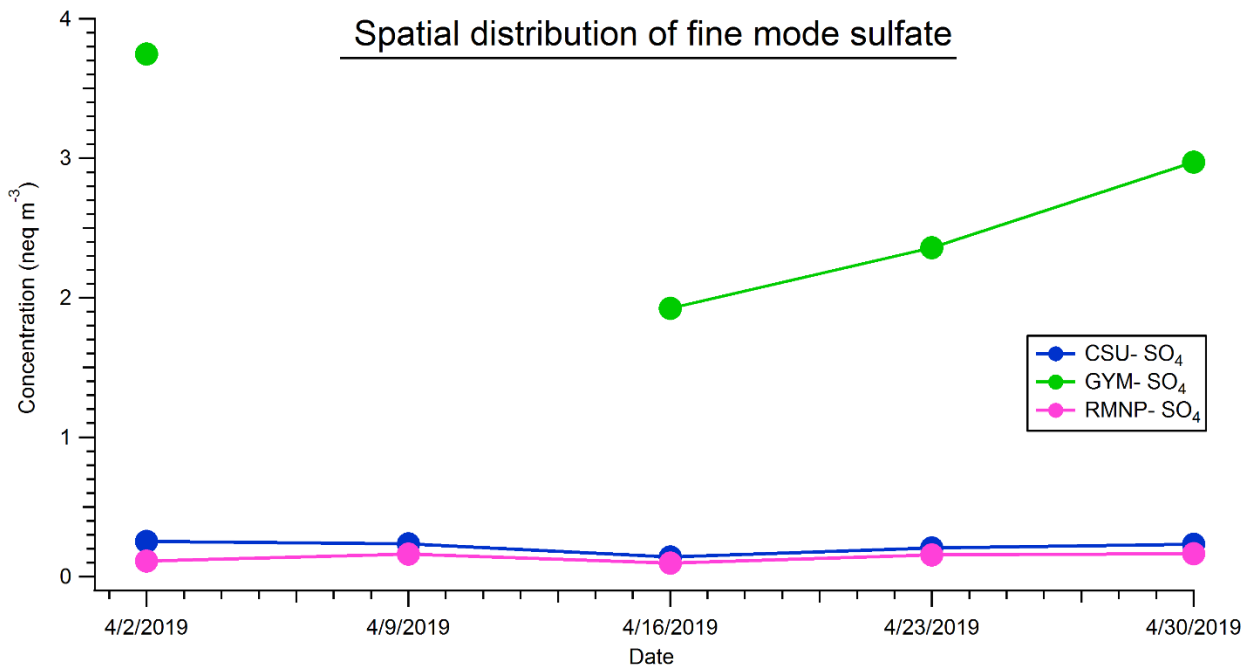
Figure 6. Spatial distribution of fine mode sulfate for Greeley, Fort Collins, and RMNP.

Although, in the case of sulfate, there is less of a clear spatial distribution trend as was observed for ammonium and nitrate.

While our main interest in this work lies in the nitrogen species present in the fine mode aerosol, it is important to consider the gas phase species that participate in gas-particle partitioning reactions. In Figure 7 particulate ammonium and gaseous ammonia (a) and particulate nitrate and gaseous nitric acid (b) concentrations are shown for the three measurement sites. Together gaseous ammonia and $PM_{2.5}$ ammonium comprise N(-III), nitrogen in the -3 oxidation state. There were higher gaseous ammonia concentrations in Greeley, reflecting its proximity to agricultural ammonia sources. The difference in the ammonium concentrations across the three sampling sites was smaller than the difference in ammonia concentrations at each site. Gas phase ammonia is removed relatively quickly from the atmosphere through dry deposition and chemical reaction while fine mode particulate ammonium can be transported longer distance to relatively remote locations.   Particulate nitrate is in greater concentration relative to gaseous nitric acid at all three measurement sites and shows similar differences between gas and particle species for each site. Greeley shows the greatest average concentrations of both gas and particle phase N(V) (nitrogen in the +5 oxidation state: nitrate plus nitric acid) while RMNP shows the smallest concentrations of both phases. This is to be expected given the large amount of emission sources near the Greeley site and minimal amount of emission sources near the RMNP site.
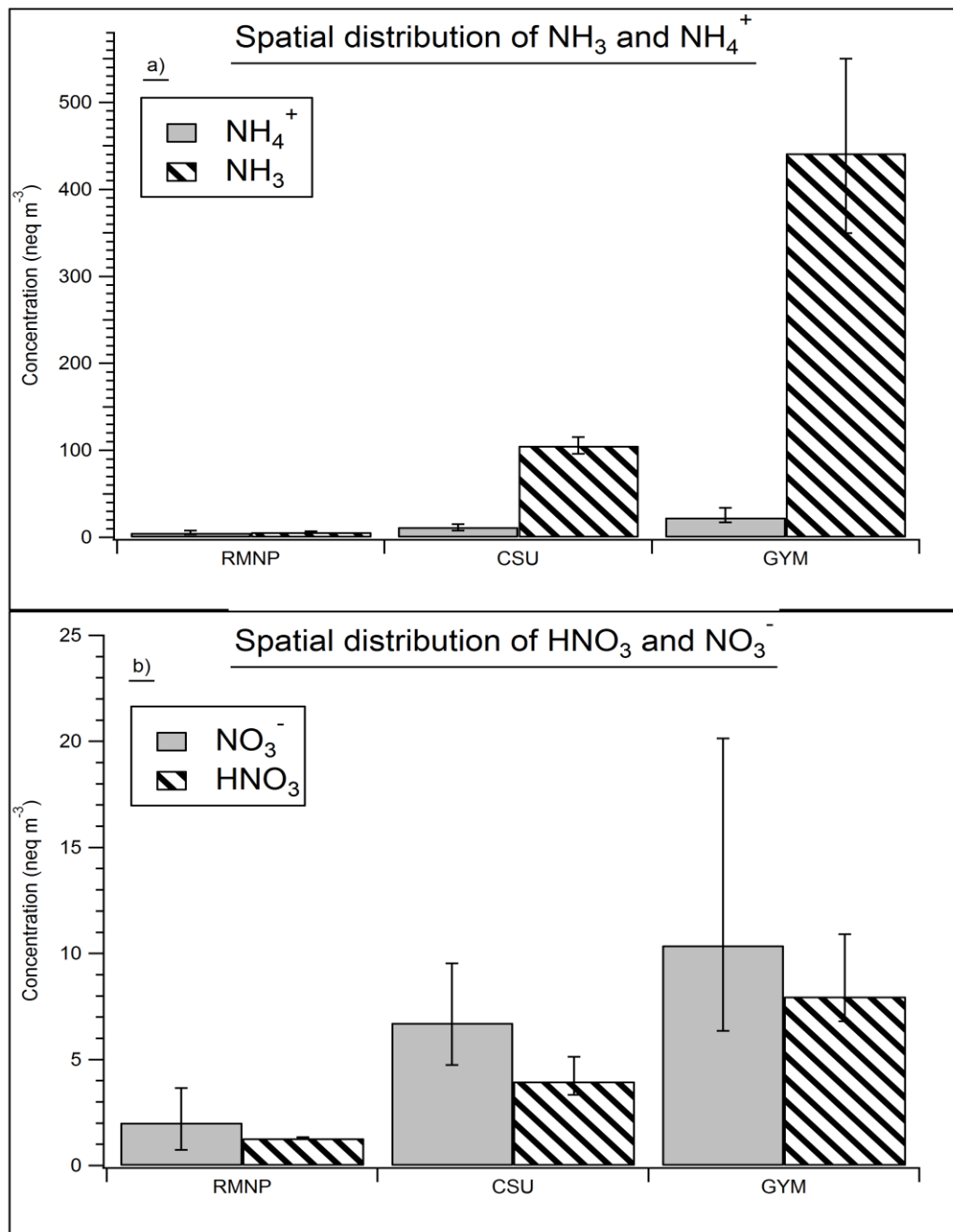
Figure 7. Gas and particle phase concentrations are shown for N(-III) and N(V).

3.2 Organic nitrogen spatial distributions

In the TN analysis we looked at the contributions of ammonium and nitrate to TN but

the organic nitrogen content of the fine mode aerosol at these three sites was not addressed.

Using the TN measurement and inorganic N species, there is evidence of organic nitrogen in samples collected at Fort Collins and RMNP and no evidence of ON at Greeley. However, using the amine IC method described in the methods section we were able to detect some amines at all three sites. On average the contribution of all quantified amines to TN was 0.97 % at RMNP, 1.4 % at Fort Collins, and 1.1 % at Greeley.

Figure 8 show plots of methylamine (a), dimethylamine (b), and trimethylamine (c) spatial distributions. Methylamines showed the same general trend as ammonium with the highest concentrations generally occurring in Greeley. With the exception of dimethylamine, RMNP had the lowest concentration of methylamines. In the case of dimethylamine, Fort Collins and RMNP were observed to have nearly identical concentrations with little variation throughout the month (Figure 8b). Concentrations of dimethylamine in Fort Collins and RMNP generally were not detected above the MDL and were, therefore, replaced with half the MDL. Trimethylamine was observed to be very low in concentration yet was still found above the limit of detection for all three sites with the exception of the sample collected in RMNP on 4/30/2019 that was slightly below the MDL. As can be seen from Figure 8c, trimethylamine exhibited a similar trend on 4/23/2019, as previously seen for ammonium, when Greeley and Fort Collins showed similar concentrations. The most concentrated day for Greeley for both ammonium and the three methylamines occurred on 4/2/2019. The most concentrated day for ammonium in Fort Collins and RMNP occurred on 4/9/2019. Greeley and Fort Collins showed the highest methylamine, dimethylamine, and trimethylamine concentrations on 4/2/2019. Trimethylamine concentrations were also highest at RMNP on this date.
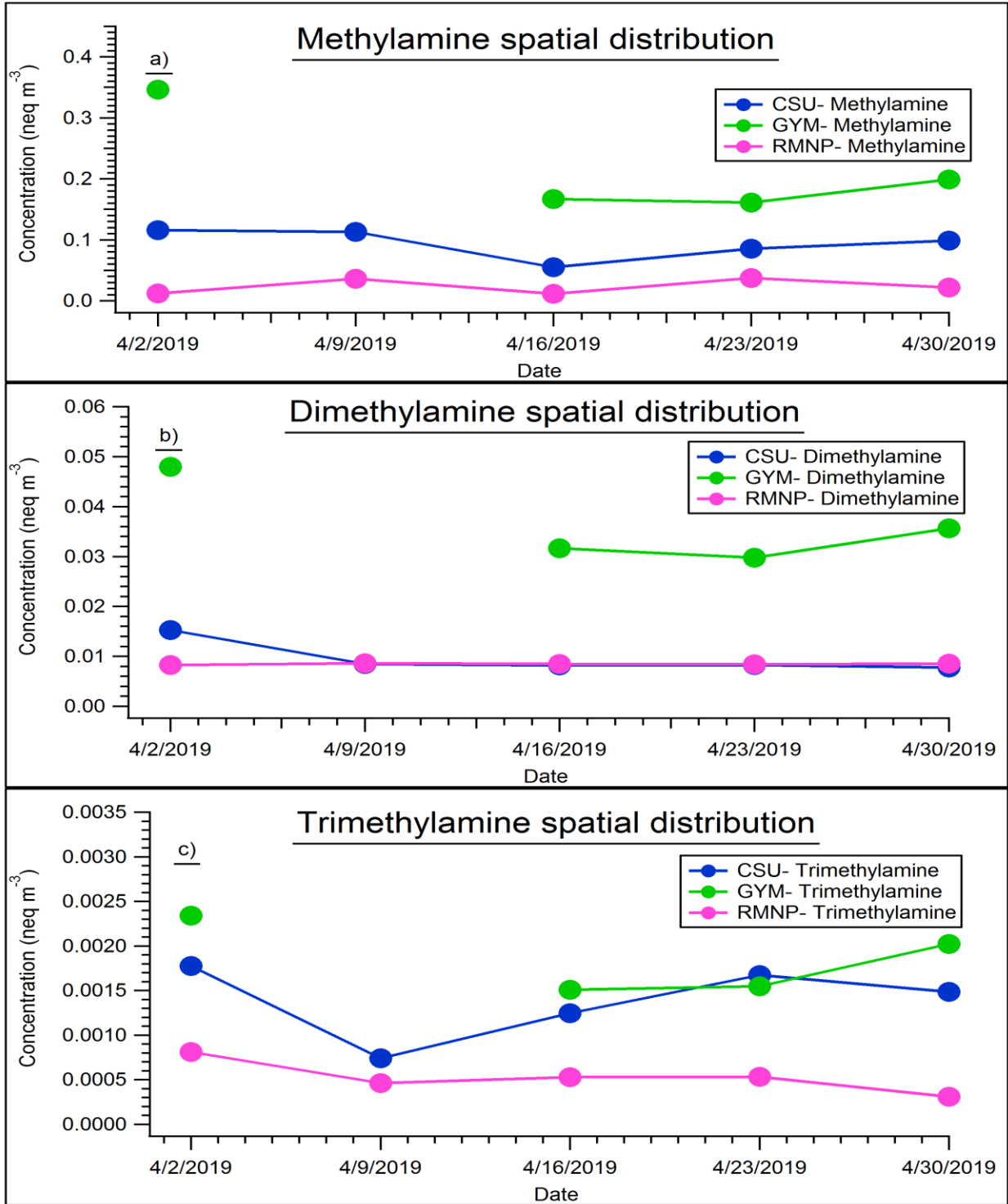
Figure 8. Methylamine (a), dimethylamine (b), and trimethylamine (c) spatial concentration distributions are shown for the month of April 2019.

In addition to the methylamines, plots of other amines are presented in Figure 9. Due to the lack of variation in methylamine concentrations over time (i.e. throughout the sampling month), the time-weighted average concentration was calculated for the entire month and plotted for each site to evaluate spatial variation across sites rather than changes in time. The error bars describe the variability across the sampling period and represent the maximum and minimum concentrations observed at each site. The concentrations observed for allylamine (Figure 9a) were very small across all sites and were often below the detection limit for RMNP and Fort Collins. The highest concentrations were observed in Greeley. Dipropylamine (Figure 9b) also showed little evident variation between the different sampling dates and concentrations were found to be highest in Greeley and below the detection limit for RMNP and Fort Collins. In contrast to the other amines shown, iso-butylamine (Figure 9c) concentrations between Fort Collins and Greeley are very similar, possibly suggesting similar sources in the two locations.   RMNP exhibited much lower concentrations of iso-butylamine, consistent with fewer local sources and dilution, oxidation, and/or deposition reducing concentrations during transport from the Front Range.
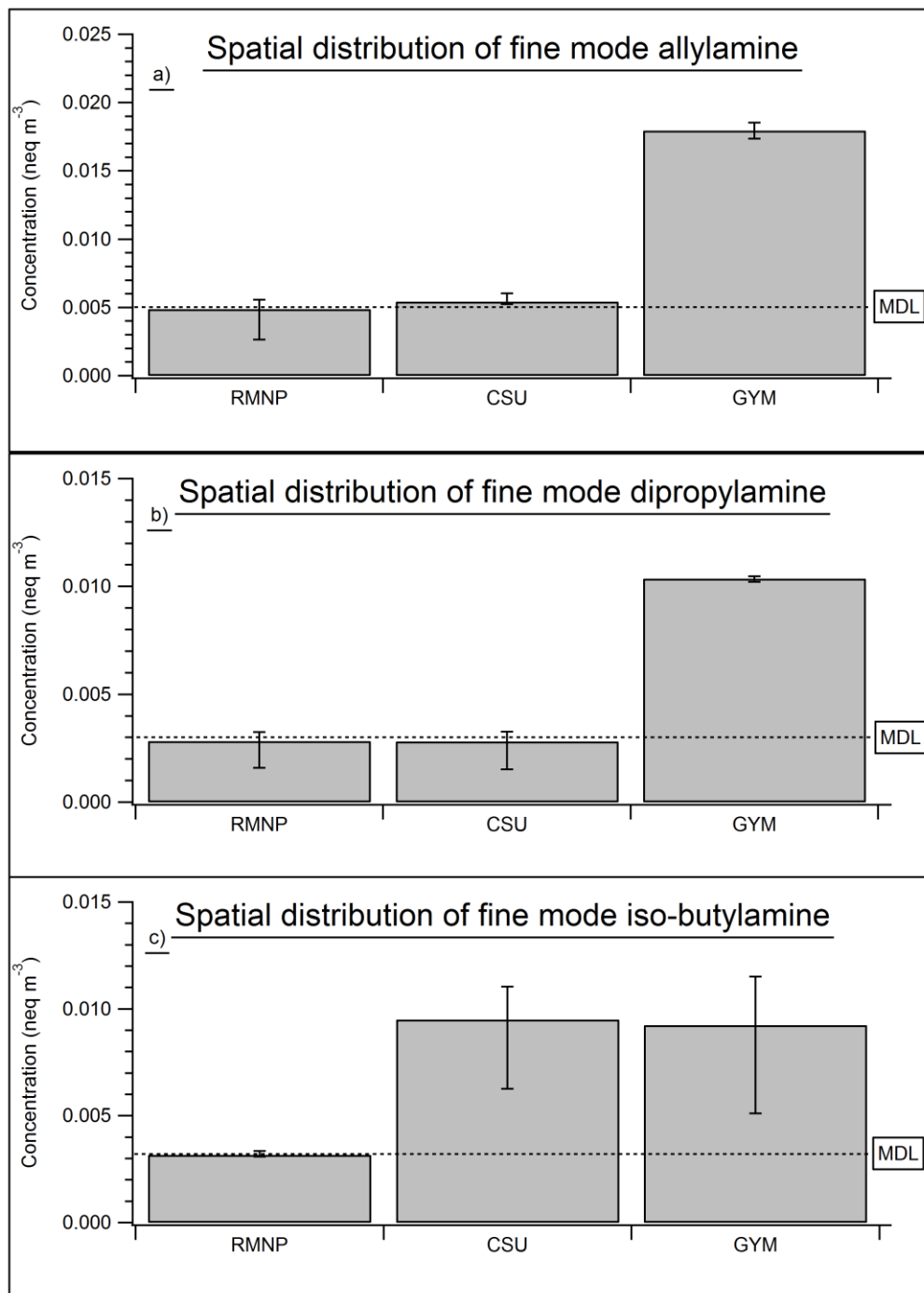
Figure 9. Spatial distributions for allylamine (a), dipropylamine (b) and iso-butylamine (c) are shown above.

Animal husbandry is a known source of amines but other source types can contribute to amine emissions, including iso-butylamine and dipropylamine from tobacco smoke and from agricultural sources. Some amines, such as amylamine, can be emitted from the beer fermentation and grain-drying processes; the beer industry has a large impact in Northern Colorado, particularly in Fort Collins. In contrast to the other amines shown here, the amylamine spatial distribution (Figure 10) shows consistently higher concentrations in Fort Collins. RMNP still shows the lowest concentrations overall, but Greeley concentrations are not much higher. The highest concentration was observed in Fort Collins on 4/23/2019.
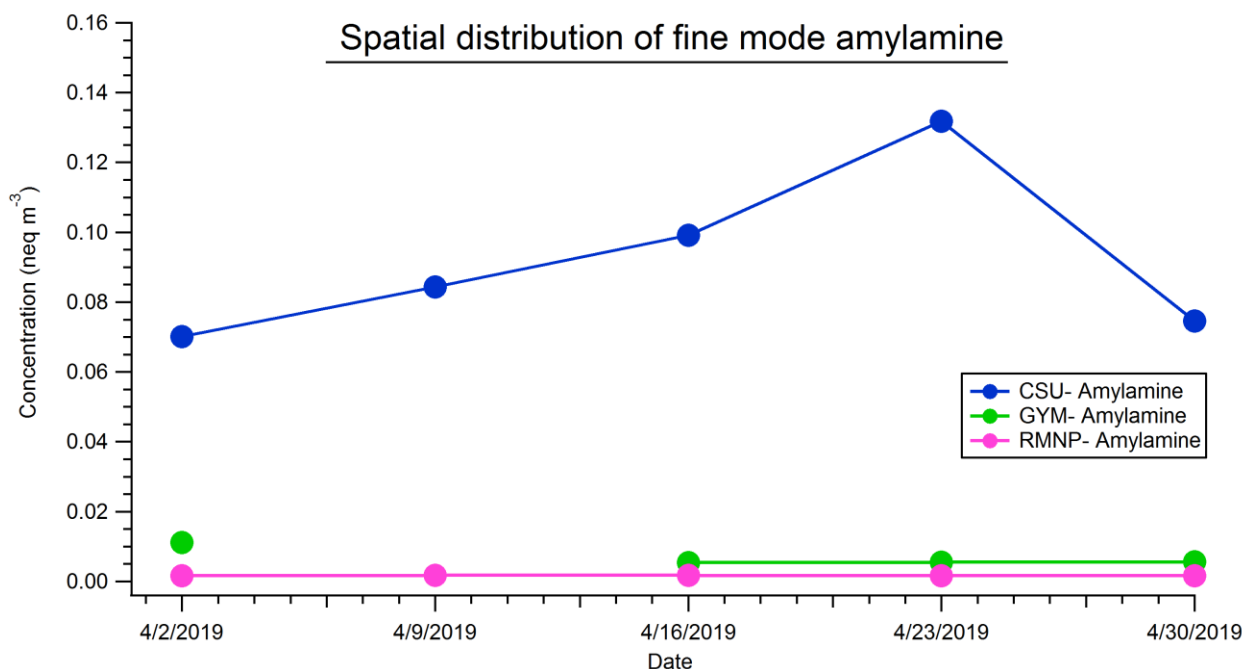
Figure 10. Spatial distribution of fine mode amylamine for Greeley (GYM), Fort Collins (CSU), and RMNP is shown above.

3.3 MOUDI size distributions

Size distribution measurements were made in August, 2018 and January, 2019. Plots of ammonium, nitrate, sulfate, oxalate, and various amines are shown in this section to illustrate

their size distributions. The plots also illustrate the Twomey inversion as it compares to the raw

MOUDI stage concentration data. The Twomey algorithm smooths and allows for more

accurate representation of particle species' size distribution data by taking MOUDI stage

collection efficiencies into consideration. The smooth lines (beginning with Figure 11) show the

inverted data from the adapted Twomey algorithm while the bars show the measured

concentrations for each MOUDI collection stage.

Figure 11 shows the size distribution data for ammonium (a), nitrate (b), and sulfate (c)

on 8/24/2018.   In all three cases, the Twomey fit represents the data well, even when coarse

aerosol is the dominant mode, as observed for nitrate. Nitrate is present in the coarse mode

during the summer sampling periods likely in the form of mineral nitrate salts. Magnesium and

calcium data supports the formation of soil dust-derived nitrate salts with peaks for these

species in the coarse mode overlapping the coarse mode nitrate peak. A smaller submicron

nitrate mode, presumably ammonium nitrate, is also observed. Ammonium nitrate is typically

not very abundant in the summertime atmosphere due to the tendency for ammonium nitrate

to dissociate and return ammonia and nitric acid to the gas phase under high temperature

conditions. The sulfate size distribution for this summer sampling period shows a commonly

observed submicron mode for this species, but also indicated the ability of the inversion to

identify a potential sulfate droplet mode (reflecting aqueous sulfate production in cloud drops)

around 1 to 2 microns. A small sulfate coarse mode is also apparent. The ammonium

distribution is dominated by a fine particle, submicron mode, where ammonium appears to be

paired with sulfate and some nitrate. A small droplet mode is also apparent for ammonium,

likely reflecting its pairing with sulfate in this size range.
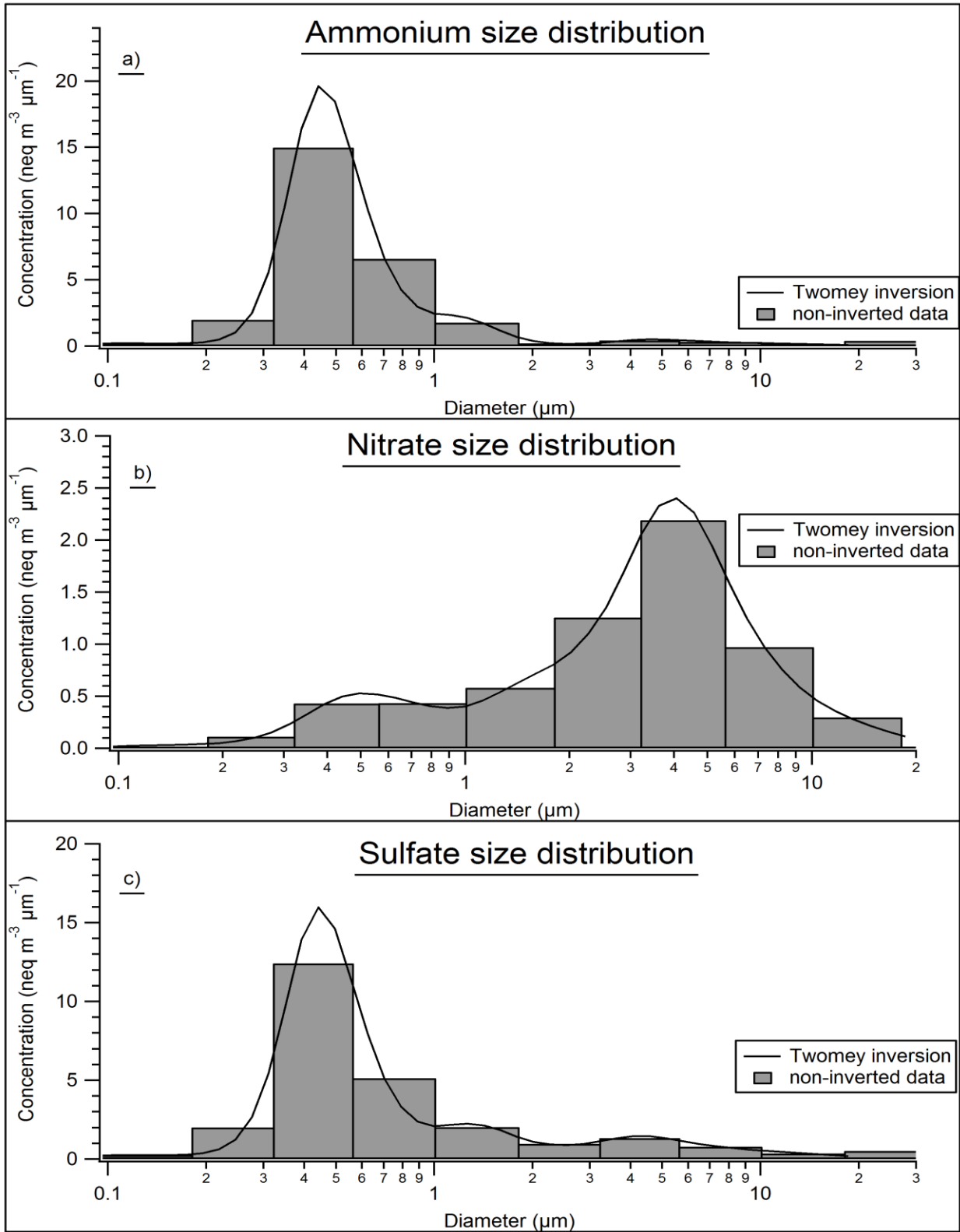
Figure 11. A comparison between ammonium (a), nitrate (b), and sulfate (c) is shown above for the sample collected on

8/24/2018.

Evidence of a droplet mode was not only found for sulfate but for oxalate as well, although oxalate (like sulfate) was primarily present in a submicron aerosol mode. An example of this droplet mode is shown in Figure 12. Interestingly, other organic acids, including acetate and succinate, also show some evidence of a droplet mode during the summer sampling periods, although this mode was not as clearly defined as observed for sulfate and oxalate. Generally, a droplet mode is more prevalent during periods of higher humidity and is largely found to be an effect of aqueous-phase chemistry (Hering and Friedlander, 1982; Meng and Seinfeld, 2007; Wang et al., 2012). During these periods of greater humidity and/or cloud presence, constituents in the atmosphere under-go aqueous phase chemistry and produce new particles that are larger and of different composition than would otherwise occur with a dry particle. The sampling periods of 8/17/18, 8/21/18 and 8/24/18 suggest aqueous processing.
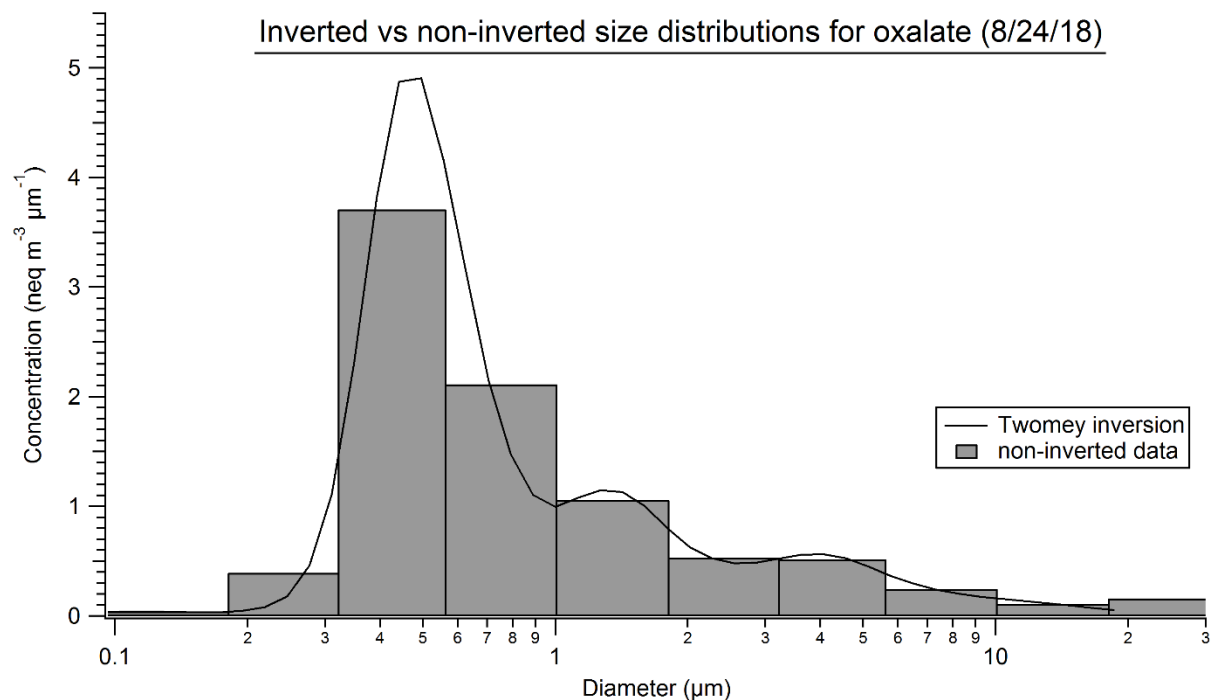
Figure 12. Non-inverted data compared to the Twomey inversion is shown for oxalate during the 8/24/18 sampling period. Evidence of droplet mode occurs here.

40

The summertime nitrate for the period of 8/17/19 shows a peak in the general droplet mode range. Typically, evidence of a droplet mode is found by a small bump riding on the dominant fine mode peak; yet, nitrate, during the 8/17/19 period, shows a very definitive peak for fine mode (peak max = 0.6 µm), droplet mode (peak max = 1.6 µm), and coarse mode (peak max = 4.3 µm). However, a comparison to raw data shows that this peak is likely an artifact caused by the Twomey inversion.
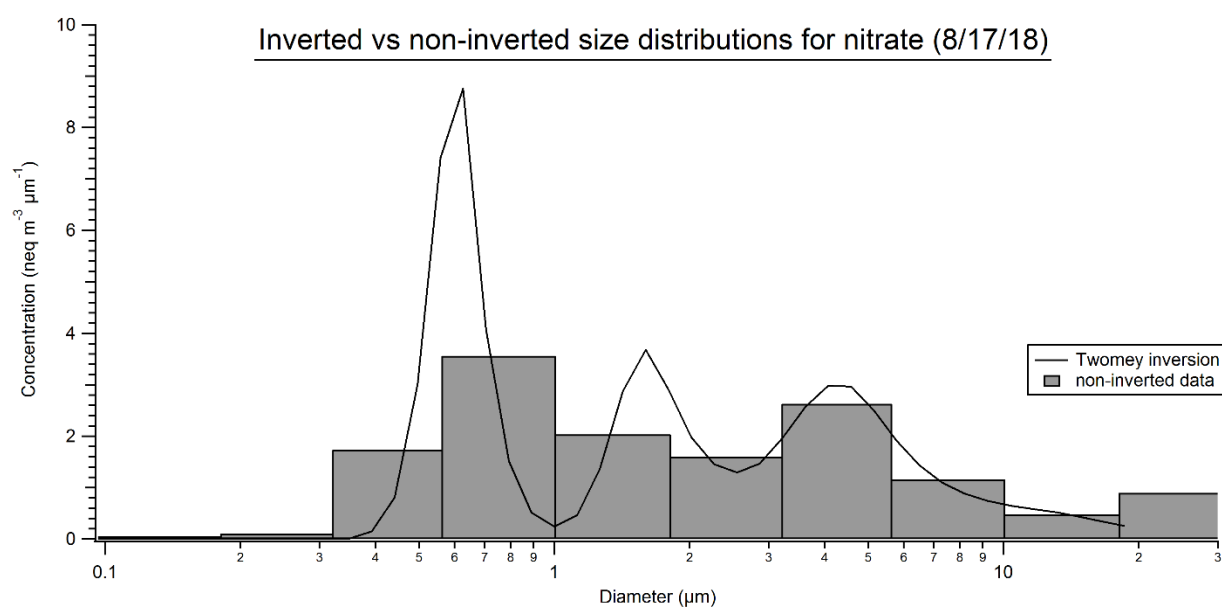
Figure 13. An artifact caused by the Twomey inversion is shown in the nitrate sample during 8/17/19. The peak at 1.6 um is not an actual evidenced droplet mode as can be seen by the raw data.

In addition to inorganic ions and organic acids, the Twomey inversion was fitted to the MOUDI measurements of amine data. Figure 14 shows size distributions for methylamine (a), dimethylamine (b), and trimethylamine (c) for the sample collected on 1/15/19. Trimethylamine and dimethylamine both show size distribution peaks around 0.4 µm, but methylamine shows a broader maximum around 0.55 µm, suggesting other processes driving formation of larger

particle sizes. While trimethylamine is dominant in the fine mode, there is some suggestion of trimethylamine existing in the coarse mode, as well, in very small concentrations.

Amines were observed to be present primarily in the fine mode with most of the mass in all samples falling between 0.2 and 1 μm. Generally, the amines that were measured in greater concentrations in the fine mode consistently above the MDL were trimethylamine, dimethylamine, and methylamine. There is almost no evidence of coarse mode amines and some of the amines measured were not clearly observed in the fine or coarse mode for either season, suggesting concentrations of these are insignificant. Amine coarse mode peaks are difficult to ascertain because much of the coarse mode data is masked by the effect of the treatment of values that fall below the MDL. When data points were found to be below the MDL, then the data was replaced with half of the value of the MDL causing difficulty in ascertaining the coarse mode distributions for these three amines. Table 4 shows a more complete list of amines that were and were not detected above the MDL. Several amines were only slightly above the MDL and are indicated as such in the table. For example, amylamine, even when detected, the concentration was only just above the MDL causing greater uncertainty in the peak maxima. Overall, the winter showed negligible concentrations of most amines with the exception of the methylamines.

Table 4. A list of the amines that were or were not detected is shown here for summer and winter seasons. Amines that were detected slightly above the MDL are indicated with the word, "slight." Amines that were and were not detected above the MDL are indicated with a Yes or No, respectively.

Amines	Summer (2018)	Winter (2019)
Propylamine	No	No
Dipropylamine	No	No
Ethanolamine	No	No
Diethanolamine	No	No

1,4-diaminobutane	No	No
Tert-butylamine	No	No
Sec-butylamine	Slight	No
Triethylamine	Slight	No
butylamine	Slight	No
Allylamine	Slight	No
Diethylamine	Slight	No
Iso-butylamine	Slight	Slight
Amylamine	Slight	Slight
Trimethylamine	Yes	Yes
Dimethylamine	Yes	Yes
methylamine	Yes	Yes
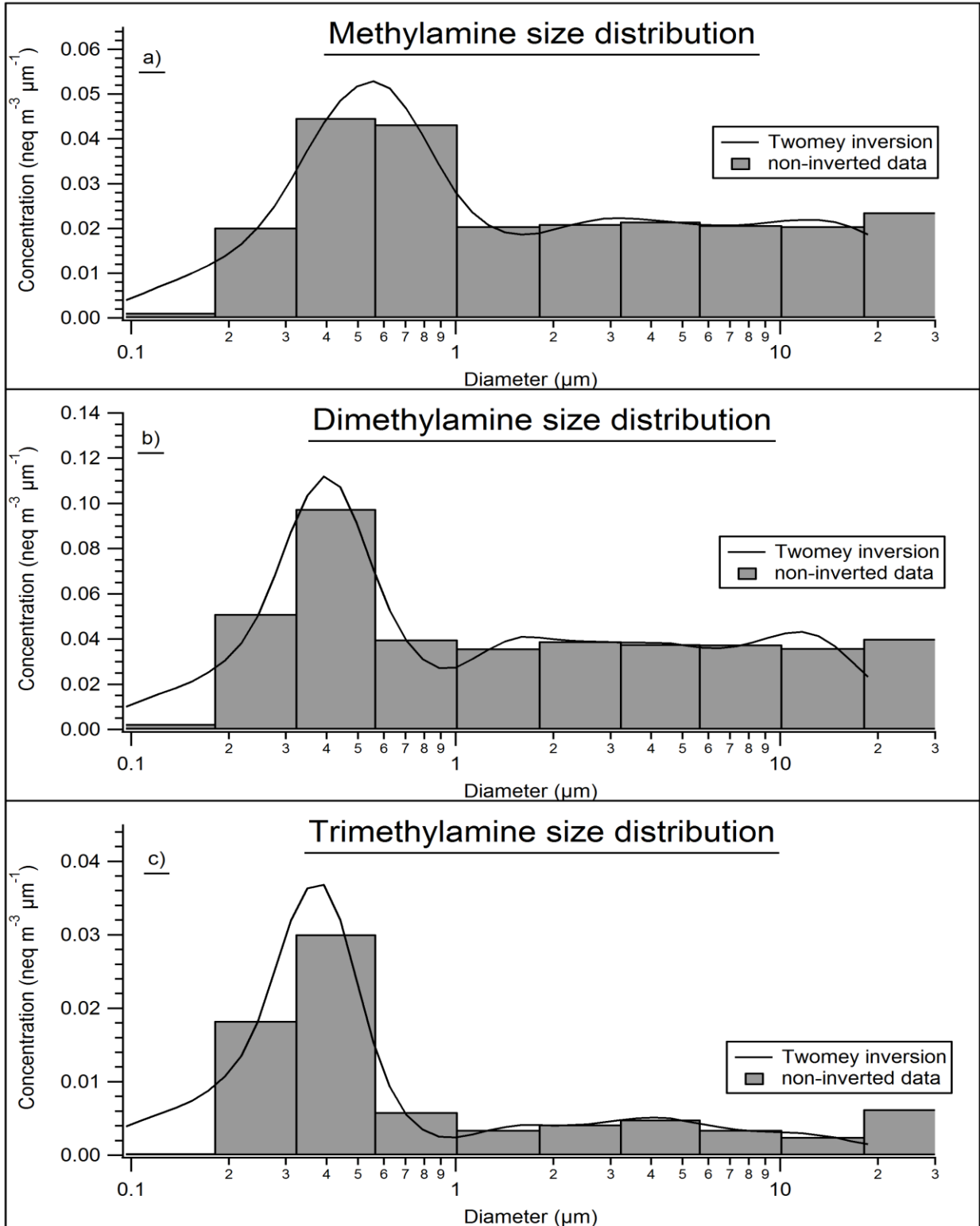
Figure 14. Size distributions for methylamine (a), dimethylamine (b), and trimethylamine (c) are shown above for the

1/15/19 sampling period.

3.4 Size distribution ionic comparison

In previous work, there are often indications that excess ammonium, above what is needed for neutralization of sulfate, is attributed to ammonium nitrate. In the winter samples presented here, ammonium neutralizes both sulfate and nitrate completely. Figure 15 shows the ammonium observed during the 1/15/19 period was in slight excess to nitrate and sulfate combined.   Some of the "excess" ammonium could be associated with oxalate or succinate, both of which were found in small concentrations. Note, also, the presence of a dominant find mode of ammonium nitrate in this winter sample, in strong contrast to the coarse mode nitrate that dominated the summer sample discussed above. Ammonium nitrate formation is often thermodynamically favored under wintertime conditions. The distribution maximum of sulfate occurs at 0.45 μm while the maxima for ammonium and nitrate occur at ~0.32 μm. The size difference between nitrate and sulfate size distributions is not unusual and reflects different origins for these species in the atmosphere. Note the absence of any significant coarse particle mode for either nitrate or sulfate in this winter sample.
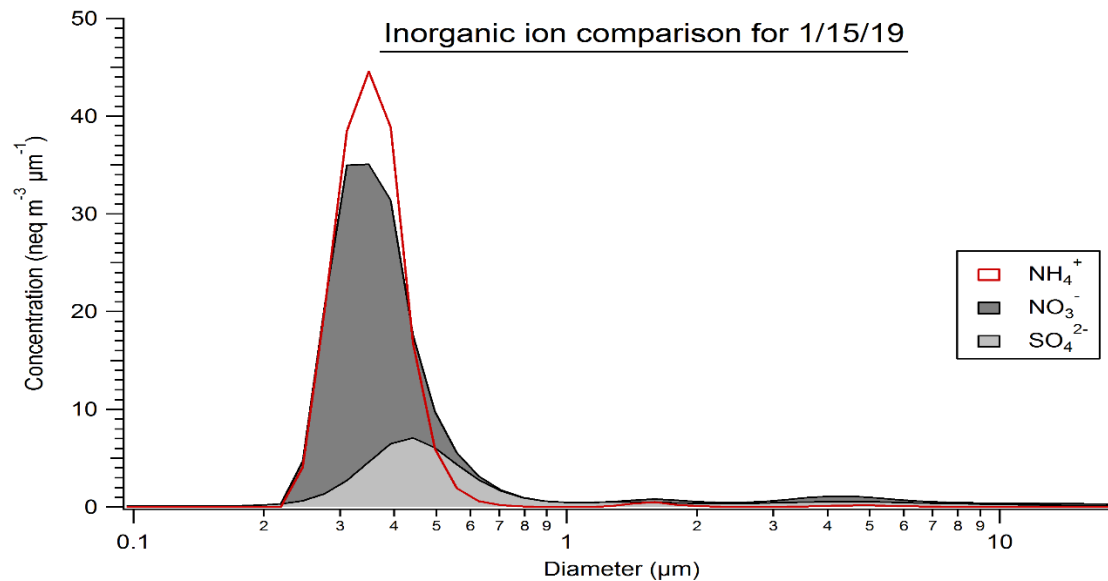
Figure 15. Equivalents of ammonium are compared to the sum of nitrate and sulfate equivalents and ammonium was observed to be plentiful to neutralize both nitrate and sulfate.

A second winter particle size distribution example is shown for the sampling period of 1/25/19 in Figure 16. During this period, the concentration of ammonium was almost exactly equivalent to the sum of nitrate and sulfate concentrations in the fine mode range. Once again, no significant coarse mode is present for either nitrate or sulfate.
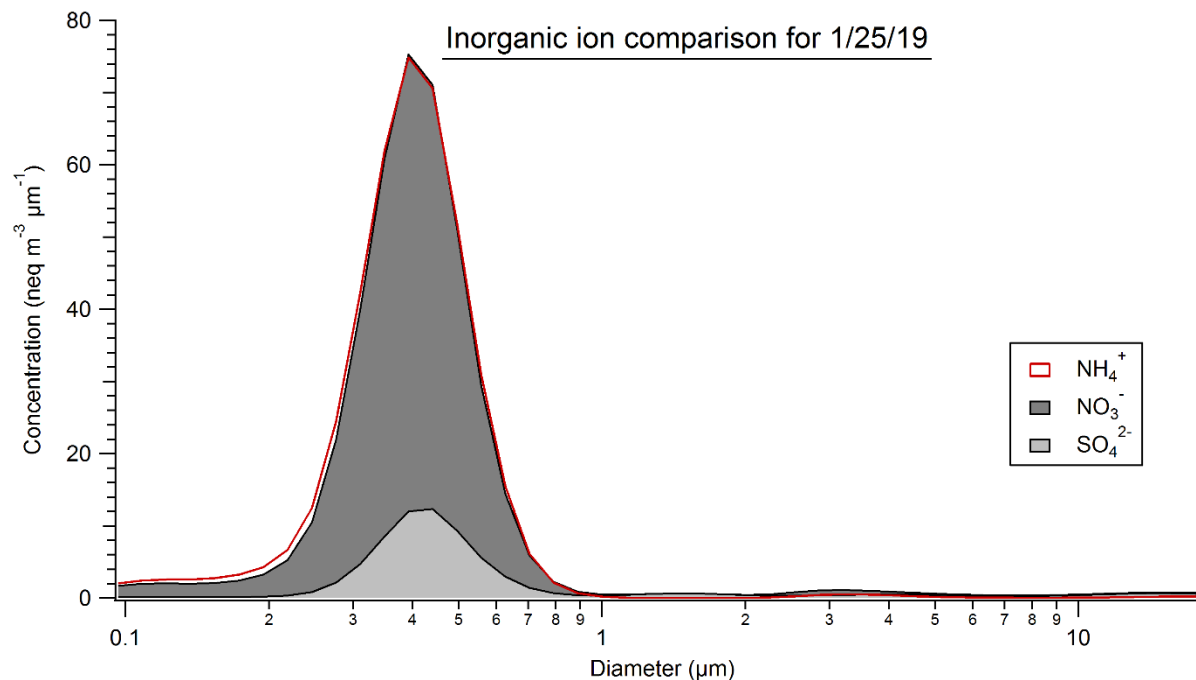
Figure 16. Winter sampling periods show almost exact neutralization of sulfate and nitrate by ammonium in the fine mode.

Summer sampling periods (eg., the 8/24/2019 sample shown in Figure 17a) show ammonium to be in excess, relative to the sum of sulfate and nitrate, in the fine mode and to be deficient in the coarse mode. Excess fine mode ammonium here has likely reacted with organic acids (see Figure 12 for the presence of fine mode oxalate in this sample). Sulfate in the summer time exhibits evidence of a droplet mode that is formed during periods of higher relative humidity (RH). The neutralization of sulfate in the droplet mode by ammonium is evidenced by ammonium present in the droplet mode range. Ammonium displays a droplet mode peak that overlaps the droplet mode of sulfate (Figure 17a). The deficiency of ammonium in the coarse mode occurs because nitrate and sulfate here are typically paired with mineral cations (Figure 17b) as a result of reaction with coarse particle soil dust. Figure 18 confirms the correlation between coarse nitrate plus coarse sulfate and coarse magnesium and coarse calcium. Calcium and magnesium are known mineral cations found in soil dust.
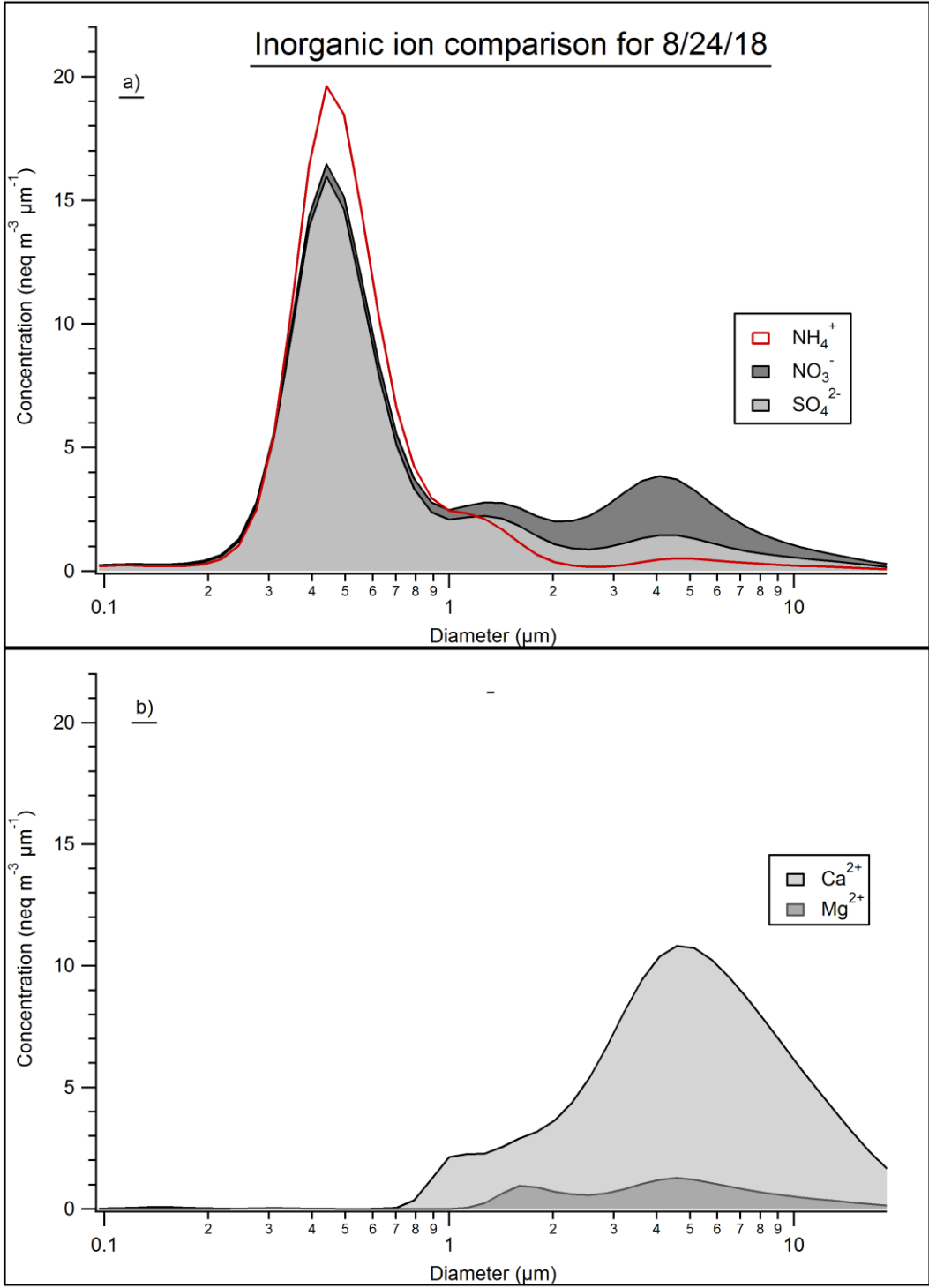
Figure 17. Summer sampling periods for 8/24/2019 (a) show ammonium to be in excess in the fine mode, as was the case in the winter. However, there is now presence of coarse nitrate and sulfate that are in the form of salts with mineral cations (b) rather than ammonium. Nitrate and sulfate are stacked to show comparison to ammonium and calcium and magnesium are stacked to show comparison to coarse nitrate and sulfate.
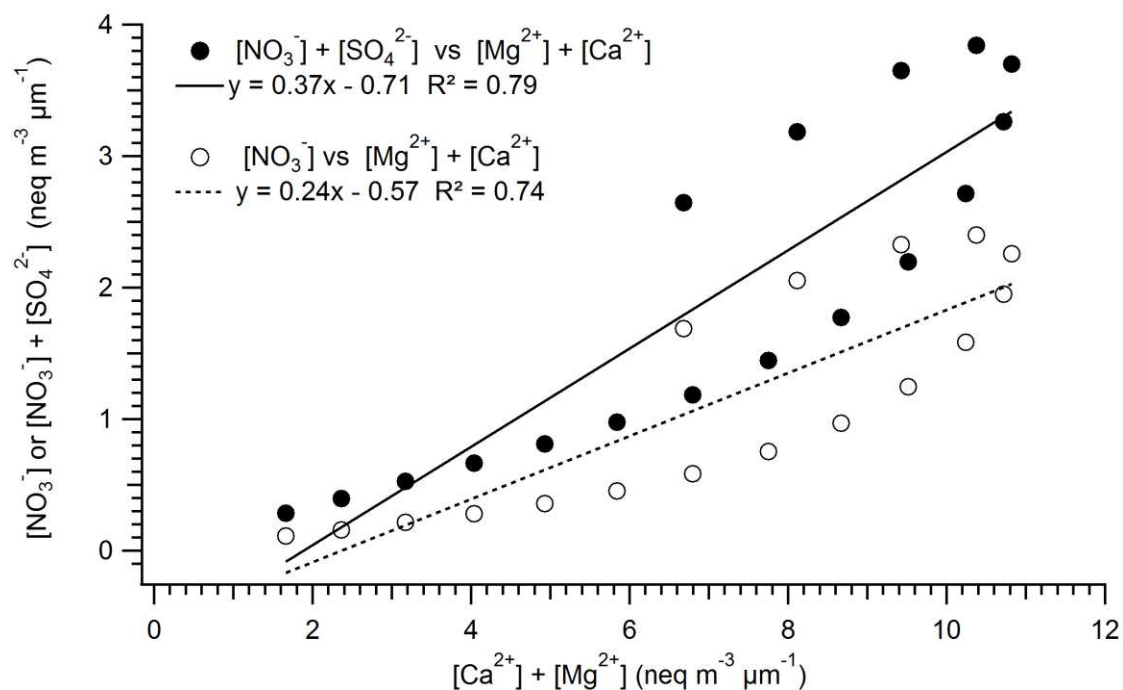
Figure 18. A correlation was observed between coarse nitrate and coarse sulfate vs coarse magnesium and coarse calcium for the 8/24/2019 sample.

3.5 Seasonal trends

Concentrations of inorganic nitrogen in PM were found to be smaller during the summer season compared to the winter. Figure 19 shows the summer and winter concentrations for ammonium. Interestingly, the particle sizes corresponding with the peak maxima are typically larger for the summer season. The largest particle maxima occurred when the RH was also found to be high during the midday. Since the particles were not dried prior to entry into the MOUDI impactor, these size distribution shifts likely reflect hygroscopic aerosol particle growth.

Higher temperatures during the summer can explain the greater ammonium concentrations observed for the winter. While ammonia emissions increase at warmer

temperatures in the summer, most of the ammonia under these conditions is found in the gas

phase due to the semi-volatile nature of ammonium nitrate.
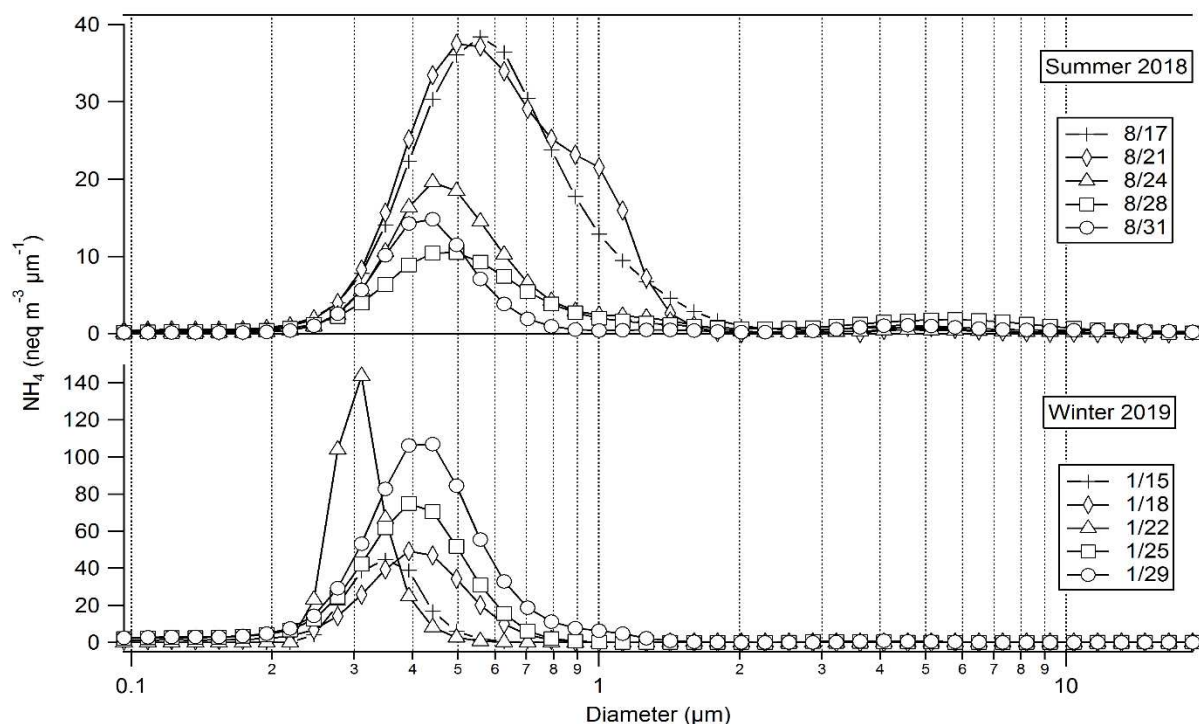
Figure 19. A seasonal comparison for the size distribution of ammonium is shown above. Summer showed smaller concentrations and larger maximum particle size compared to winter sampling.

A larger particle diameter maximum during the summertime compared to wintertime

was a consistent trend for all measured species; however, a greater concentration during the

winter was not always observed for all measured species. For example, dimethylamine and

trimethylamine were observed at greater concentrations during the summer season but

methylamine showed greater average concentrations in the winter. Figure 20, Figure 21, and

Figure 22 show methylamine, dimethylamine, and trimethylamine seasonal trends. In all cases,

the peak maxima occur at larger particle sizes during the summertime, likely an effect of higher

RH and associated particle hygroscopic growth.
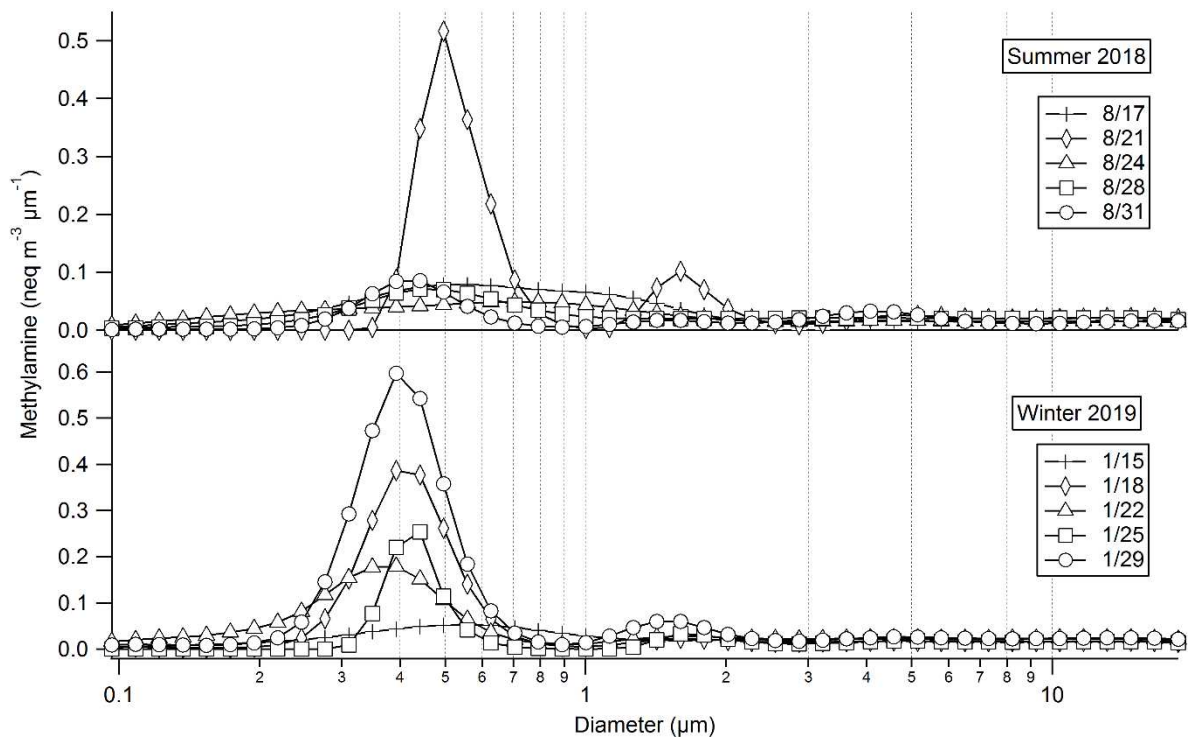
Figure 20. A seasonal comparison for the size distribution of methylamine is shown above. Methylamine is the only amine that shows the same trend as inorganic nitrogen with greater concentrations occurring in the wintertime.
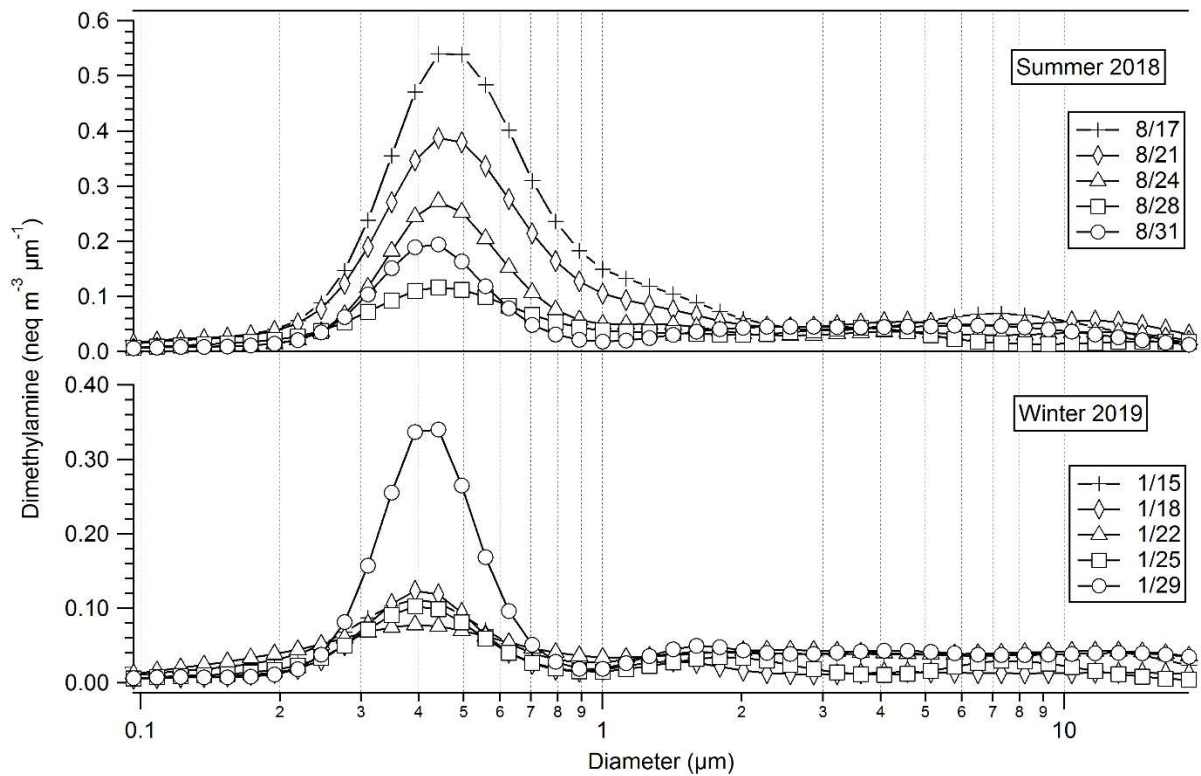
Figure 21. A seasonal comparison for the size distribution of dimethylamine is shown above. Dimethylamine differs from methylamine as the greatest average concentration occurs in the summertime.
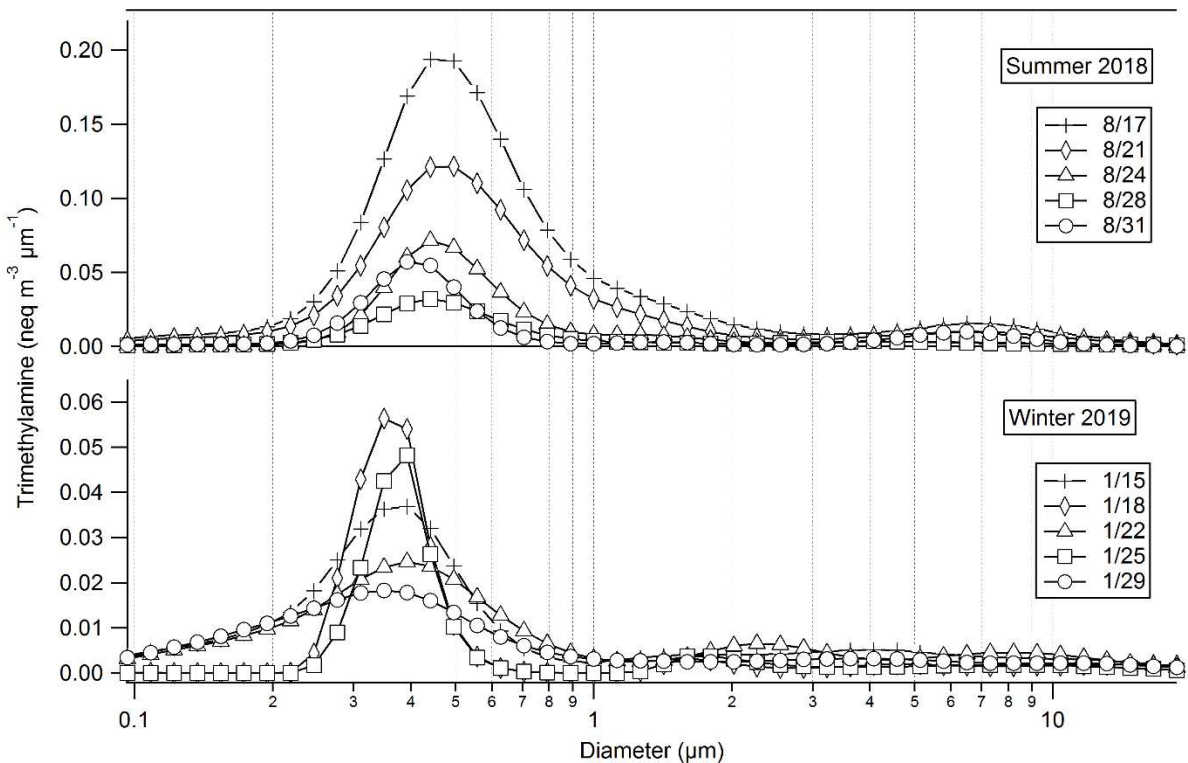
Figure 22. A seasonal comparison for the size distribution of trimethylamine is shown above. Trimethylamine is observed to be in greater concentration during the summertime in contrast to inorganic nitrogen.

Seasonal trends for OA were also analyzed. These species were almost exclusively found in the fine mode during both the summer and winter sampling. However, formate, oxalate, malonate and acetate were observed to have small amounts in the droplet mode around 1 μm during the summertime. These species are known products of aqueous phase atmospheric chemistry (Sullivan et al., 2016). Of the OA species measured many were found to be at or less than 1 neq m^{-3} μm^{-1} total mass. These include propionate, butyrate, MSA, pyruvate, cis-pinonate, valerate, glyoxalate, maleate, and phthalate. Figure 23 shows the seasonal trends for one of the more abundant species, oxalate. As to be expected, a larger peak maximum in the fine mode occurs during the summer sampling periods when

photochemistry is more active and oxalic acid production should increase. Greater oxalate

concentrations in the summertime may also reflect seasonal sources such as bacterial and

metabolic processes in vegetation and soil that are enhanced during periods of increased

agricultural activity, as well as, biomass burning. There is high variability in the coarse mode

range for oxalate that is likely an artifact caused by the interpretation of data below the

detection limit. There is little strong evidence here of any significant coarse mode oxalate.
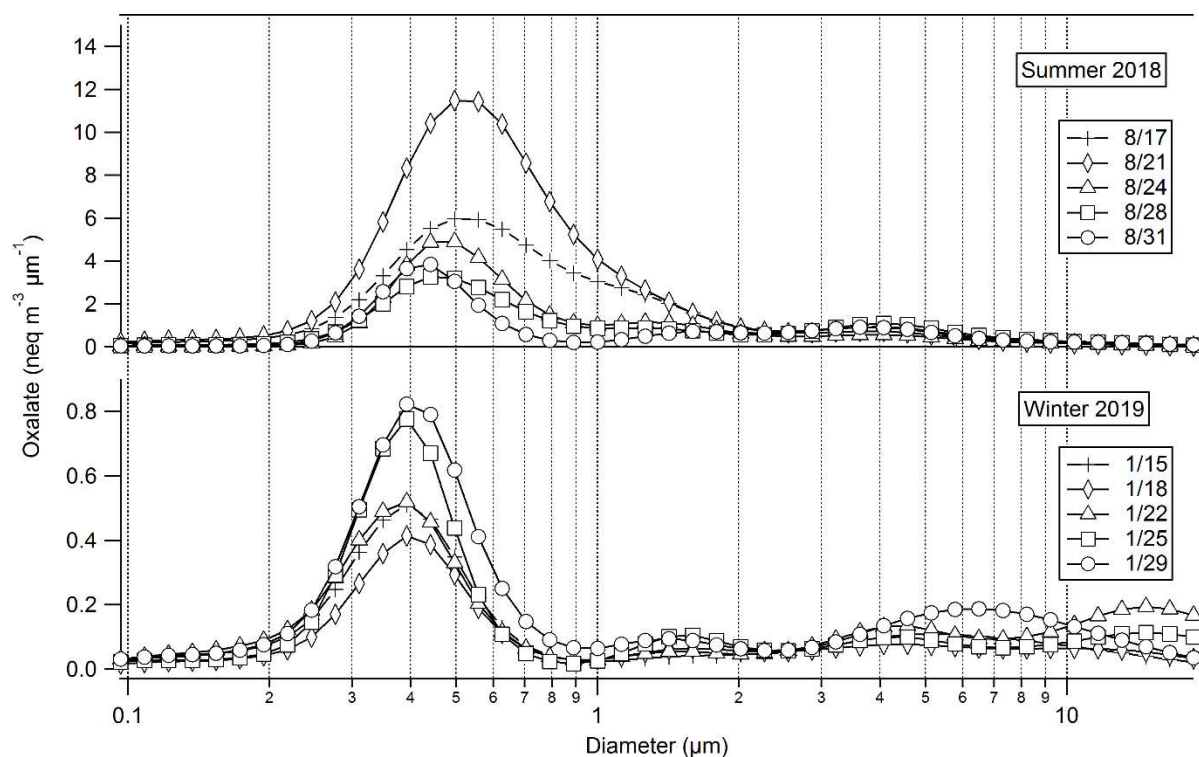
Figure 23. Seasonal trends for oxalate are shown above. The summertime saw greater concentrations of oxalate compared to winter. Coarse mode variability is likely an artifact of the code caused by the MDL.

Figure 24 and Figure 25 show the seasonal trends for nitrate and sulfate. As discussed

earlier, coarse mode nitrate and sulfate are greater in the summertime and are likely correlated

with calcium and magnesium (see Figure 17). During the summer there is almost no fine mode

nitrate on several days. A lack of fine mode nitrate is consistent with warmer temperatures

pushing the ammonia-nitric acid-ammonium nitrate gas-particle equilibrium towards the gas

phase. Two samples in the summer (8/17/2019 and 8/21/2019) show increased particulate

nitrate that is likely an effect of higher humidity during these periods. Higher RH values

increase the equilibrium constant for ammonium nitrate formation.

Sulfate was observed to have similar concentrations between the summer and winter

sampling periods. When day-time humidity was increased, as was the case during the 8/17/18

and 8/21/18 samples, there was greater evidence of sulfate in a droplet mode at approximately

1.3 µm.
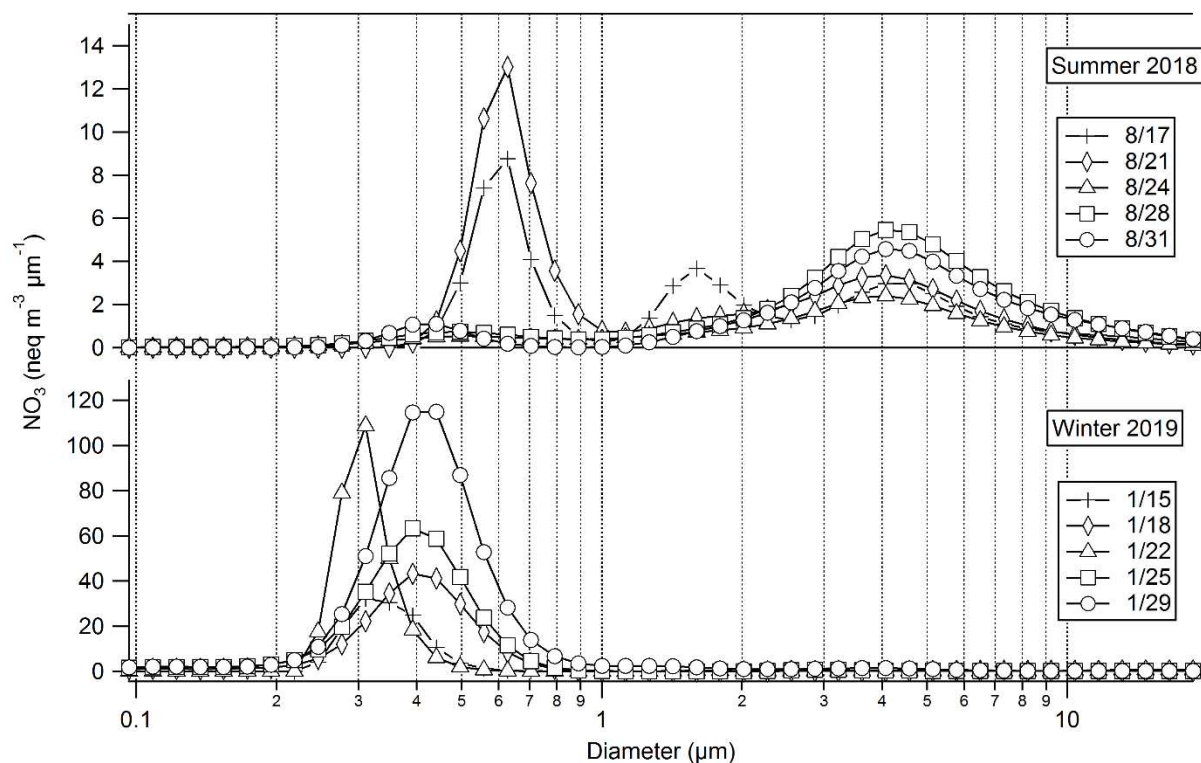
Figure 24. A seasonal comparison for the size distribution of nitrate is shown above. Similar to ammonium, the greatest

concentrations in fine mode occurred during the winter and the peak maximums were associated with larger particle sizes
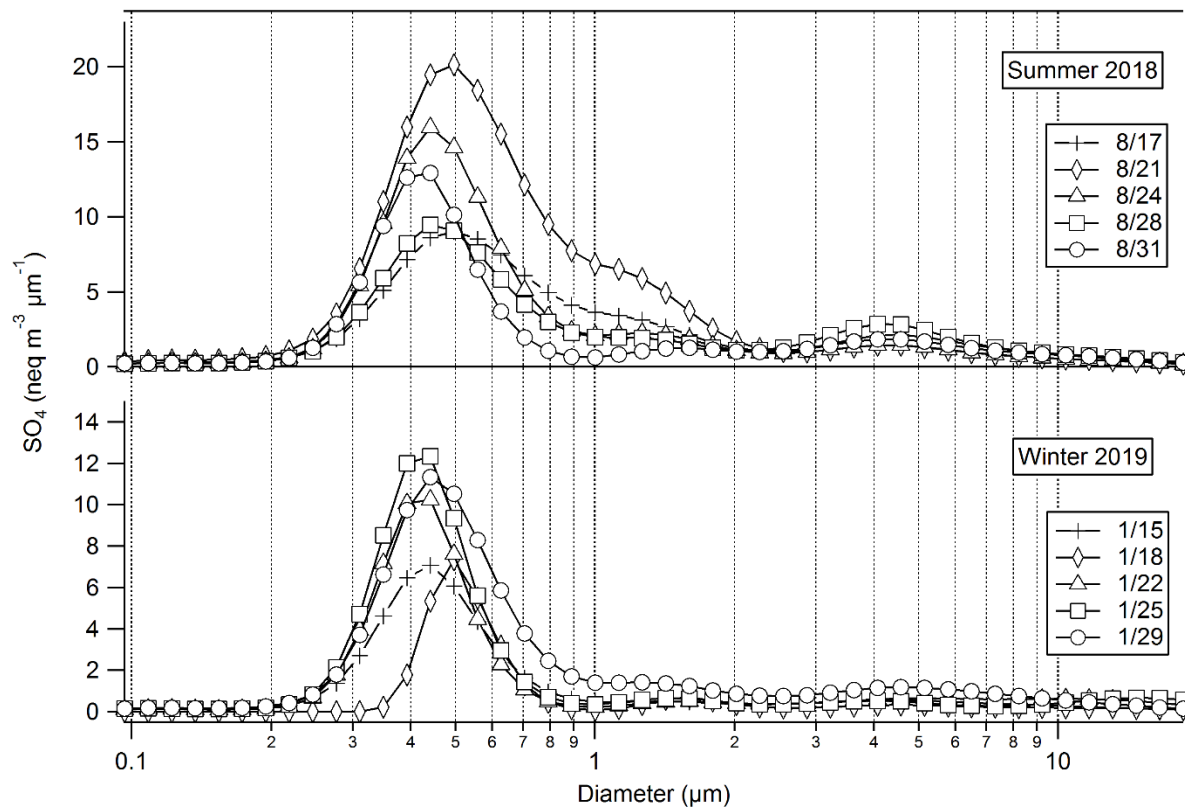
Figure 25. Seasonal trends for sulfate are shown above. Similar concentrations for both summer and winter suggest a common source year-round.

3.6 Ionic charge balance

To assess the ionic balance for the samples collected in the Fort Collins region, the OA

and inorganic anions were summed and compared to the sum of the amines and inorganic

cations. Plots were generated to reflect the anion/cation ratios for the summer and winter

MOUDI sampling periods. While there may still be other ions not measured here that could

further affect the anion/cation balance, comparison of the major ions measured is still useful.

In the summertime, there was a shift between anion deficit at sizes larger than 1 μm and cation

deficit at sizes smaller than 1 μm. Figure 26a shows the ionic balance for the 8/24/18 MOUDI

sample, exemplifying this charge balance shift. Smaller particles have an anion surplus of

around 20 % and larger particles have an anion deficit. The deficit may reflect the presence of

mineral carbonate species not measured here. There was a closer charge balance across key

size ranges of PM in the wintertime. Figure 26b shows an example of wintertime charge

balances for the 1/25/2019 sample period. The charge balance is very close to 1.0 throughout

the heart of the submicron aerosol mode that dominates wintertime aerosol mass.

Ammonium and amines summed are found to neutralize sulfate and nitrate almost

entirely in the fine mode range for both winter and summer seasons. An assessment of anion

to cation ratios with ammonia, amines, sulfate, and nitrate show an a/c ratio between 0.8-1.1

for summer and winter sampling. A larger anion surplus in the fine mode during the summer is

likely caused, in part, by increased organic acid concentrations such as acetate, formate,

succinate, and malonate in the fine mode during the summer compared to the winter. The

anion deficit seen in the coarse mode for summer samples is caused, in part, by increased

calcium concentrations and could reflect that the carbonate was not measured or simply that

relative concentration errors are bigger where size distribution has little mass.
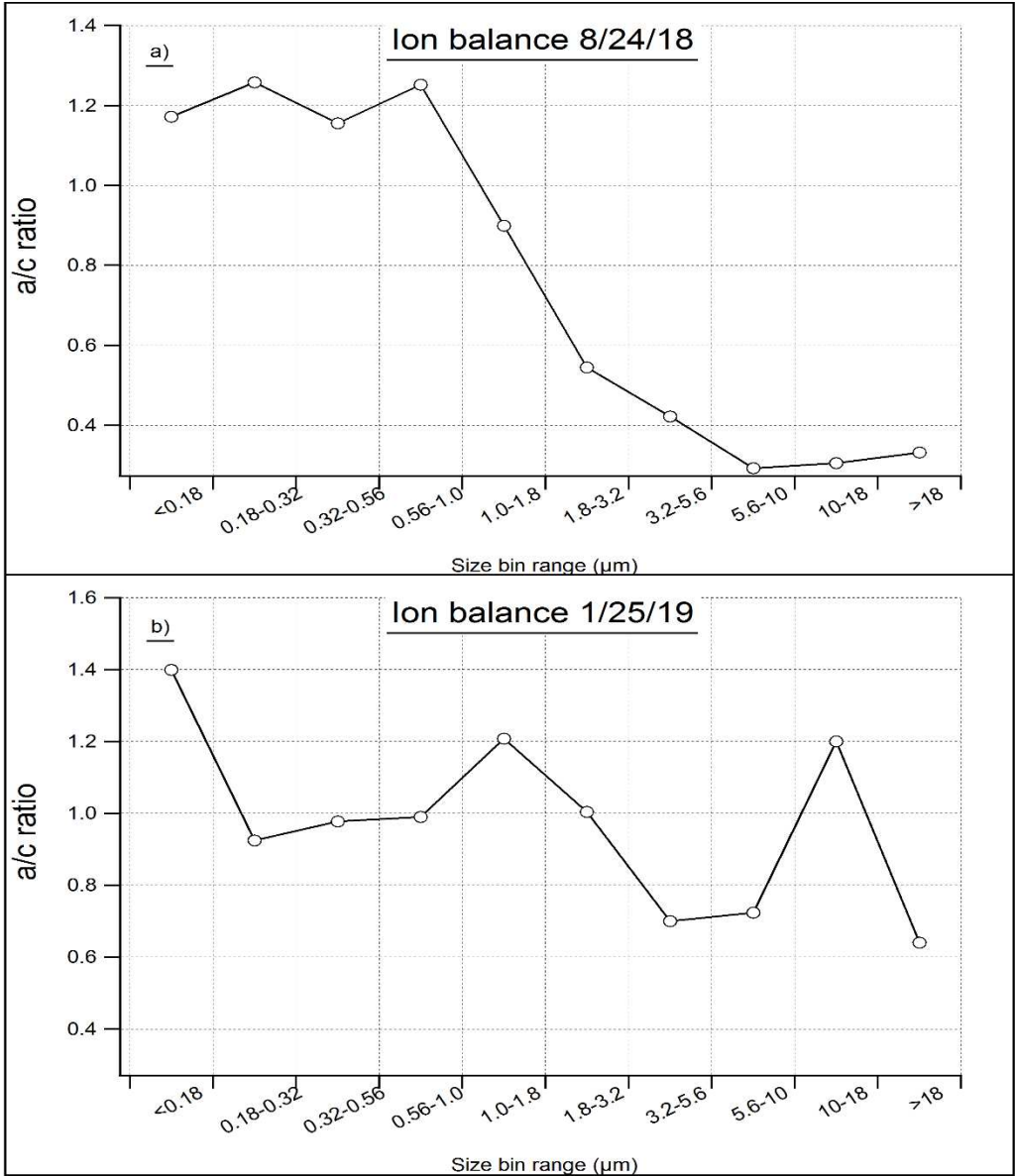
Figure 26. Ion balances for sample representing summer (a) and winter (b) seasons are shown here. Summer samples showed a shift between cation deficits to anion deficits from small to large particle sizes, respectively.

4. Conclusions and Recommendations for Future Work:

4.1 TN analysis

While TN analysis alone was not effective at identifying organic nitrogen, amines were still detected above the MDL by ion chromatography. Organic nitrogen is difficult to quantify, due to its measurement by difference between total reactive nitrogen and the sum of measured inorganic nitrogen species concentrations, and could have a large MDL for the TOC-TN instrument. More study is needed to identify what the organic nitrogen detection limit is for sample analysis using a TOC-TN analyzer for PM analysis. An assessment of error associated with detection of ammonium, nitrate, and TN shows that, even though the inorganic nitrogen content exceeded the TN found in Greeley, there is possibility of organic nitrogen present in the samples. High concentrations of ammonium and nitrate at Greeley potentially mask the organic nitrogen that was otherwise expected to be observed. Blank nylon filter samples showed some variability and high background relative to the collected samples. While TN was observed above the MDL in all samples, organic nitrogen determined by difference may not have been above the MDL. Analysis of organic nitrogen in filter samples has proven to be difficult without proper methods developed for identification of specific species in the organic nitrogen group. This work attempted to quantify several different amine species and their formation in fine mode aerosol, as well as, provide a new method for the detection of amines on filters using ion chromatography methods that are already used for inorganic species.

4.2 Spatial distributions

Of the inorganic nitrogen species identified, Greeley showed nearly equal contributions of nitrate and ammonium to TN. Greeley has close proximity to important emission sources such as the livestock industry and, due to this proximity, has more gas-phase ammonia (Figure 7) compared to the other two sites measured during the same time period. Nitrate was more prevalent in the form of PM at all three sites compared to gas likely due to an abundance of ammonia to react with and favorable conditions (lower temperatures and higher RH) for ammonium nitrate particle formation. Eventually, nitrate-containing PM is diluted during transport away from sources and also lost through deposition and/or evaporation. The decrease in particulate nitrate concentrations across the three sites supports this conclusion. While ammonia is initially observed in the gas-phase near agricultural sources, a shift to particulate ammonium dominance occurs at Fort Collins and RMNP, indicating the importance of PM in chemical transport to remote locations. Gas-phase ammonia was, surprisingly, unchanging between Fort Collins and RMNP during our measurement period, a pattern not consistent with longer term observations of this spatial gradient. While there could have been increased periods of easterly winds bringing ammonia-rich air masses to RMNP, I venture that the increased ammonia (g) in RMNP could have been transported in particulate forms and then re-emitted from surfaces after wet or dry deposition occurred. Decreased ammonium particulate at RMNP compared to Fort Collins and Greeley might reflect rain wash-out and deposition during transport. More analysis is needed during other seasons and in more locations for better spatial resolution of organic nitrogen and TN concentrations to determine trends in Northern Colorado.

Generally, spatial distributions for all species analyzed in this study showed similar trends of having the greatest concentrations observed in Greeley and the smallest concentrations in RMNP. There is some variability to which species had similar Greeley/Fort Collins concentrations or similar Fort Collins/RMNP concentrations. Greeley and Fort Collins have some similar sources that could yield similar concentrations for particular species. Sulfate concentration showed little difference between RMNP and Fort Collins, suggesting a localized source is generating higher concentrations in Greeley, alone. This is also potentially attributed to other sources of sulfate east of Greeley that could be affecting concentrations observed at the Greeley site. For example, a power plant east of Greeley in Brush, Colorado is a known source of sulfur dioxide, the precursor to sulfate formation. In addition to this power plant, there are many oil and gas developments east of Greeley that could also be attributing to the elevated sulfate concentrations observed at this site.

In the particle phase at all sites, sulfate is likely neutralized by both ammonium and amines as size distribution data show similar peak maxima in the fine mode. Nitrate is also likely neutralized by both ammonium and amines; however, summertime nitric acid appears to be reacting with suspended soil dust particles leading to the formation of coarse mode PM.

Unsurprisingly, particulate amines were found to be most concentrated in Greeley. Greeley is closest to the most feeding operations (cattle, swine, poultry, and sheep farms) and agricultural operations, both of which are known to be sources of amines. Methylamine is highest in Greeley, but Fort Collins is nearly as high as Greeley. Especially interesting is the increased dimethylamine concentration observed in Greeley. Dimethylamine can be emitted by chemical manufacturing companies, including the oil and gas industry and leather

manufacturing. Likely, there are elevated dimethylamine concentrations in Greeley attributed to the proximity of these industries relative to the sampling location. Iso-butylamine was observed at nearly the same concentration in both Greeley and Fort Collins. Dairy farms are a large source of iso-butylamine emissions (Ge et al., 2011) and there are dairy farms surrounding both site locations. Allylamine shows elevated concentrations in Greeley but not much is known about allylamine sources. Typically, allylamine is used as an industrial solvent (Soucy, 2014). The quantification of industrial sources that use allylamine is not assessed in this work. However, examining industries that use allylamine and other amines in industrial processes would help to further explain the spatial trends that are seen in this work. Dipropylamine is also emitted from industrial sources, in addition to being found naturally in tobacco leaves, but direct emissions from different industries have not been studied in depth yet. Amylamine was unique in its spatial trends as it had significantly higher concentrations in Fort Collins compared to the other site locations. Amylamine has a strong emission influence from the beer and wine industry, which is prevalent in Fort Collins.

RMNP is often thought of as a remote location with few sources nearby; therefore, overall, it is expected for RMNP to have lower concentrations of most air pollutants. Fort Collins and Greeley both have similar local sources that could be attributed to the trends seen in this study. Differences in particular industrial sector sources are likely the cause of differences in observed amine concentrations and further study into the types of industries and their emissions at each location is needed to better understand amine spatial trends.

4.3 Seasonal size distributions

While a bimodal mass distribution is typically observed for ambient PM, there is evidence here that several species had a seasonally dependent trimodal distribution evidenced with a third mode in the so-called "droplet mode" range. Past work with cascade impactors in California during the Southern California Air Quality Study (SCAQS) has supported the findings of trimodal ammonium and sulfate distributions (John et al., 1990). The data presented here are consistent with trimodal distributions that were observed for most summer samples for these species along with oxalate (Figure 11a, Figure 11c, and Figure 12); although, ammonium had nearly insignificant coarse mode peaks. Summer and winter sulfate show indications of a droplet mode around 1-1.5 μm with smaller droplet mode concentrations during the winter. Sulfate is known to be highly efficient at forming this droplet mode through aqueous chemistry in clouds and fogs and could explain why droplet mode was identified in the winter despite periods of lower relative humidity. A lack of coarse mode sulfate in the winter suggests few reactions between sulfur dioxide or sulfuric acid and suspended soil particles during this season. Coarse mode sulfate observed during the summer is likely the result of increased soil dust, allowing for sulfur dioxide oxidation or sulfuric acid condensation on larger pre-existing aerosol as evidenced by overlap of sulfate peaks with calcium and magnesium peaks (Figure 17).

Possible reasons for what initially appeared to be excess particulate nitrate, relative to available ammonium, in the MOUDI samples for winter could be contributions of other unknown cation species in neutralization of excess sulfate and nitrate (Lee et al., 2008). I surmise that the cation species, in addition to ammonium, needed for neutralization of the excess nitrate and sulfate are likely the amines observed in this study. Many gas-phase amines

are stronger bases than ammonia and can compete in reactions to form nitrate and sulfate salts (Murphy et al., 2007). Further assessment of ionic charge balances showed that ammonium and amines nearly neutralize nitrate and sulfate in the fine mode range with anion to cation ratios between 0.8 and 1.1 for fine particles during both summer and winter seasons.

Coarse mode nitrate has been observed to come from reactions of nitric acid with sea salt or soil dust (Lee et al., 2008). Depending on the region of study, more or less coarse mode nitrate is associated with soil dust reactions. In this work, coarse mode nitrate and sulfate was found to be correlated with calcium and magnesium (Figure 18), consistent with reaction of nitric acid or its precursors with suspended soil particles. There is reduced dust emitted from agricultural activity and other sources during the winter months and therefore, fewer reactions occur on coarse mode aerosol.   Nitrate, sulfate, calcium and magnesium show coarse mode peak maxima between 4 and 5 μm diameters for all summer samples. As coarse mode nitrate is commonly found in rural locations, the coarse nitrate found here is likely attributed to reactions with soil dust. As amines were not observed in the coarse mode size range, nitrate and sulfate in this size range are not attributed to amines.

Some amines exhibited higher concentrations in the summer, but most showed higher concentrations in the winter. Trimethylamine and dimethylamine both showed elevated summer concentrations compared to the winter, suggesting an affinity for the particle phase despite their high volatility. Methylamine showed similar concentrations in both summer and winter. Most other amines were found to be more concentrated in PM during the winter, similar to ammonium. Gas-phase amines were not assessed in this work and the gas-particle portioning of amines cannot be confirmed here; however, because animal agriculture is a

dominant source of many amines, there are likely significant concentration of gas-phase amine emissions during warmer summer conditions. While agriculture is a dominant source of ammonium and amines, other sources of these species are potentially significant, as well. Amine sources include a wide range of industrial processes. For example, amylamine was produced in tons during the 70s and is used in textiles, chemical manufacturing, pharmaceutical processes, beer and wine production and other similar industries (Daniel et al., 2015; Thomas, 1990). Such industries don't have a seasonal dependence and are likely using amines year-round.

Incorporations of amines into PM have important implications for remote locations, such as RMNP, where amines were detected above the MDL during the spring season. Through incorporation into submicron aerosol particles, amines can be transported over longer distances to remote locations, affecting the nitrogen loading in sensitive ecosystems. However, more study into both PM and gas-phase amines is needed during the winter and summer season to understand the effect of chemical transport of amines and their fates during transport from sources to remote locations.

4.4 Amine trends

Amines have importance in forming fine mode PM but not much is known about the fates of many amines. Some recent work has investigated more closely oxidation reactions of amines in the presence of key oxidants such as ozone, nitrous oxides, and the hydroxyl radical (Malloy et al., 2009; Murphy et al., 2007). Primary, secondary, and tertiary amines are known to

form aminium salts and tertiary amines are especially capable of acting as precursors to secondary organic aerosol (Malloy et al., 2009; Silva et al., 2008).

Trimethylamine can compete with ammonium for protons in acidic particles through direct dissolution and form aminium salts while in the particle phase (Pratt et al., 2009); thus, despite being observed in small concentrations during this study, amines that have the ability to compete with ammonium should be considered in understanding amine chemistry and PM formation. While nitrate and sulfate are significant in reacting with amines through acid-base pathways, organic acids are also capable of reacting with amines and forming aminium salts (Williams et al., 2010). The organic acids seen in the same size ranges as amines in this work suggest that these compounds may have an important role in forming aminium salts that remain in particle phases despite the high volatility, individually and relatively, of both amines and organic acids.

Failure to measure amine concentrations is one source of apparent cation deficiencies when considering aerosol charge balance. When amines measured in this study were summed with ammonia and compared to the equivalent sum of nitrate and sulfate, the result is a nearly neutral particle no matter the size in the winter and summer. This charge balance should also consider other trace species, such as organic acids. While a detailed assessment into organic acid sources and seasonal dependence is not addressed here, fine mode organic acids were found to be more concentrated in the summer compared to the winter, likely due to increased summertime photochemical production, and helped correct an apparent cation deficit in the fine particle mode during the summer.

Amines can react with organic acids and change PM composition. Amines, like ammonia, are volatile and have an affinity for the gas-phase in warmer temperatures. Organic acids are also volatile compounds, but their reactions with amines can secure them in the particles phases for extended periods due to decreased volatility (Barsanti et al., 2009). While previous work has not extensively investigated amines and their potential for reaction with organic acids, there has been some work on the effect of ammonium sulfate and its role in increasing organic acid partitioning to aqueous aerosol (Yli-Juuti et al., 2013). If amines are reacting with sulfate in a similar way as ammonium, then amines could also be enhancing the increased organic acid concentrations in fine mode PM observed in this study.

References:

Baron, J.S., Rueth, H.M., Wolfe, A.M., Nydick, K.R., Allstott, E.J., Minear, T.J., Moraska, B., 2000. Ecosystem responses to nitrogen deposition in the Colorado Front Range. Ecosystems 3, 352–368.

Barsanti, K.C., McMurry, P.H., Smith, J.N., 2009. The potential contribution of organic salts to new particle growth. Atmospheric Chemsitry Phys. 9, 2949–2957.

Beem, K.B., Raja, S., Schwandner, F.M., Taylor, C., Lee, T., Sullivan, A.P., Carrico, C.M., McMeeking, G.R., Day, D., Levin, E., Hand, J., Kreidenweis, S.M., Schichtel, B., Malm, W.C., Collett Jr., J.L., 2010. Deposition of reactive nitrogen during the Rocky Mountain Airborn Nitrogen and Sulfur (RoMANS) study. Environ. Pollut. 158, 862–872.

Benedict, K.B., Carrico, C.M., Kreidenweis, S.M., Schichtel, B., Malm, W.C., Collett, Jr, J.L., 2013. A seasonal nitrogen deposition budget for Rocky Mountain National Park. Ecol. Appl. 23, 1156–1169.

Benedict, K.B., Prenni, A.J., Sullivan, A.P., Evanoski-Cole, A.R., Fischer, E.V., Callahan, S., Sive, B.C., Zhou, Y., Schichtel, B.A., Collett Jr., J.L., 2018. Impact of Front Range sources on reactive nitrogen concentrations and deposition in Rocky Mountain National Park. PeerJ 6:e4759.

Bethea, T., Narayan, R.S., 1972. Identification of beef cattle feedlot odors. Trans. ASAE 15, 1135–1137.

Bobbink, R., Hicks, K., Galloway, J., Spranger, T., Alkemade, R., Ashmore, M., Bustamante, M.,

Cinderby, S., Davidson, E., Dentener, F., Emmett, B., Erisman, J.W., Fenn, M., Gilliam, F.,

Nordin, A., Pardo, L., De Vries, W., 2010. Global assessment of nitrogen deposition

effects on terrestrial plant diversity: a synthesis. Ecol. Appl. 20, 30–59.

Brown, S.S., Ryerson, T.B., Wollny, A.G., Brock, C.A., Peltier, R., Sullivan, A.P., Weber, R.J., Dube,

W.P., Trainer, M., Meagher, J.F., Fehsenfeld, F.C., Ravishankara, A.R., 2006. Variability in

nocturnal nitrogen oxide processing and its role in regional air quality. Science 311, 67–

70.

Cisneros, R., Bytnerowicz, A., Schweizer, D., Zhong, S., Traina, S., Bennett, D.H., 2010. Ozone,

nitric acid, and ammonia air pollution is unhealthy for people and ecosystems in

southern Sierra Nevada, California. Environ. Pollut. 158, 3261–3271.

Daniel, D., Dos Santos, V.B., Vidal, D.T.R., Do Lago, C.L., 2015. Determination of biogenic amines

in beer and wine by capillary electrophoresis–tandem mass spectrometry. J.

Chromatogr. 14, 121–128.

Dod, R.L., Gundel, L.A., Benner, W.II., Novakov, T., 1984. Non-ammonium reduced nitrogen

species in atmospheric aerosol particles. Sci. Total Environ. 36, 277–282.

Fekete, A., Malik, A.K., Kumar, A., Schmitt-Kopplin, P., 2010. Amines in the Environment. Crit.

Rev. Anal. Chem. 40, 102–121. https://doi.org/10.1080/10408340903517495

Filipy, J., Rumburg, B., Mount, G., Westberg, H., Lamb, B., 2006. Identification and

quantification of volatile organic compounds from a dairy. Atmos. Environ. 40, 1480–

1494.

Ge, X., Wexler, A.S., Clegg, S.L., 2011. Atmospheric amines - Part I. A review. Atmos. Environ. 45, 524–546.

Gebhart, K.A., Schichtel, B.A., Malm, W.C., Barna, M.G., Rodriguez, M.A., Collett Jr., J.L., 2011. Back-trajectory-based source apportionment of airborne sulfur and nitrogen concentrations at Rocky Mountain National Park, Colorado, USA. Atmos. Environ. 45, 621–633.

Hering, S.V., Friedlander, S.K., 1982. Origins of aerosol sulfur size distributions in the Los Angeles Basin. Atmos. Environ. 16, 2647–2656.

Hutchinson, G., Mosier, A., Andre, C.E., 1982. Ammonia and amine emissions from a large cattle feedlot. J. Environ. Qual. 11, 288–293.

Jen, C.N., Bachman, R., Zhao, J., McMurry, P.H., Hanson, D.R., 2016. Diamine-sulfuric acid reactions are a potent source of new particle formation. Geophys. Res. Lett. 43, 867–873.

Jen, C.N., McMurry, P.H., Hanson, D.R., 2014. Stabilization of sulfuric acid dimers by ammonia, methylamine, dimethylamine, and trimethylamine. J. Geophys. Res. Atmospheres 119, 7502–7514.

John, W., Wall, S.M., Ondo, J.L., Winklmayr, W., 1990. Modes in the size distributions of atmospheric inorganic aerosol. Atmos. Environ. 24A, 2349–2359.

Krzymien, M., Day, M., Shaw, K., Zaremba, L., 1999. An investigation of odors and volatile organic compounds released during composting. J. Air Waste Manag. Assoc. 49, 804–813.

Lee, T., 2007. Characterizing ionic components of aerosol in rural environments: Temporal

variability, size distributions, and the form of particle nitrate (PhD dissertation).

Colorado State University.

Lee, T., Yu, Z.-Y., Ayres, B., Kreidenweis, S.M., Malm, W.C., Collett Jr., J.L., 2008. Observations of

fine and coarse particle nitrate at several rural locations in the United States. Atmos.

Environ. 42, 2720–2732.

Liggio, J., Li, S.-M., Vlasenko, A., Stroud, C., Makar, P., 2011. Depression of ammonia uptake to

sulfuric acid aerosols by competing uptake of ambient organic gases. Environ. Sci.

Technol. 45, 2790–2796.

Mace, K.A., Artaxo, P., Duce, R.A., 2003. Water-soluble organic nitrogen in Amazon Basin

aerosols during the dry (biomass burning) and wet seasons. J. Geophys. Res. 108, 4512.

Makela, J.M., Yli-koivisto, S., Hiltunen, V., Seidl, W., Swietlicki, E., Teinila, K., Sillanpaa, M.,

Koponen, I.K., Paatero, J., Rosman, K., Hameri, K., 2016. Chemical composition of

aerosol during particle formation events in boreal forest. Tellus B Chem. Phys. Meteorol.

53, 380–393.

Malloy, Q.G.J., Qi, L., Warren, B., Cocker III, D.R., Erupe, M.E., Silva, P.J., 2009. Secondary

organic aerosol formation from primary aliphatic amines with NO3 radical. Atmospheric

Chemsitry Phys. 9, 2051–2060.

Marple, V.A., Rubow, K.L., Behm, S.M., 1991. A microorfice uniform deposit impactor (MOUDI):

Description, calibration, and use. Aerosol Sci. Technol. 14, 434–446.

McGregor, K.G., Anastasio, C., 2001. Chemistry of fog waters in California's Central Valley: 2. Photochemical transformations of amino acids and alkyl amines. Atmos. Environ. 35, 1091–1104.

Meng, Z., Seinfeld, J.H., 2007. On the source of the submicrometer droplet mode of urban and regional aerosols. Aerosol Sci. Technol. 20, 253–265.

Miner, J.R., Hazen, T.E., 1969. Ammonia and amines: Components of swine-building odor. Trans. ASAE 12, 772–774.

Mosier, A.R., Andre, C.E., Viets, F.G., 1973. Identification of aliphatic amines volatilized from cattle feedyard. Environ. Sci. Technol. 7, 642–644.

Murphy, S.M., Sorooshian, A., Kroll, J.H., Ng, N.L., Chhabra, P., Tong, C., Surratt, J.D., Knipping, E., Flagan, R.C., Seinfeld, J.H., 2007. Secondary Aerosol Formation From Atmospheric Reactions of Aliphatic Amines. Atmospheric Chemsitry Phys. 7, 2313–2337.

Passant, N.R., Richardson, S.J., Swannell, R.P.J., Gibson, N., Woodfield, M.J., van Der Lugt, jan P., Wolsink, J.H., Hesselink, P.G.M., 1993. Emissions of volatile organic compounds (VOCs) from the food and drink industries of the European community. Atmos. Environ. 27, 2555–2566.

Pitts, J.N., Grosjean, D., Vancauwenberghe, K., Schmid, J.P., Fitz, D.R., 1978. Photo-oxidation of aliphatic-amines under simulated atmospheric conditions - formation of nitrosamines, nitramines, amides, and photo-chemical oxidant. Environ. Sci. Technol. 12, 946–953.

Pratt, K.A., Hatch, L.E., Prather, K.A., 2009. Seasonal Volatility Dependence of Ambient Particle Phase Amines. Environ. Sci. Technol. 43, 5276–5281.

Rabaud, N.E., Ebeler, S.E., Ashbaugh, L.L., Flocchini, R.G., 2003. Characterization and quantification of odorous and non-odorous volatile organic compounds near a commercial dairy in California. Atmos. Environ. 37, 933–940.

Rappert, S., Müller, R., 2005. Odor compounds in waste gas emissions from agricultural operations and food industries. Waste Manag. 25, 887–907.

Rogge, W., Hildermann, L., Mazurek, M., Cass, G., 1993. Sources of fine organic aerosol. 2. Noncatalyst and catalyst-equipped automobiles and heavy-duty diesel trucks. Environ. Sci. Technol. 27, 636–651.

Rogge, W., Hildermann, L., Mazurek, M., Cass, G., Simonelt, B., 1994. Sources of fine organic aerosol. 6. Cigarette smoke in the urban atmosphere. Environ. Sci. Technol. 28, 1375–1388.

Rogge, W., Hildermann, L., Mazurek, M., Cass, G., Simonelt, B., 1991. Sources of fine organic aerosol. 1. Charbroilers and meat cooking operations. Environ. Sci. Technol. 25, 1112–1125.

Schade, G.W., Crutzen, P.J., 1995. Emission of aliphatic amines from animal husbandry and their reactions: Potential source of N2O and HCN. J. Atmospheric Chem. 22, 319–346.

Seinfeld, J.H., Pandis, S.N., 2006. Atmospheric Chemistry and Physics, Second Edition. ed. John Wiley & Sons, INC.

Silva, P.J., Erupe, M.E., Price, D., Elias, J., 2008. Trimethylamine as Precursor to Secondary Organic Aerosol Formation via Nitrate Radical Reaction in the Atmosphere. Environ. Sci. Technol. 42, 4689–4696.

Silvern, R.F., Jacob, D.J., Kim, P.S., Marais, E.A., Turner, J.R., Campuzano-Jost, P., Jimenez, J.L., 2017. Inconsistency of ammonium-sulfate aerosol ratios with thermodynamic models in the eastern US: a possible role of organic aerosol. Atmospheric Chemsitry Phys. 17, 5107–5118.

Sollinger, S., Levsen, K., Wünsch, G., 1994. Indoor pollution by organic emissions from textile floor coverings: Climate chamber studies under static conditions. Atmos. Environ. 28, 2369–2378.

Sollinger, S., Levsen, K., Wünsch, G., 1993. Indoor pollution by organic emissions from textile floor coverings: Climate chamber studies under dynamic conditions. Atmos. Environ. 27, 183–192.

Soucy, N.V., 2014. Allylamine, in: Encyclopedia of Toxocology (Third Edition). Reference Module in Biomedical Sciences, pp. 149–151.

Sullivan, A.P., Hodas, N., Turpin, B.J., Skog, K., Keutsch, F.N., Gilardoni, S., Paglione, M., Rinaldi, M., Decesari, S., Facchini, M.C., Poulain, L., Herrmann, H., Wiedensohler, A., Nemitz, E., Twigg, M.M., Collett Jr., J.L., 2016. Evidence for ambient dark aqueous SOA formation in the Po Valley, Italy. Atmospheric Chemsitry Phys. 16, 8095–8108.

Thomas, C.E., 1990. 1.2 - n-Amylamine, in: Nitrogen and Phosphorus Solvents, Ethel Browning's Toxicity and Metabolism of Industrial Solvents. Elsevier, pp. 11–16.

Tsai, C.-J., Chen, M.-L., Ye, A.-D., Chou, M.-S., Shen, S.-H., Mao, I.-F., 2008. The relationship of odor concentration and the critical components emitted from food waste composting plants. Atmos. Environ. 42, 8246–8251.

Twomey, S., 1975. Comparison of constrained linear inversion and an iterative nonlinear algorithm applied to the indirect estimation of particle size distributions. J. Comput. Phys. 18, 188–200.

Wang, X., Wang, W., Yang, L., Gao, X., Nie, W., Yu, Y., Xu, P., Zhou, Y., Wang, Z., 2012. The secondary formation of inorganic aerosols in the droplet mode through heterogeneous aqueous reactions under haze conditions. Atmos. Environ. 63, 68–76.

Williams, B.J., Goldstein, A.H., Kreisberg, N.M., Hering, S.V., Worsnop, D.R., Ulbrich, I.M., Docherty, K.S., Jimenez, J.L., 2010. Major components of atmospheric organic aerosol in southern California as determined by hourly measurements of source marker compounds. Atmospheric Chemsitry Phys. 10, 11577–11603.

Williams, M.W., Hood, E., Caine, N., 2001. Role of organic nitrogen in the nitrogen cycle of a high-elevation catchment, Colorado Front Range. Water Resour. Res. 37, 2569–2581.

Winklmayr, W., Wang, H.-C., John, W., 1990. Adaptation of the Twomey Algorithm to the Inversion of Cascade Impactor Data. Aerosol Sci. Technol. 13, 322–331.

Yli-Juuti, T., Zardini, A.A., Eriksson, A.C., Hansen, A.M.K., Pagels, J.H., Swietlicki, E., Svenningsson, B., Glasius, M., Worsnop, D.R., Riipinen, I., Bilde, M., 2013. Volatitly of organic aerosol: Evaporation of ammonium sulfate/succinic acid aqueous solution droplets. Environ. Sci. Technol. 47, 12123–12130.

Yokelson, R., Susott, R., Ward, D., Reardon, J., Griffith, D., 1997. Emissions from smoldering combustion of biomass measured by open-path Fourier transform infrared spectroscopy. J. Geophys. Res. 102, 18865–18877.

Yu, X.-Y., Lee, T., Ayres, B., Kreidenweis, S.M., Collett, Jr, J.L., Malm, W., 2005. Particulate

nitrate measurement using nylon filters. J. Air Waste Manag. Assoc. 55, 1100–1110.

Yu, X.-Y., Lee, T., Ayres, B., Kreidenweis, S.M., Malm, W., Collett Jr., J.L., 2006. Loss of fine

particle ammonium from denuded nylon filters. Atmos. Environ. 40, 4797–4807.

Zhang, Y.L., Lee, X.Q., Cao, F., 2011. Chemical Characteristics and sources of organic acids in

precipitation at a semi-urban site in Southwest China. Atmos. Environ. 45, 413–419.

Appendix A:

Many species were analyzed but were not discussed in this work. The figures in this section summarize the data collected for all of the species analyzed during the MOUDI sampling campaign in Fort Collins during August 2018 and January 2019. The following sections list seasonal trends of amines, organic acids, and other inorganic ions. The figures represent the Twomey inversion corrected data. In some samples, the species were not detected above the MDL and the code interpreted the raw data as a relatively straight horizontal line. When this happened the relevant specie was determined to be undetectable by ion chromatography methods. Only two amines, dipropylamine and 1,4 diaminobutane, were not observed in any samples collected from the MOUDI in August 2018 or January 2019.

Amines:
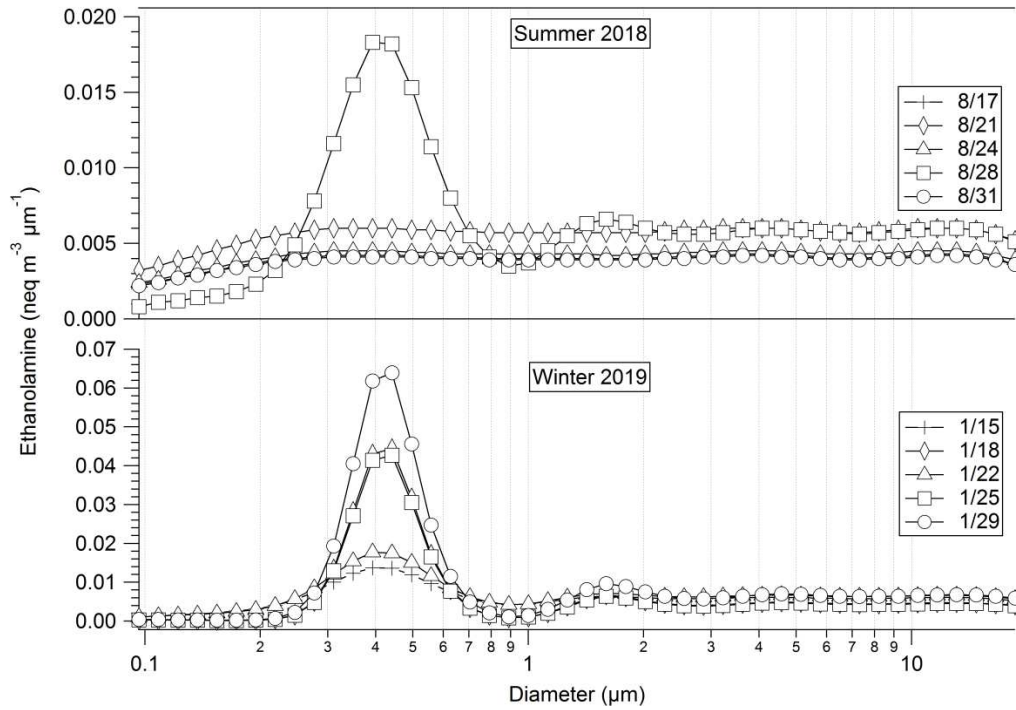
Figure A1. Seasonal trends of ethanolamine are shown above. Only the sample collected on 8/28/2018 during the summer detected ethanolamine in the fine mode. Winter samples were observed to have trace amounts of ethanolamine in fine mode.
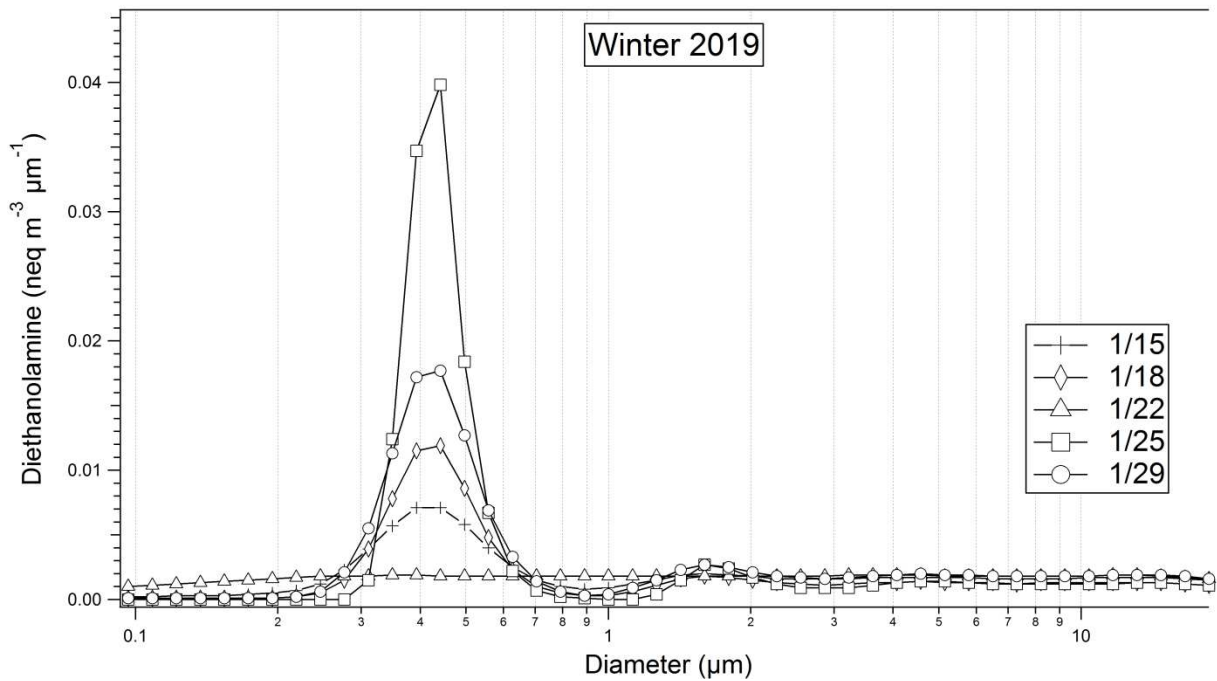
Figure A2. Diethanolamine was not observed in any summer samples but was observed in small amounts for almost all winter samples.
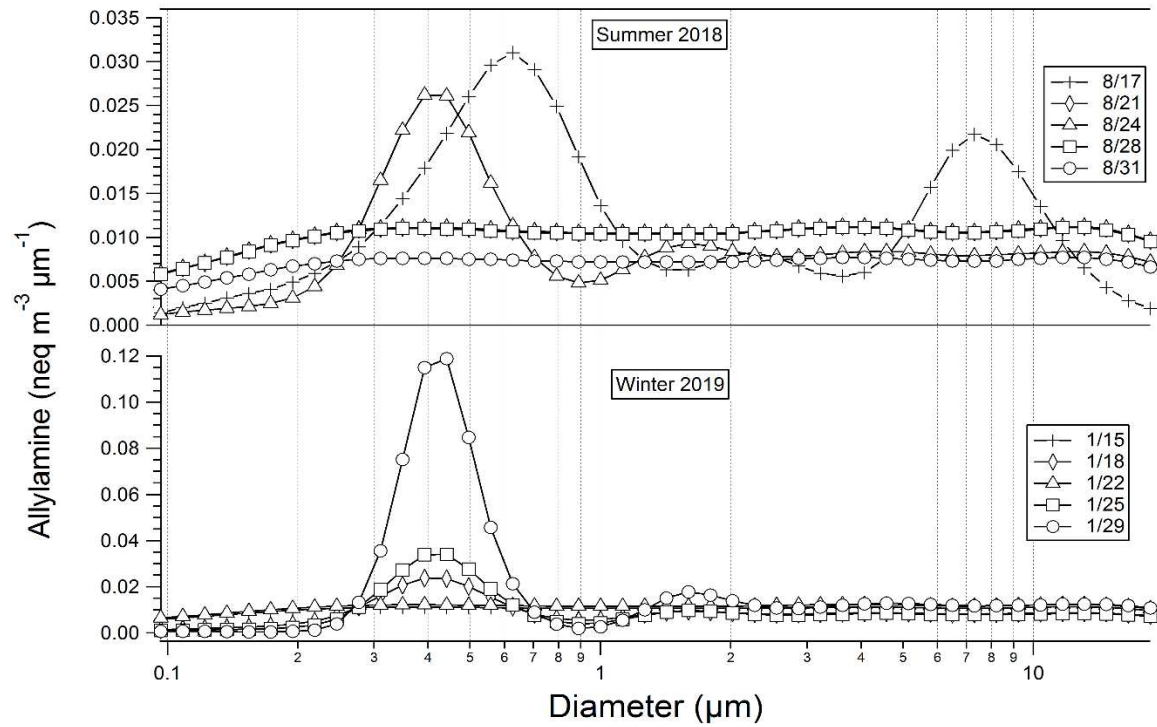
Figure A3. Seasonal trends for allylamine show an interesting coarse peak in the sample collected on 8/17/2019. Because this was not replicable in other samples it is not clear if this was a contamination or truly evidence of coarse allylamine. However, it is possible as this period experienced high day-time relative humidity.
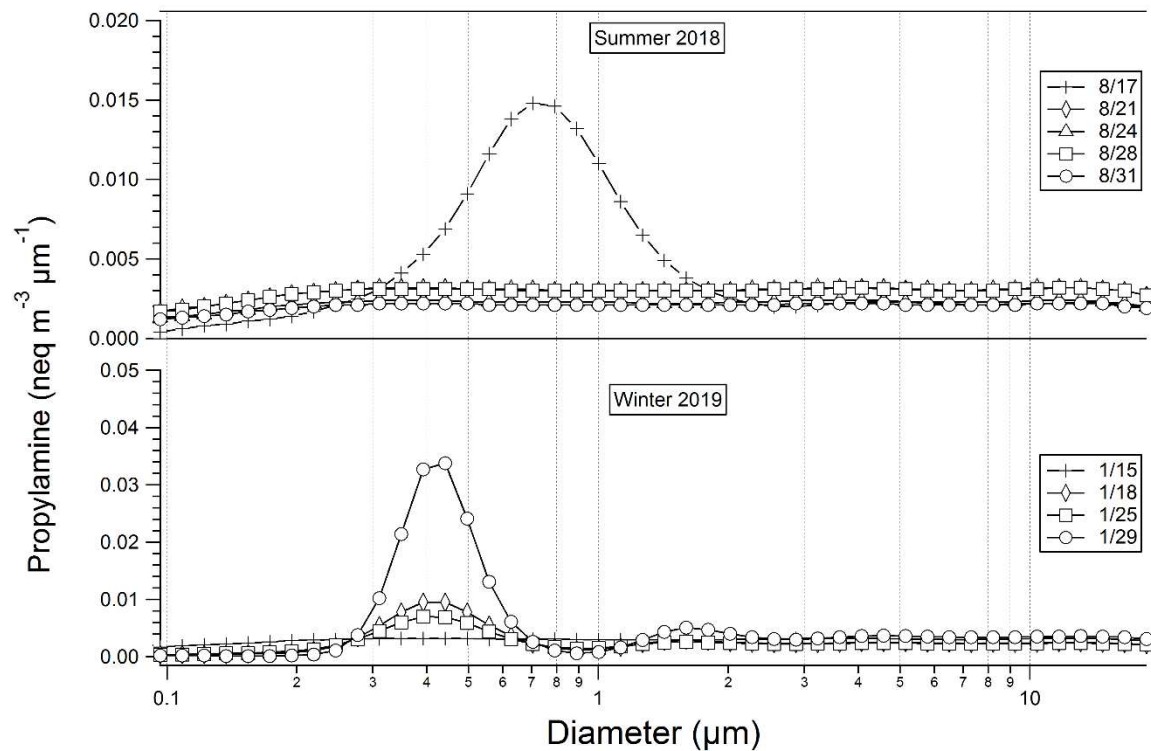
Figure A4. Seasonal trends for propylamine are shown above. A small amount of propylamine was observed in fine mode during the winter and in one sample collected during the summer likely due to the high RH in that sampling period.
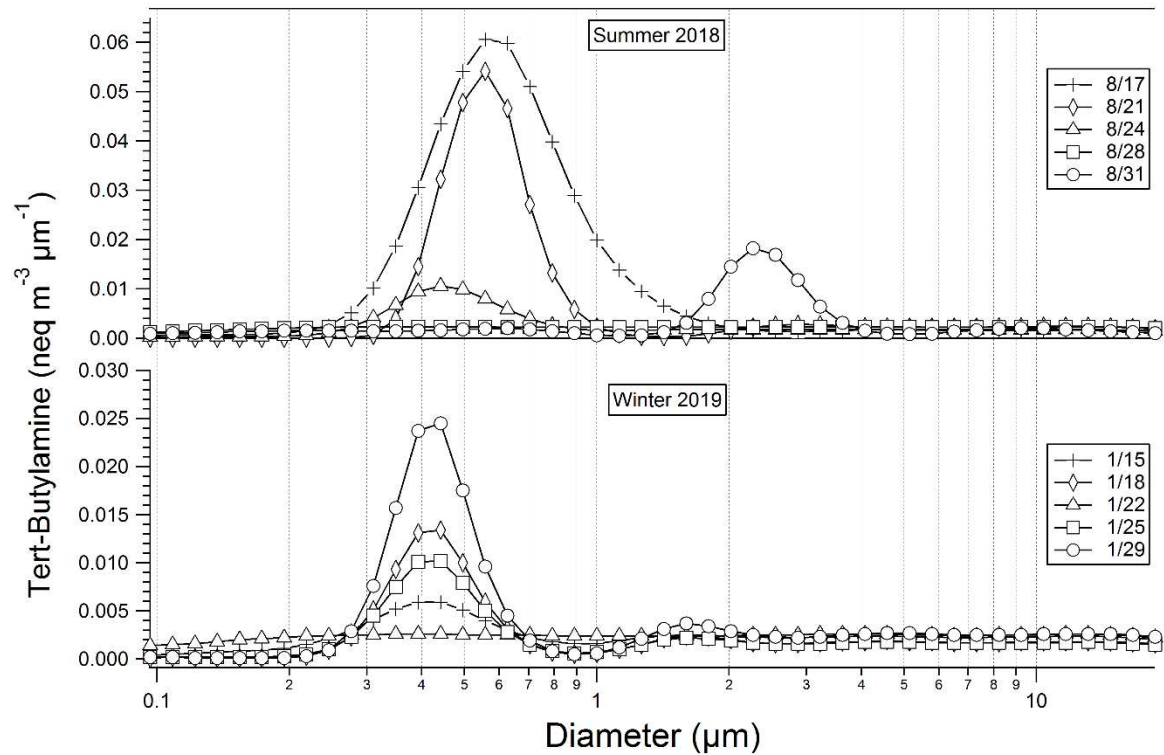
Figure A5. Seasonal trends for tert-butylamine are shown above.
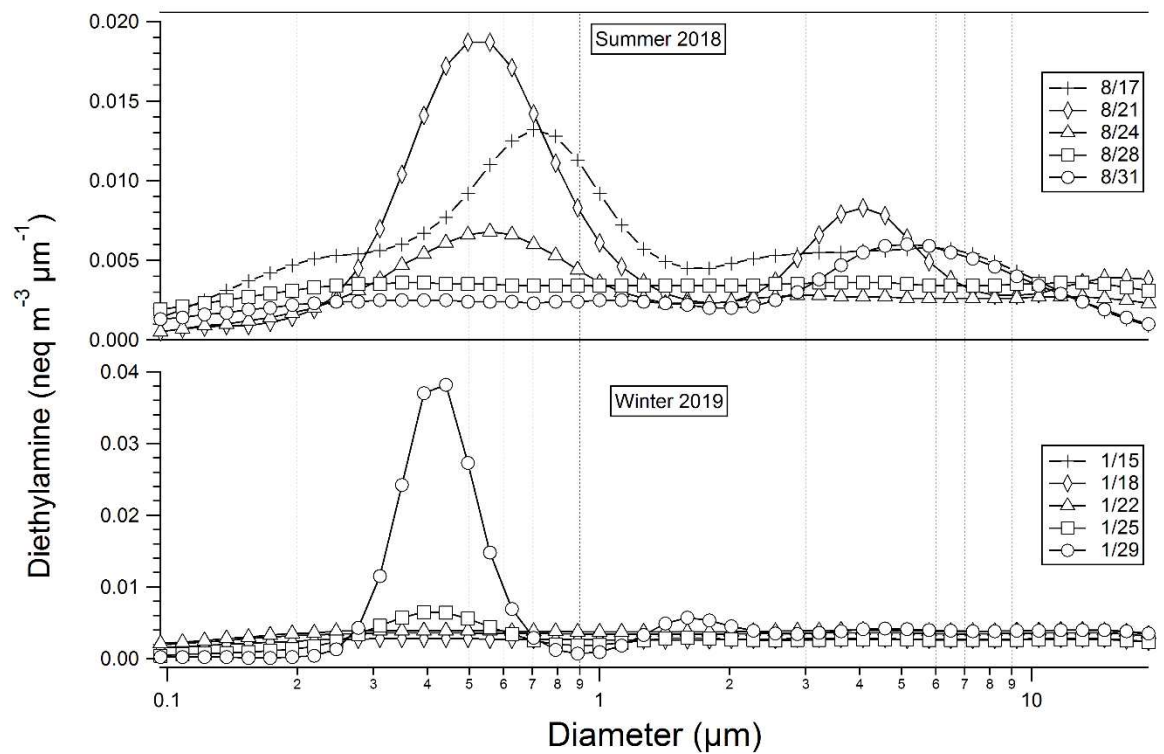
Figure A6. Diethylamine size distributions were interesting during the summer season because a possible coarse mode was detected slightly above MDL for at least one sample collected 8/21/2018. Winter concentrations were generally undetectable.
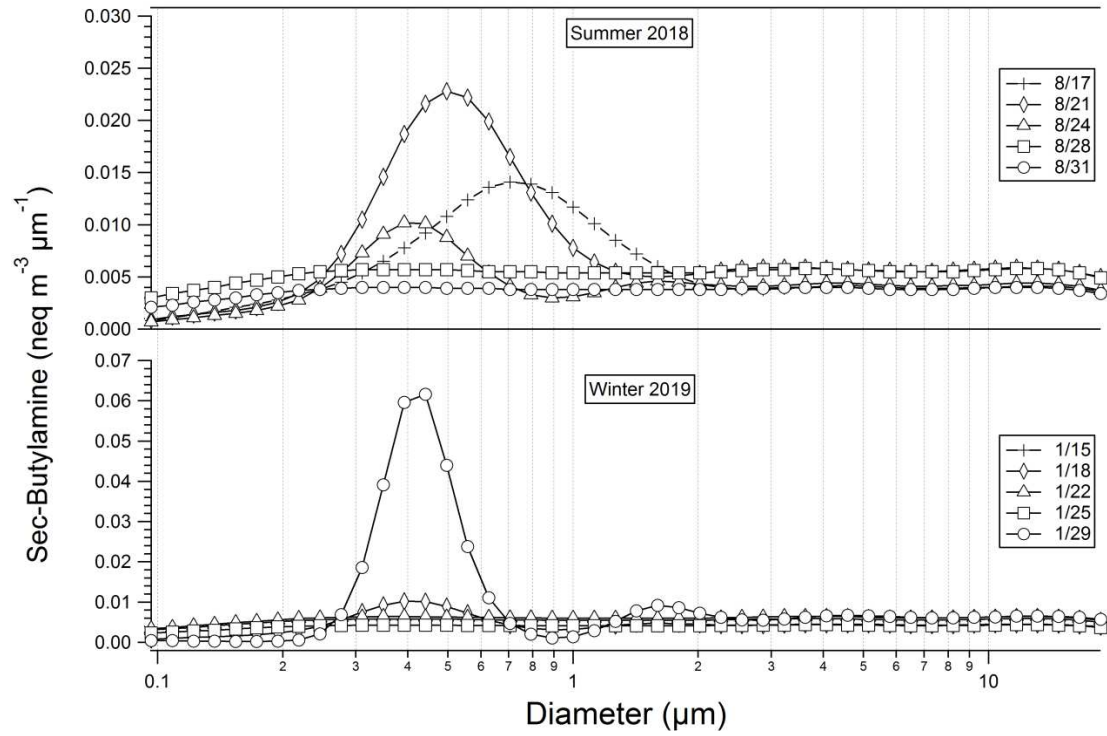
Figure A7. Sec-butylamine seasonal size distributions are shown above.
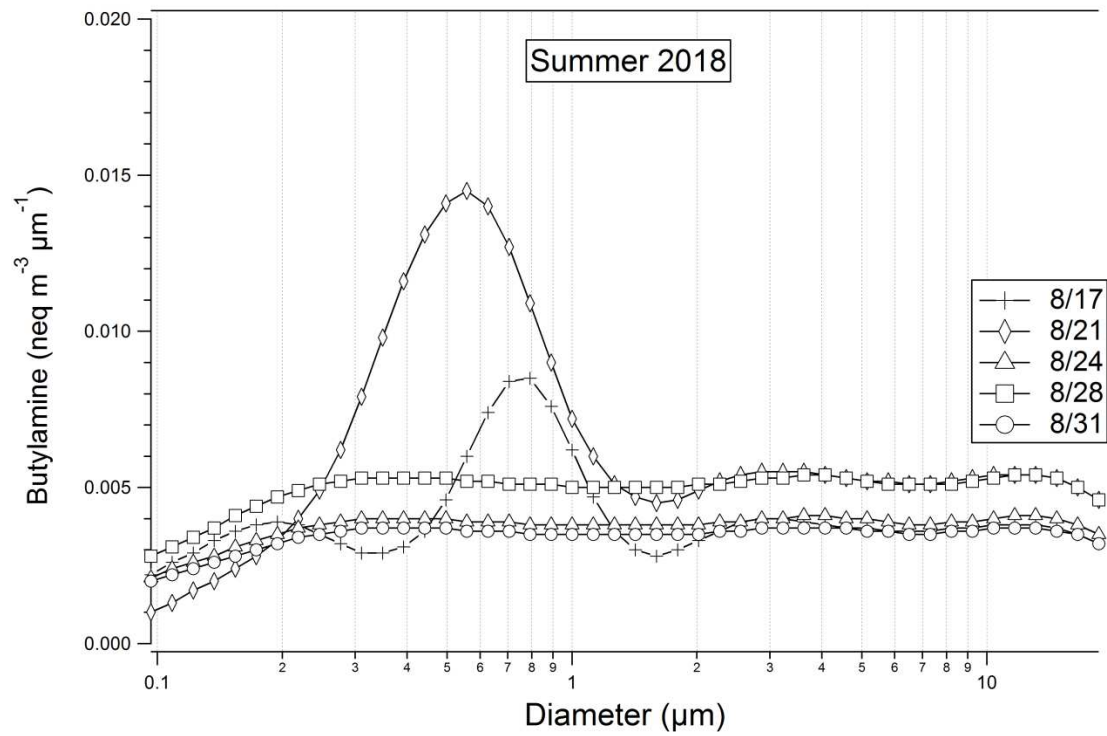
Figure A8. Butylamine was not detected in any winter samples and was only detected in trace amounts during two summer sampling periods were day-time RH was relatively high.
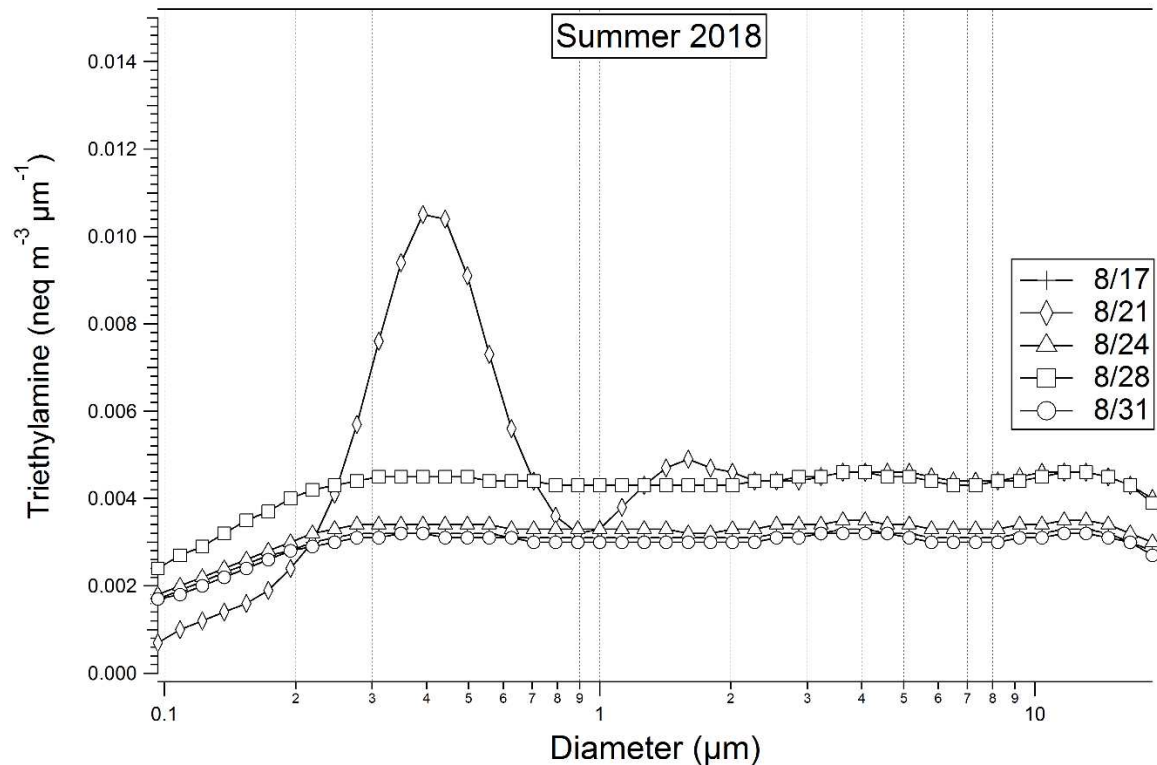
Figure A9. Triethylamine was also not detected in any winter time samples collected in this work. Only the sample collected on 8/21/2018 showed evidence of triethylamine in the fine mode.

Organic Acids:
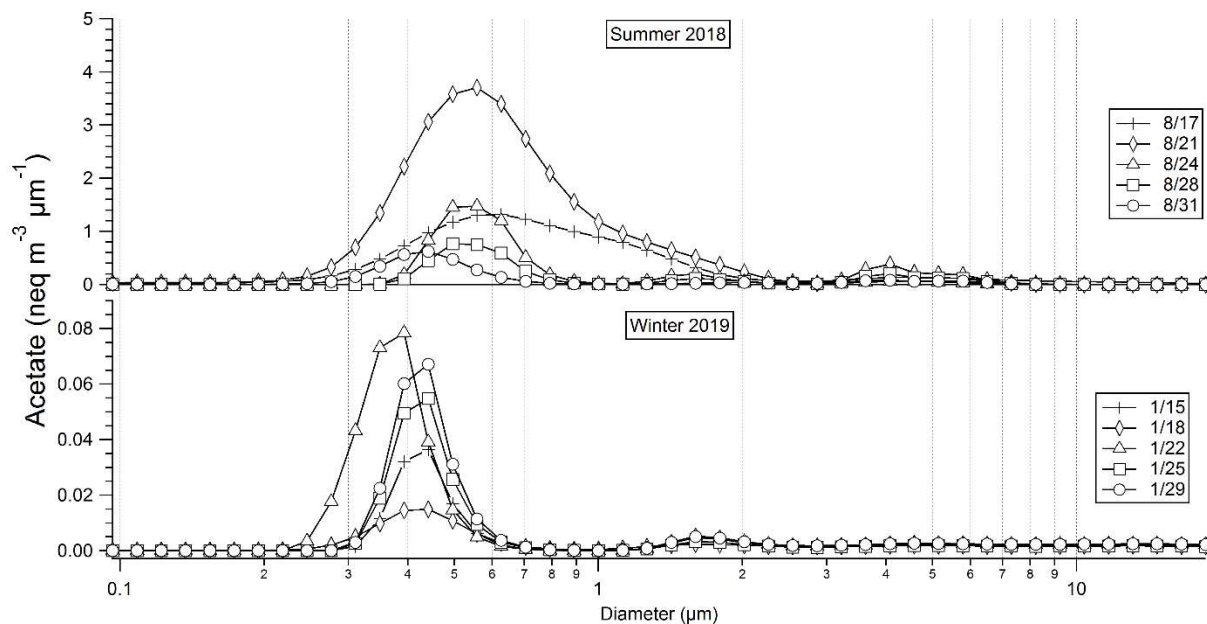
Figure A10. Acetate size distributions are shown above. Greater summer time concentrations were observed in the fine mode compared to winter.
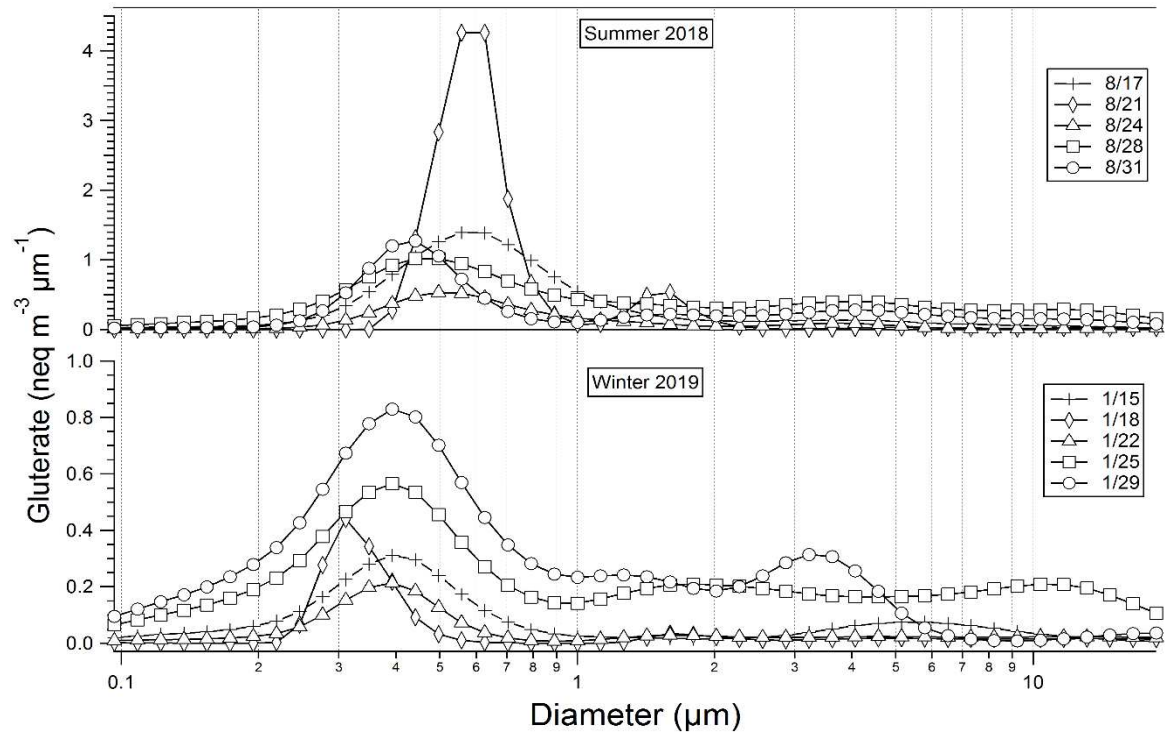
Figure A11. Gluterate seasonal size distributions are shown above.
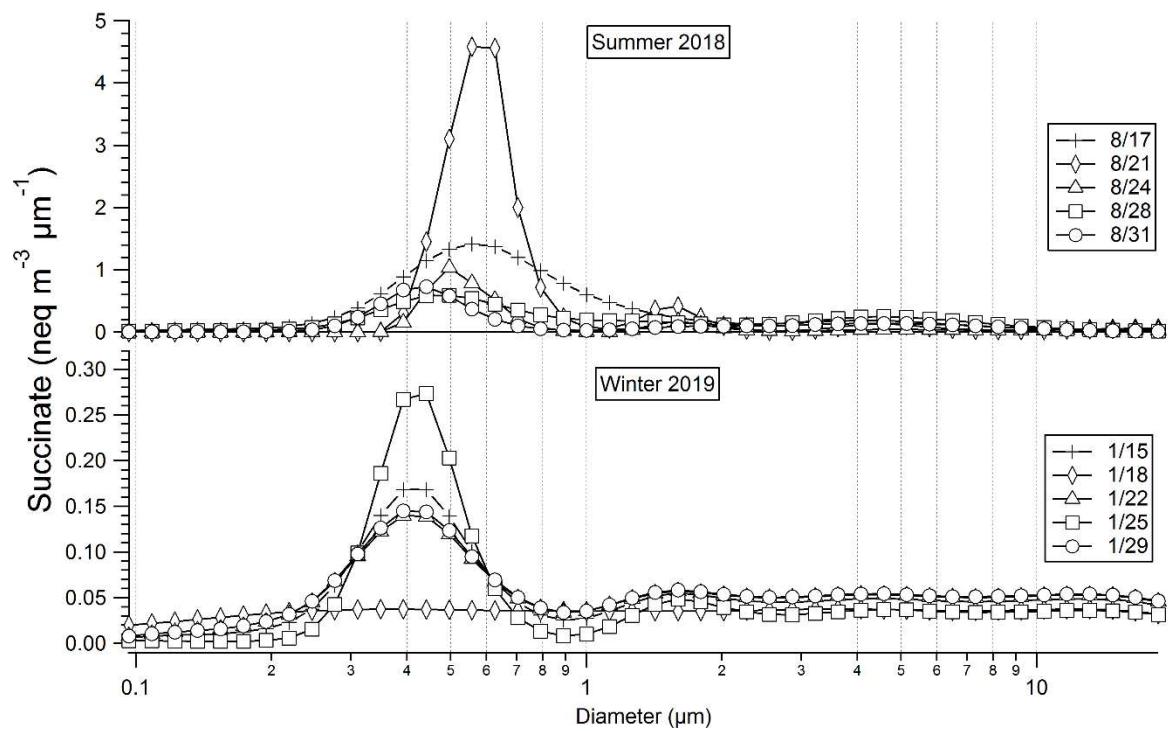
Figure A12. Following trends of other organic acids, greater succinate concentrations were observed in the summer season.
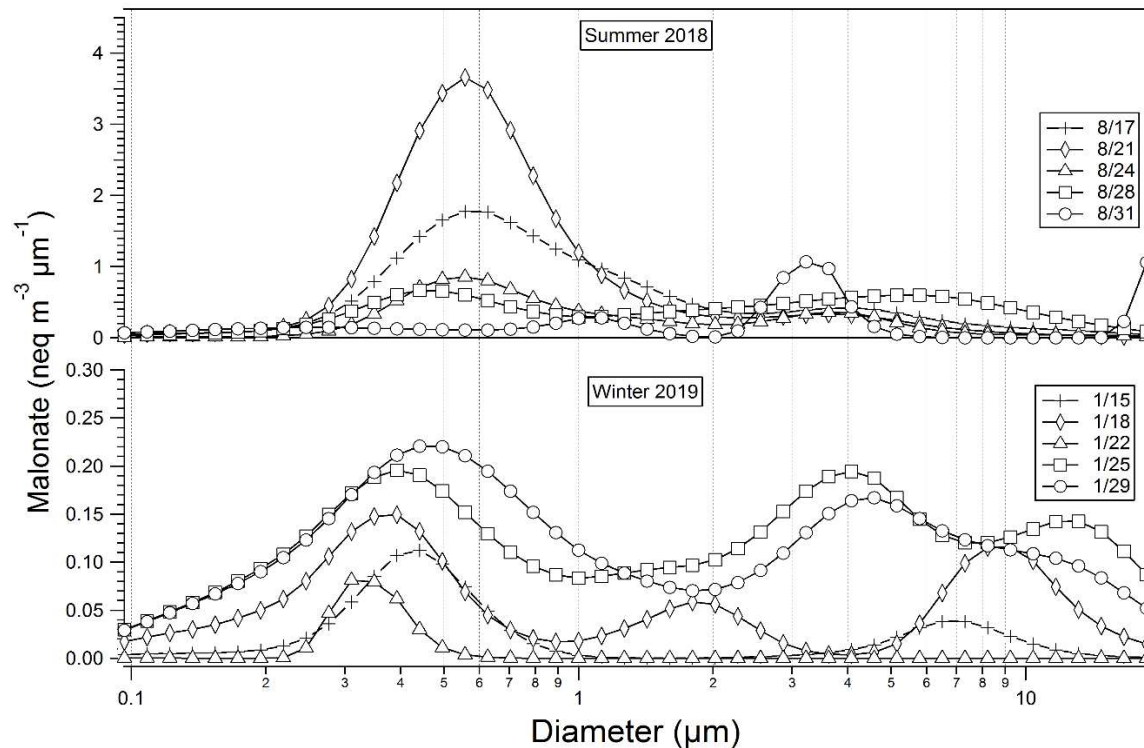
Figure A13. Winter malonate size distributions were interesting as can be seen in the bottom of the figure above. There appears to be evidence of fine and coarse modes and even potentially a droplet mode during the winter season. More sampling during the winter is needed to determine the validity of the results shown here.
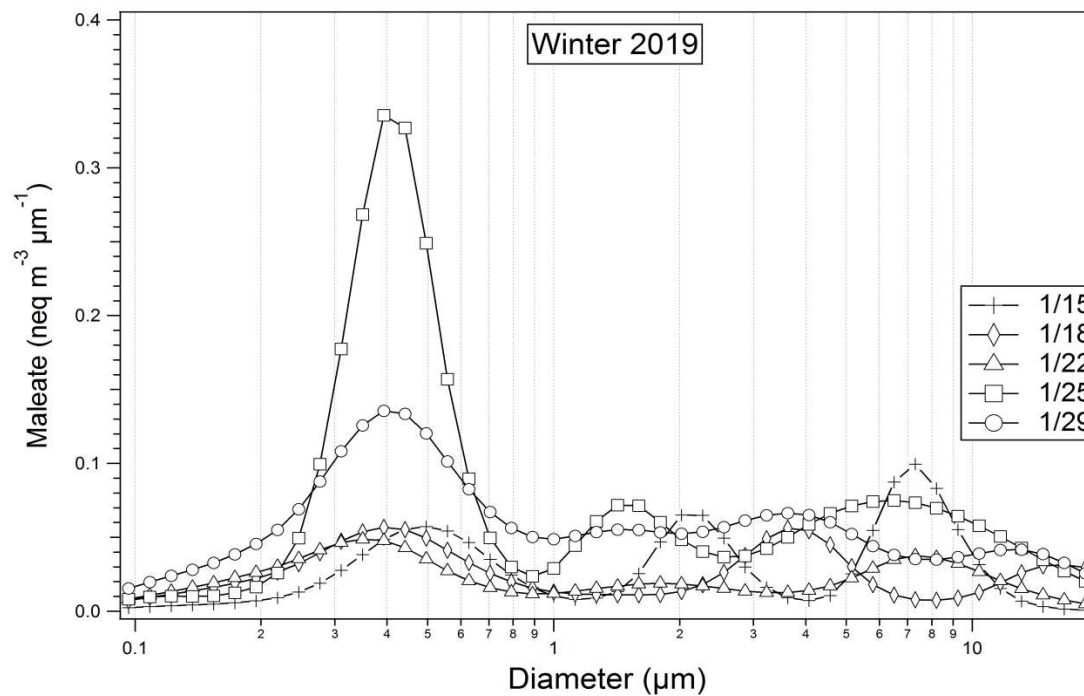
Figure A14. While most organic acids were observed in greater concentrations in the summer, size distributions of maleate show that detection was only possible in the winter. The erratic peaks in the droplet and coarse modes are values below the MDL and cannot be ascertained as having the trend they are displaying.
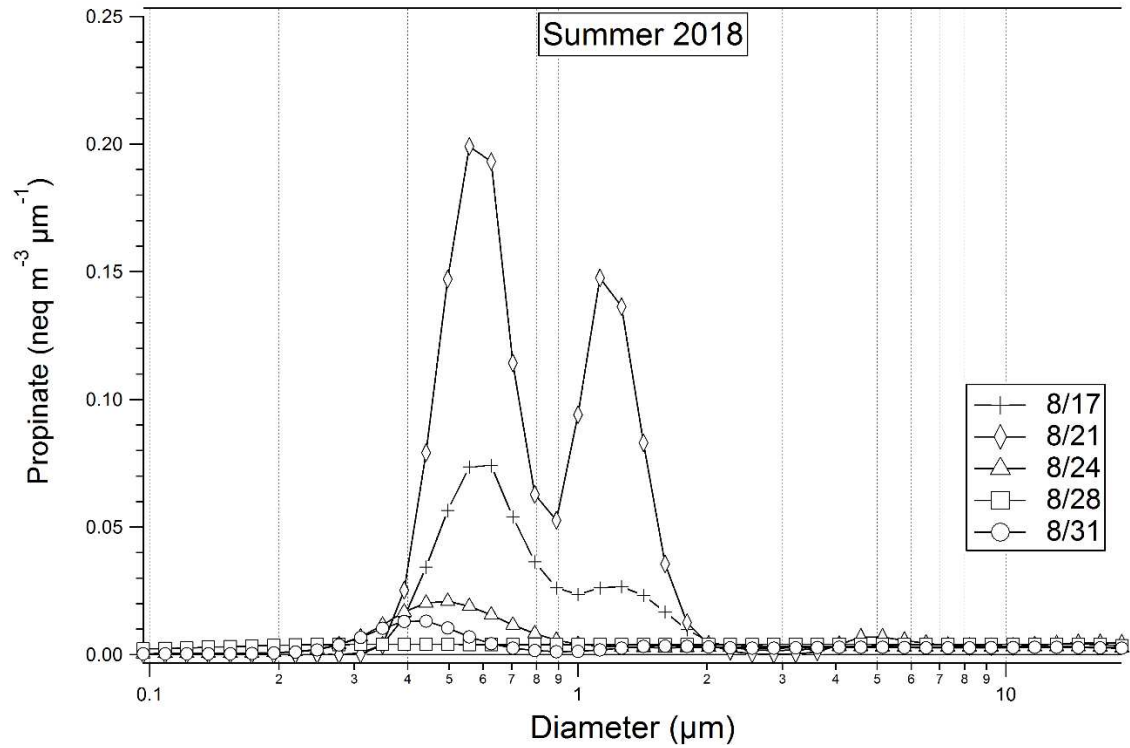
Figure A15. Propinate shows evidence of a droplet mode as well as a fine mode. The sharpness of the droplet mode peak on 8/21/2018 is likely an overestimation made by the Twomey algorithm rather than a real-life droplet mode peak.
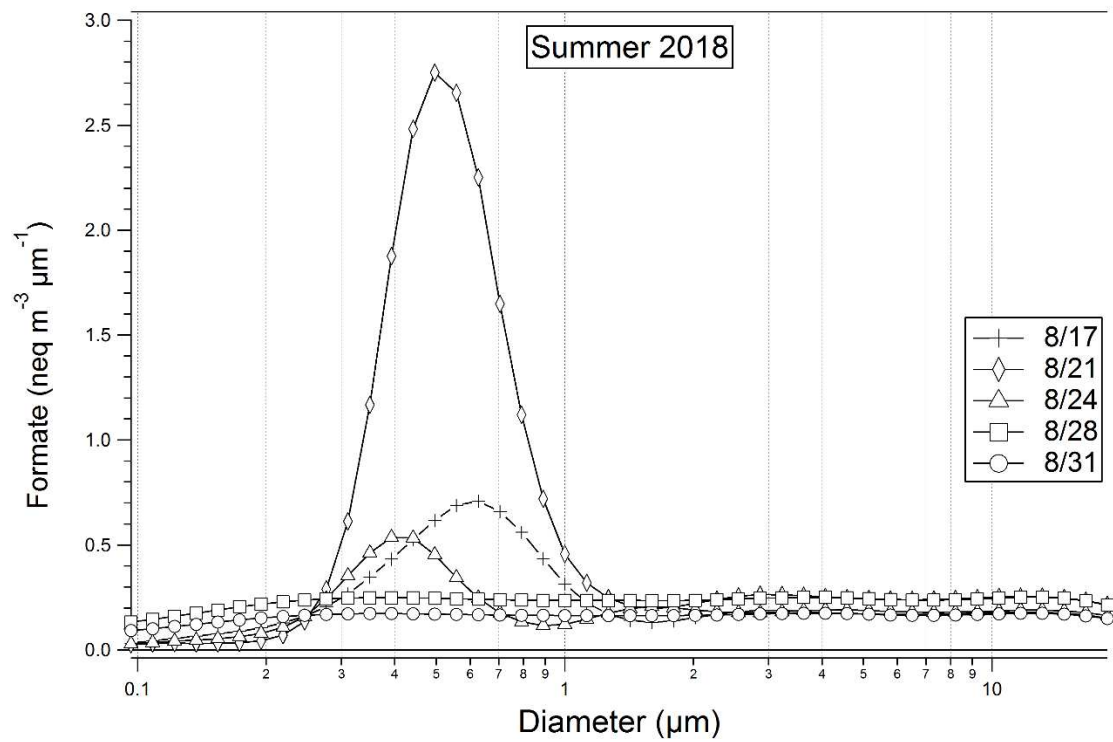
Figure A16. Formate size distributions are shown above. Formate was only detected in samples collected in the summer.
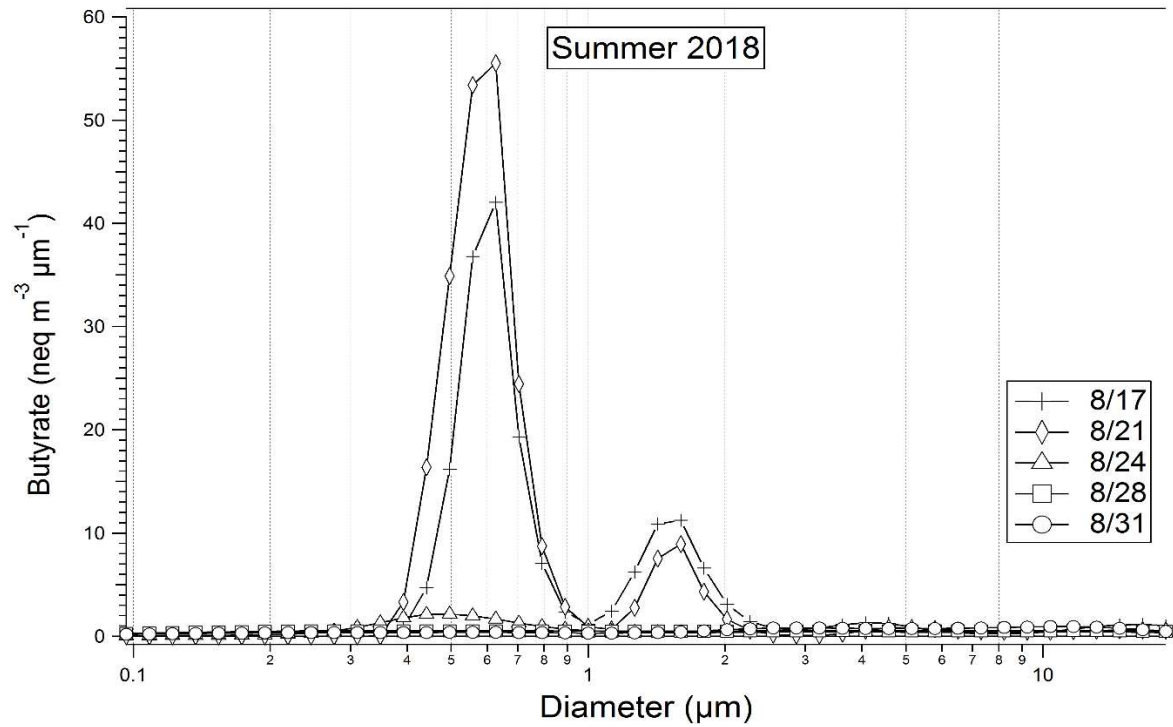
Figure A17. Similar to other organic acids, butyrate was only observed in the summer. There appears to be evidence of a large droplet mode during the two samples collected when day-time RH was relatively high.
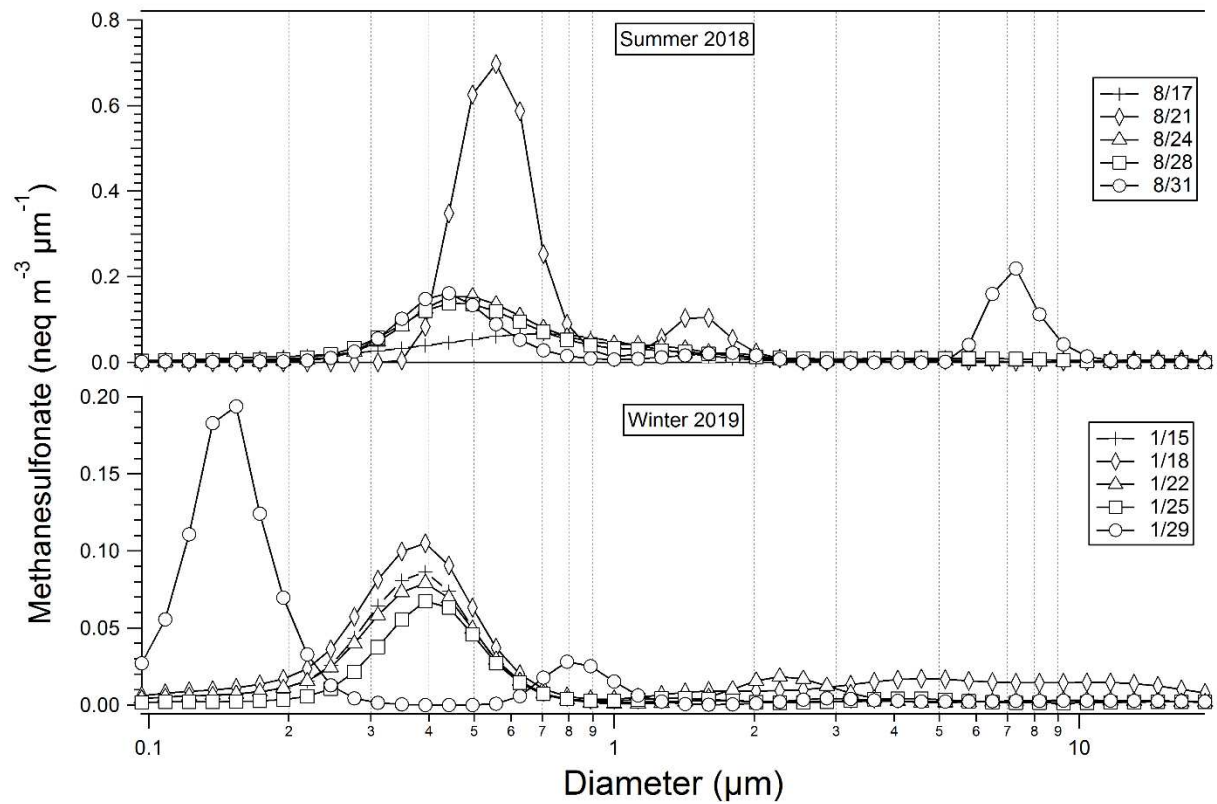
Figure A18. Methanesulfonate size distributions for summer and winter seasons are shown above.
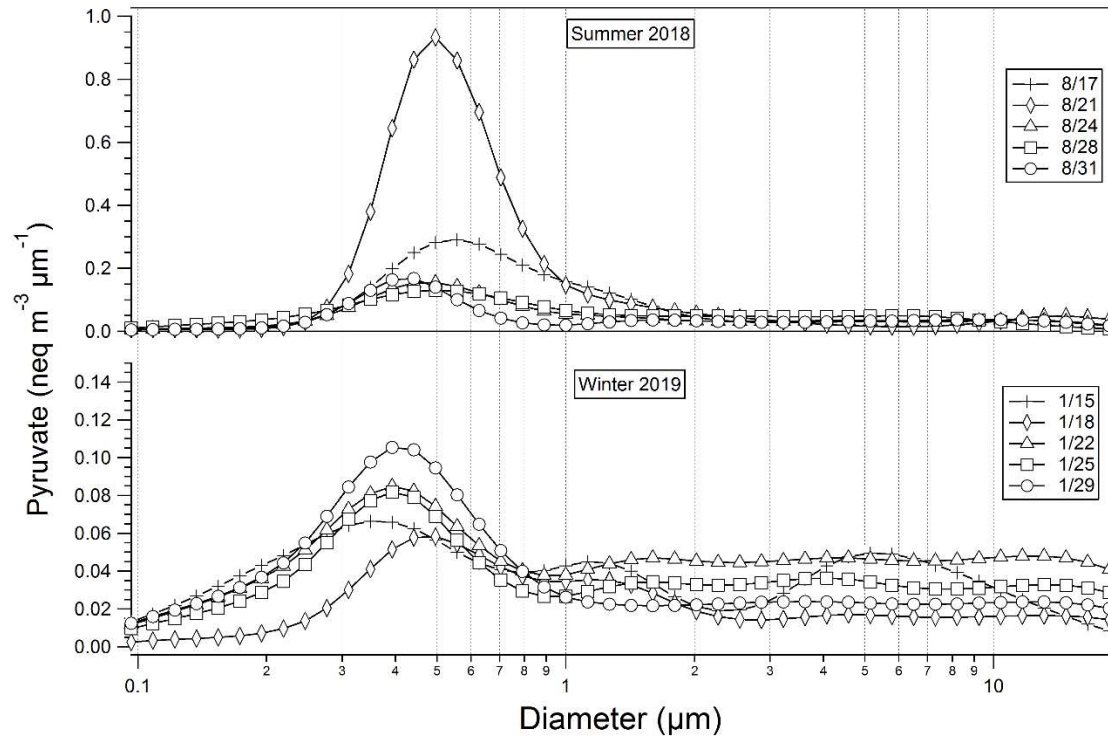
Figure A19. Pyruvate was only slightly above the MDL during the winter season, causing distributions to be uncertain, particularly in the coarse size range.
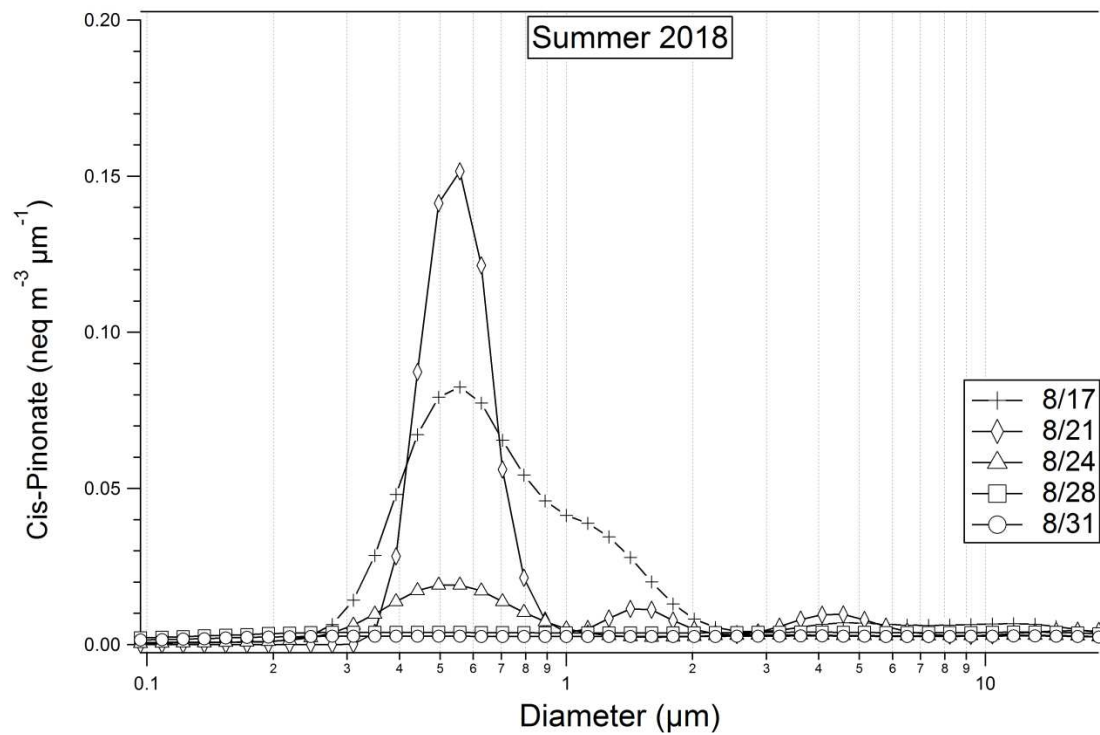
Figure A20. Cis-pinonate showed evidence of a droplet mode during the sampling period of 8/17/2018 and possibly during 8/21/2018 period when RH was high.
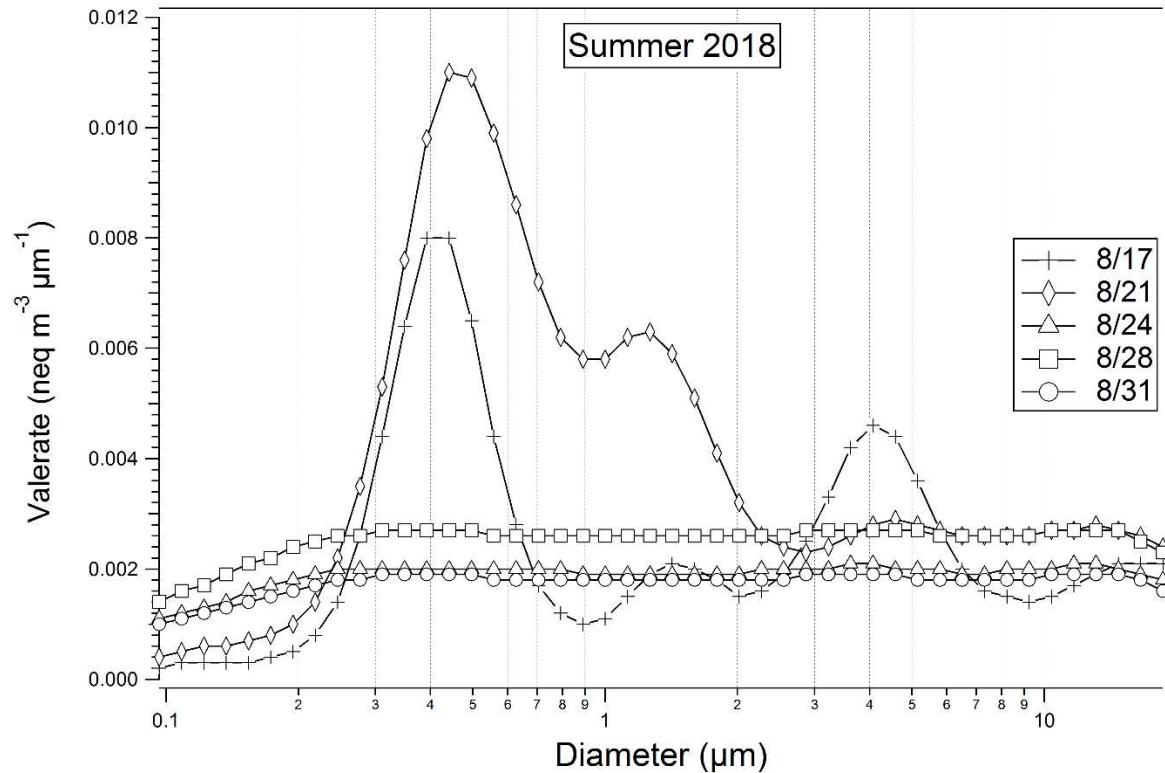
Figure A21. Valerate was observed only in the summer and was not consistently observed during each summer sampling period. Concentrations were observed to be very low but there is possibility of a droplet evidenced when RH was relatively high.
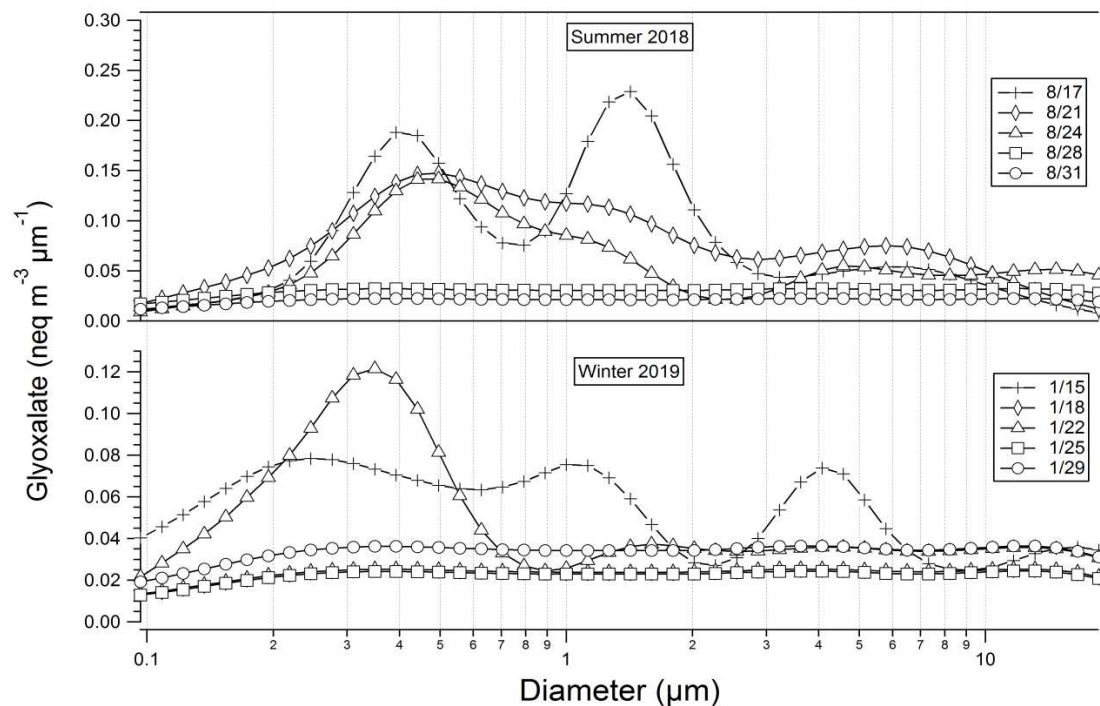
Figure A22. Glyoxalate size distributions were interesting for both seasons. Because the concentrations were low, it is not certain if the trends shown here are an effect of overestimation and underestimation by the Twomey algorithm.

Inorganic ions:
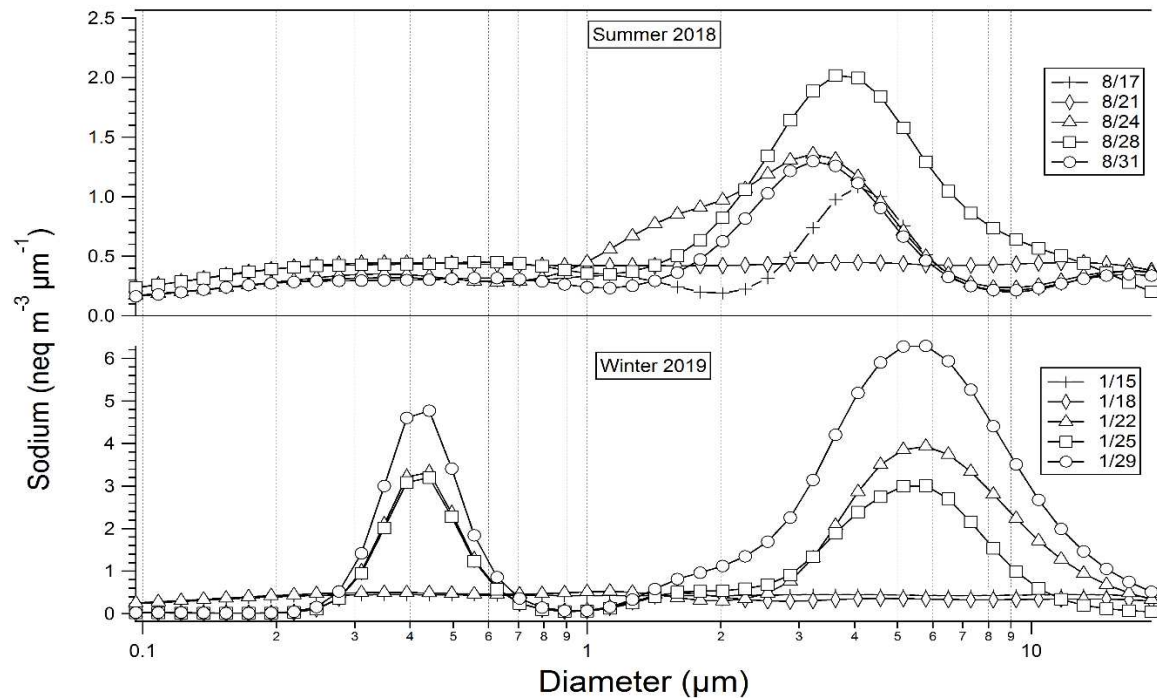
Figure A23. Sodium was dominantly observed in the coarse mode during the summer and was found in both the coarse and fine mode during the winter.
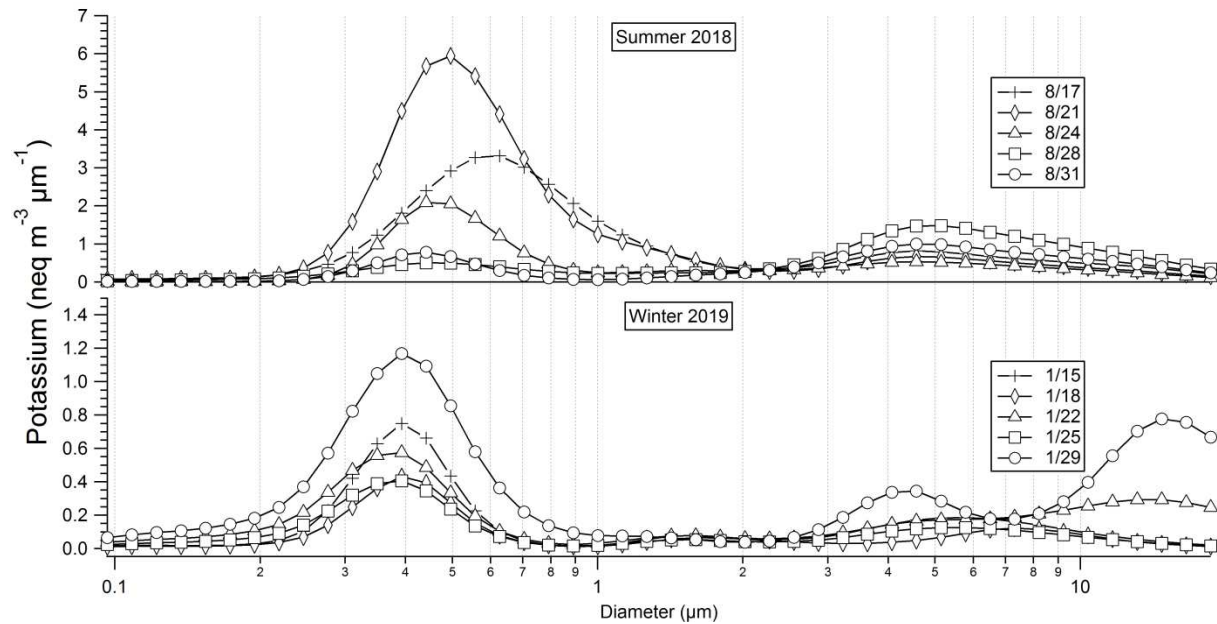
Figure A24. Potassium size distributions indicate its importance in the fine mode for both winter and summer seasons.
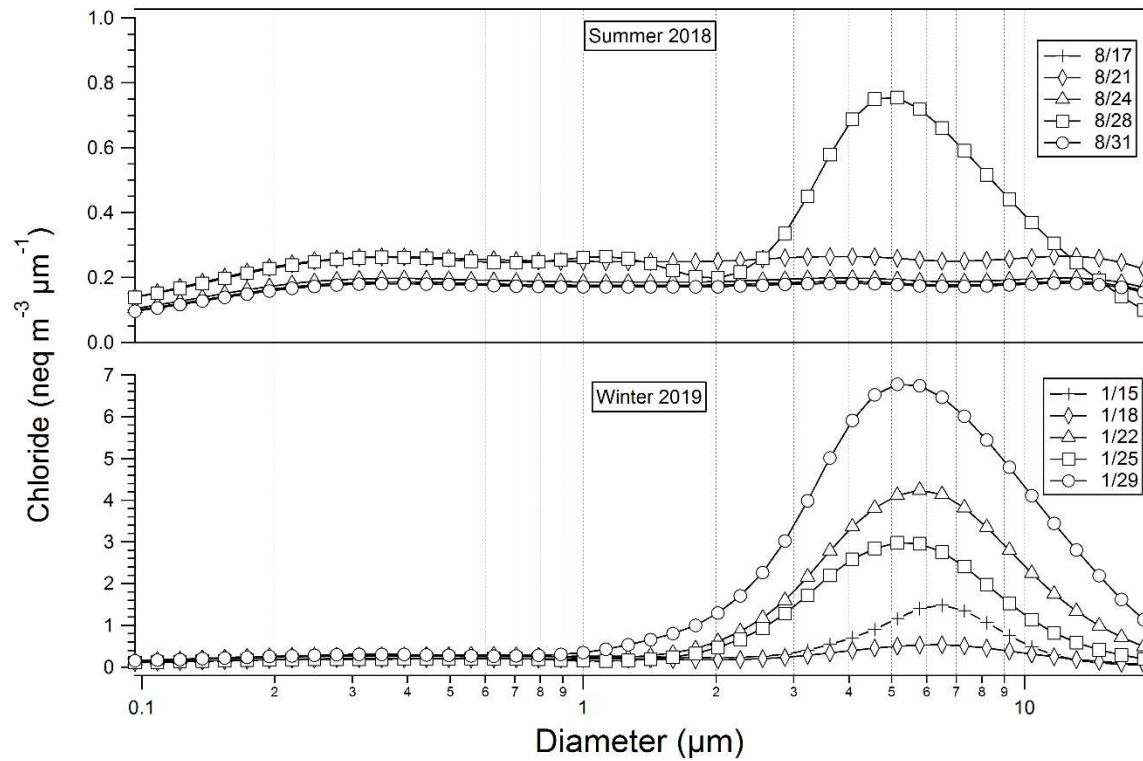
Figure A25. Chloride was found to dominate the coarse mode for the winter and summer but was generally only detected in the winter with only one sampling period in the summer indicating the presence of chloride in coarse mode.
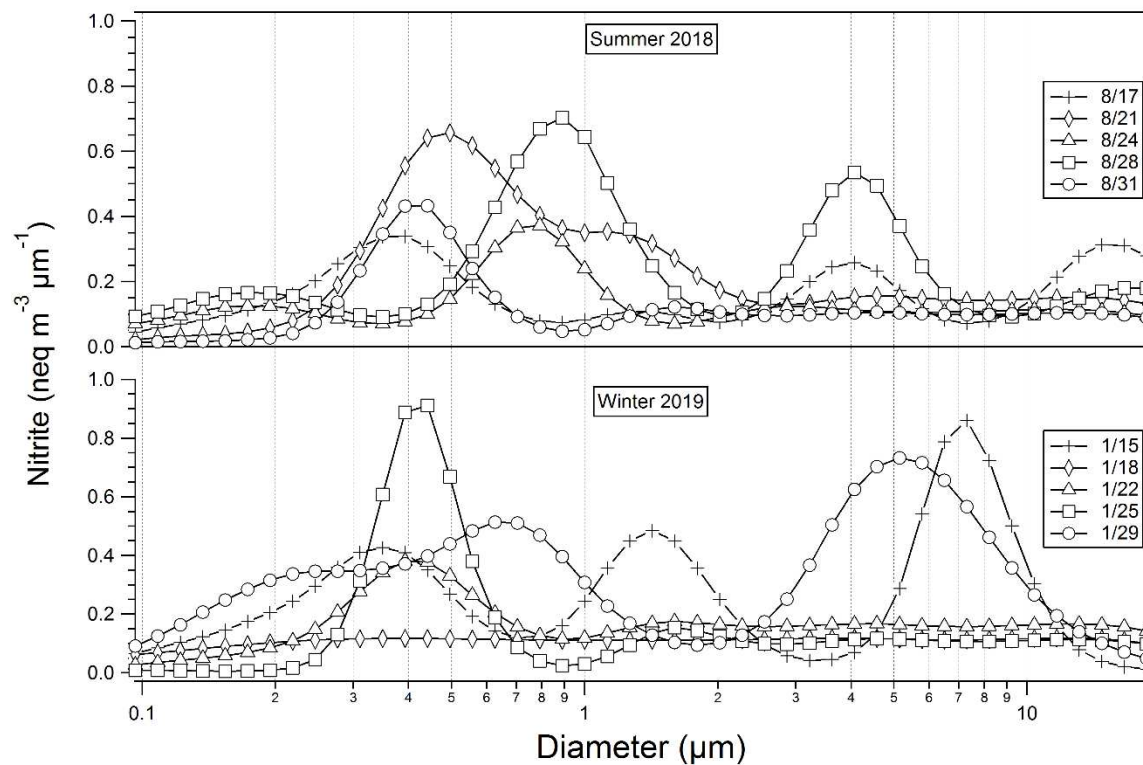
Figure A26. Nitrite did not have a consistent distribution for any sample collected in either the summer or winter. more research regarding nitrite and its' chemistry is needed to determine the trends seen by the figure above.

Appendix B:

The Twomey algorithm was adopted from previously written Fortran code as was explained in the main text above. The code encompasses many comments that explain what each element is. The first two pages of the code are comments that dictate the original creator of the code as well as an explanation of what the output files are named along with their contents.   The code is too long to be copied here as original text; however, Evelyn Bangs can be contacted for the text file of the code at ejb.bangs@beyondbb.com.

Additional files are included here that host necessary information to be used in the code. The first file includes the parameters that can be adjusted for the relevant cascade impactor being used such as the stopping criteria, curve smoothing parameters, etc. Each number in this TI.PAR file indicates the parameter used for controlling the curve fit. An example of the TI.PAR file is copied below. The different values here are explained in the comments found in the beginning several pages of the Fortran code file.

Example TI.PAR file.

```
xexp    :    0.3
xlim    :    0.01
xend    :    0.05
sigstp  :    1.05
itl     :    10
isl     :    8
ismooth :    0
ifs     :    2
```

chcnt : 100

zero   :   10.0

txtflg :   1

debug :   1

The next important file, IMPACT.PAR, contains parameters that describe the collection

efficiencies for each stage of the relevant impactor. The format for this file is considered to be

'free' and each value is separated by a space. The first column of this file contains the D50

cutpoints, the second column contains the steepness parameters, and the third column

contains the skewness parameters for each impactor stage. The values here are generally

taken from the calibration data provided by the manufacturer. The code can be adjusted to

reflect the number of stages depending on the type of impactor used. To change the number

of stages, the variable 'stgcnt' in the code must be changed to reflect the proper number of

stages/calibration data provided in the IMPACT.PAR file. An example of the IMPACT.PAR file is

given as follows.

Example IMPACT.PAR file.

D50	Steepness	Skewness
0.018	3.000	0.000
0.037	3.000	0.000
0.094	4.000	0.000
0.175	4.000	0.000
0.290	5.000	0.000
0.560	6.000	0.000
1.000	9.500	0.000

1.800	9.500	0.000
3.200	10.00	0.000
5.600	5.500	0.000
10.000	4.000	0.000
30.000	3.000	0.000

Lastly, a file containing the initial guess mass for each stage, is labeled as twomey.txt. The input data for this file is generally the raw data that was collected for each sample. This file can have up to five samples with three rows in each record. The first row contains three records: first the site name, then the sample date, and last, the species name in the format (a12, 1s, i6, t32, a12). Only the species name is included in the STG output file. The first row of numbers consists of the concentration in order of the largest stage to the smallest stage with each number separated by a space. The second row of numbers consists of the concentration uncertainties. Values of zero are entered for unused stages and any number of significant figures and decimal places can be specified. A sample concentration file is shown below:

Sample Twomey.txt file.

```
CSU  011519       NITRATE
 0.0  0.0  0.0  0.0  0.0  0.0  0.0  0.0  0.0  0.0  0.0  0.0
 0.0  0.0  0.0  0.0  0.0  0.0  0.0  0.0  0.0  0.0  0.0  0.0
CSU  011519       SULFATE
 0.0  0.0  0.0  0.0  0.0  2.1 11.6 15.0  5.1  0.0  0.0  0.0
 0.0  0.0  0.0  0.0  0.0  0.1  0.5  0.7  0.2  0.0  0.0  0.0
CSU  011519       OC
 0.0  0.0  0.0  0.0  0.0  0.3  1.5  1.9  0.6  0.0  0.0  0.0
 0.0  0.0  0.0  0.0  0.0  0.1  0.2  0.2  0.1  0.0  0.0  0.0
CSU  011519       EC
```

```
0.0  0.0  0.0  0.0  0.0  0.03 0.21 0.3  0.09 0.0  0.0  0.0

0.0  0.0  0.0  0.0  0.0  0.01 0.06 0.1  0.02 0.0  0.0  0.0

CSU  011519      FPM

0.0  0.0  0.0  0.0  0.0  3.2 17.8 23.0  7.7  0.0  0.0  0.0

0.0  0.0  0.0  0.0  0.0  0.1  0.8  1.1  0.3  0.0  0.0  0.0
```

This code can also be modified and used to determine other aspects or properties from

particle distributions that was not considered in this work and a more extensive manual can be

consulted. Contact Evelyn Bangs at ejb.bangs@beyondbb.com for access to this file.